INCORPORATING PHENOMENOLOGICAL LARGER SCALE, LEVEL-CODED MODEL ADAPTIVE PROPERTIES INTO A SMALLER SCALE MODEL TO ACHIEVE AN ADAPTIVE PULSE-CODED MODEL THAT IS CLOSER TO PHYSIOLOGY.

A Thesis Submitted in

Partial Fulfillment of the Requirements for the

Degree of Master of Science

with a

Major in Neuroscience

in the

College of Graduate Studies

University of Idaho

by

Bishnulatpam Lungsi Sharma

Major Professor: Richard B. Wells, Ph.D.

Abstract

An integration of disciplinary model ideas across disciplines of the neuroscience program is made quantitatively in this thesis. This thesis deals with the particular problem of designing a pulse-coded neural network (PCNN) and achieving an adaptive PCNN (APCNN) based on brain function. This is done by implementing the model-reference adaptation (MRA) technique where an adaptive level-coded model is the reference for the PCNN. The aim of this work is to explore methods for applying scientific reduction to higher-level network systems models in order to produce lower-scale models having closer links to neural physiology. Based on the empirical performance surface, the adaptive algorithm is a combination of gain-scheduling and steepest-descent method, resulting in adaptation of the pulse-coded model. Thus, taking the scientific reduction route an APCNN is successfully designed. Current APCNN's are designed for engineering applications, particularly image processing and hence these networks depart from biological plausibility. To our knowledge the APCNN developed in this thesis is the closest to biology amongst the available APCNNs. The adaptive property of the pulse-coded model is built upon a psycho-physiological foundation and the principles of embedding field theory.

Table of Contents

List of Figures

List of Tables

CHAPTER 1

Introduction

A major challenge for an inter-disciplinary program such as neuroscience is the integration of ideas within the disciplines to achieve a common goal. Apart from doing research in respective disciplines and catering to their audience, neuroscience as an inter-disciplinary field must cross the hurdle of discipline unification to achieve any significant strides in understanding the complexities of human brain. In other words, neuroscientists in their respective disciplines must build their research, and hence understanding, upon researches of their colleagues from other disciplines. This thesis is an essay on a quantitative method of disciplinary model integration.

If we consider respective disciplines as rungs of a ladder (Fig. 1.1), the objective of a neuroscientist should be to join the rungs for achieving the common goal of understanding how brain works. Taking the concept from systems theory this can be done on two accounts: model-order reduction (MOR) and scientific reduction (SR). MOR is the simplification of the amount of detail needed in obtaining computationally tractable models of ever more complex systems. Thus with MOR one moves towards increasing level of abstraction from mechanism to behavior. SR on the other hand is migrating scientific study and theory from the level of phenomena more directly observable by our senses to levels of increasingly refined scientific constructs.

This thesis deals with the particular problem of designing a pulse-coded neural network (PCNN) and achieving an adaptive PCNN (APCNN) based on brain function. It will be shown that this problem can be tackled by implementing the model-reference

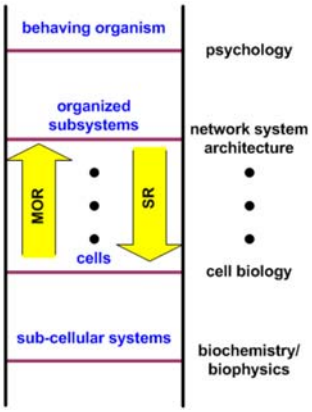

Figure 1.1. Neuroscience ladder adopted from [Wells 2011a] showing several rungs each representing scientific construct at various levels. Moving upward towards increasing level of abstraction from mechanism to behavior is model-order reduction (MOR). However, migration of scientific study from level of observable phenomenon down to increasingly refined scientific constructs is scientific reduction (SR).

principle from systems theory [Widrow & Sterns 1985]. The reference model is a network designed by Grossberg [Grossberg 1972b] which is based on psychological principles, hence described by activity level, and thus a level-coded model. This level-coded model is taken as the reference model because of its adaptive ability. A PCNN is then designed based upon the Eckhorn neuron model [Eckhorn et al. 1989b, 1990] such that it exhibits properties corresponding to those of the pre-adapted level-coded model. Finally, performance of the PCNN is evaluated against the level-coded model to achieve the adaptive property of the level-coded model, hence achieving an APCNN.

The level-coded model representing psychological phenomenon is situated close to the psychological rung while the pulse-coded model is relatively closer to the biological/physiological rung (Fig. 1.2). Therefore, the approach in this thesis is SR as we implement level-coded model in order to incorporate its properties into a model with significantly more parts, the pulse-coded model.

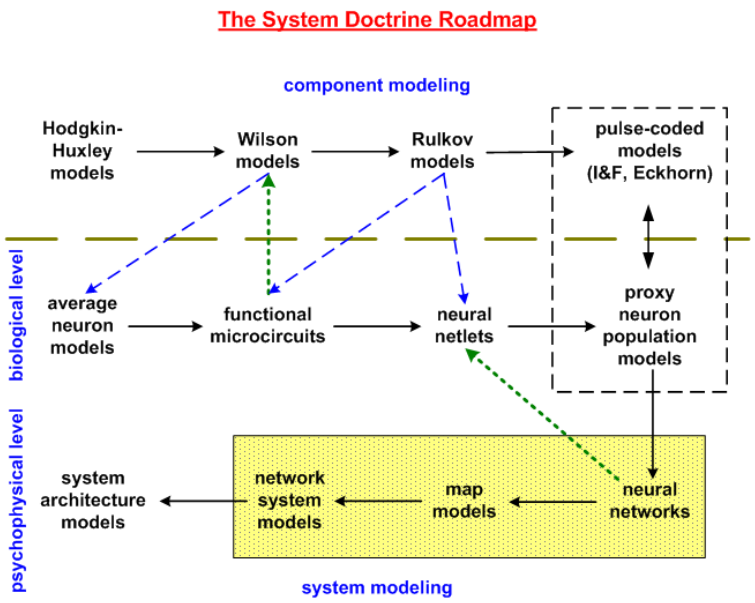

Figure 1.2. An alternate view of the neuroscience ladder (Fig. 1.1), neuroscience roadmap. The highlighted region indicates the location of this thesis with regards to the neuroscience roadmap. Thus, the level-coded model based on psychological principles is close to the psychophysical end while the pulse-coded model built using Eckhorn neuron model is relatively closer to the physiological end of the roadmap. A map model is a network of neural networks while a network of maps comprises a network system [Wells 2010, Ch.7].

Grossberg's Network

Grossberg's network (G-N) is based on psychological postulates made by Grossberg [Grossberg 1972a] which can be summarized as follows. When a subject receives shock (unconditioned stimulus) that induces fear, the subject experiences relief from fear of the shock immediately after the removal of shock stimulus. These fear and relief responses form what Grossberg calls the net-incentive motivation. In addition, the generation of fear or relief response can be reinforced by another external stimulus (conditioning stimulus). This learning of motivation patterns forms the reinforcement.

The network model derived from the above postulates has three representations: sensory, drive and motor representations (Fig. 1.3). The sensory representation sending

conditioning stimulus reinforces the drive representation. The drive representation formed by a dipole network (DN) generates motivational decisions in psychological terms. And finally, the motor representation receiving inputs from the other two representations generates action (motor) commands. The dipole network plays an important role in supporting the postulates. The unique property of the dipole network constructed by Grossberg is the rebound mechanism. That is, relief response occurs when shock input (for fear) is removed.

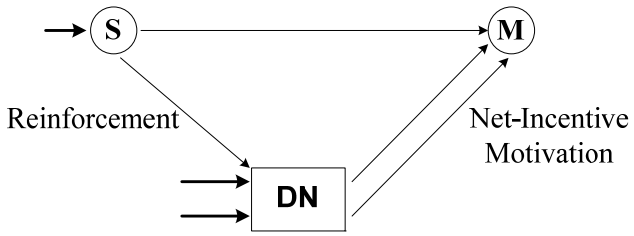

Figure 1.3. The three representations for deriving the Grossberg network; S, sensory representation receiving conditioning stimulus; DN, drive representation receiving tonic and unconditioned stimulus; and M, motor representation receiving inputs from the former two. The dipole network (DN) forms the drive representation and plays an important role in supporting Grossberg's psychological postulates. In psychological terms, outputs from DN correspond to net-incentive motivation and outputs from S to DN correspond to reinforcement. Finally, action or motor commands are generated by M.

The law of the dipole network deduced by Grossberg [Grossberg 1969a, 1969b, 1971] is expressed as

$$\dot{x}_i = -\varepsilon_i \cdot x_i + \sum_{k=1}^{n} \zeta_{ki} \cdot [x_k(t - \tau_{ki}) - \Gamma_{ki}]^+ \cdot z_{ki} + I_i, \qquad (1)$$

$$\dot{z}_{jk} = \beta_{jk} \cdot (\gamma_{jk} - z_{jk}) - \delta_{jk} \cdot [x_j(t - \tau_{jk}) - \Gamma_{jk}]^+ \cdot z_{jk} \qquad (2)$$

where $x_i(t)$ = activity of i^{th} node within the network, I_i = stimulus to i^{th} node, ζ is an excitation rate, δ is the adaptation rate, Γ denotes threshold, ε and β are the relaxation

rates, and $z_{ki}(t)$ = elastic connection strength (memory trace) from k^{th} to i^{th} node. γ is the maximum connection strength and τ is the adaptation lag. The Heaviside extractor activation function $[H]^+$ is given by, $[H]^+ = \begin{cases} H, \text{ if } H > 0 \\ 0, \text{ if } H \le 0. \end{cases}$

The law therefore describes the interaction of node activity with connection strength (synaptic weight). The external event via input I_i excites node activity $x_i(t)$ increased by an amount determined by the second term of equation (1), which is the sum of the products of preceding node activities with respective synaptic weight. The decrease in $x_i(t)$ node activity is proportional to its initial activity, given by the first term. For τ_{ki} = 0, the steady-state solution of i^{th} node activity is

if $x_i > \Gamma_{ii}$,

$$x_i = \frac{I_i - \zeta_{ii} \cdot \Gamma_{ii} \cdot z_{ii} + \sum_{k=1,k\neq i}^{n} \zeta_{ki} \cdot [x_k(t) - \Gamma_{ki}]^+ \cdot z_{ki}}{\varepsilon_i - \zeta_{ii} \cdot z_{ii}} > \Gamma_{ii}$$

else if $x_i \le \Gamma_{ii}$,

$$x_i = \frac{I_i + \sum_{k=1,k\neq i}^{n} \zeta_{ki} \cdot [x_k(t) - \Gamma_{ki}]^+ \cdot z_{ki}}{\varepsilon_i} \le \Gamma_{ii}.$$

Equation (2) on the other hand describes the rate of elastic synaptic weight formation. The steady-state weight is

$$z_{jk} = \frac{\beta_{jk} \cdot \gamma_{jk}}{\beta_{jk} + \delta_{jk} \cdot [x_j(t - \tau_{jk}) - \Gamma_{jk}]^+} \le \gamma_{jk}.$$

Note that for $\delta_{jk} = 0$, $z_{jk} = \gamma_{jk}$, a fixed value.

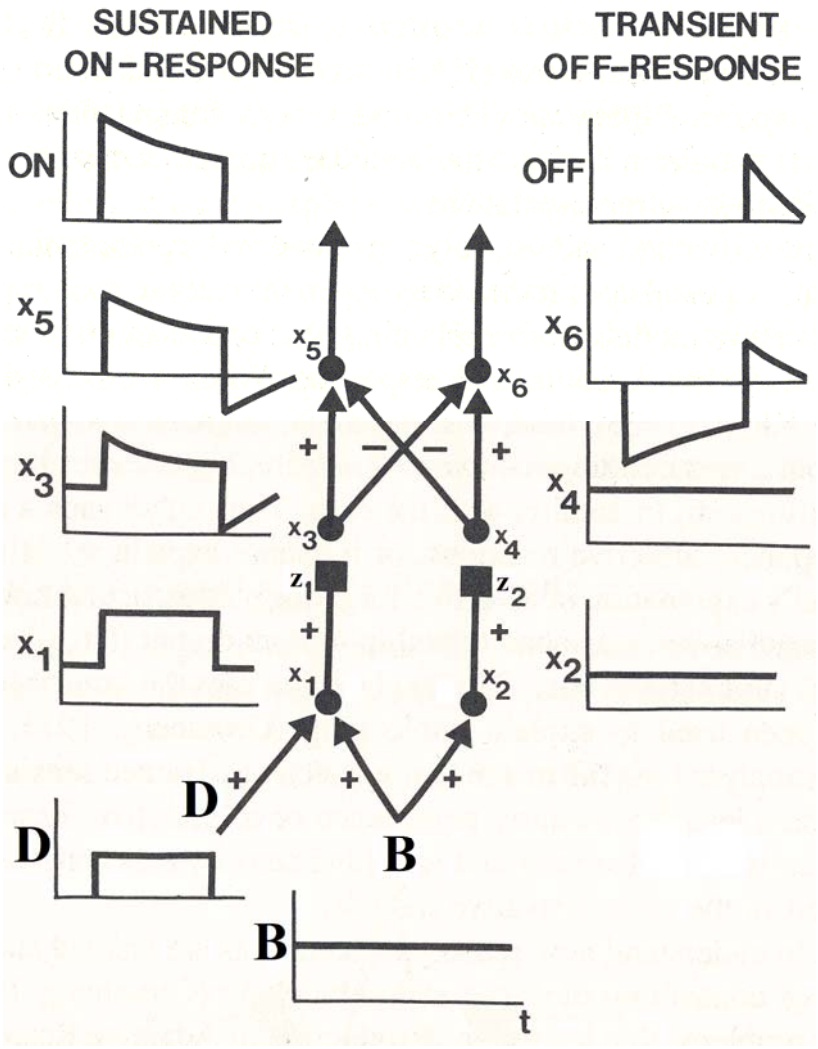

Figure 1.4. Dipole Network (DN) derived by Grossberg using equations (3) to (12) receiving bias or tonic input (B) and drive or shock input (D). x_1 and x_2 represent node activities at first stage of processing in response to respective input stimulus. x_3 and x_4 activities at second stage respond to the preceding node activities (x_1 & x_2) connected by respective elastic weights (z_1 & z_2). Input for generating x_5 and x_6 activities at third stage is the result of mutual inhibition between x_3 and x_4 activities. DN outputs are the result of x_5 and x_6 activities. The plots at the side of the network represent the node activities at respective stage of processing derived analytically with the exception of bottom and top two, which are DN inputs and outputs respectively adopted from [Grossberg et al. 1991]. $x_i < 0$ denotes below-normal-background activity.

Grossberg [Grossberg 1972b] used the principles of above two equations (Eqn. 1 & 2) to design the dipole network shown in Figure 1.4. The process describing the network is given by

$$\dot{x}_1 = -\alpha \cdot x_1 + B + D, \tag{3}$$

$$\dot{x}_2 = -\alpha \cdot x_2 + B, \tag{4}$$

$$\dot{z}_1 = \beta \cdot (\gamma - z_1) - \delta \cdot [x_1(t-\tau) - \Gamma]^+ \cdot z_1, \tag{5}$$

$$\dot{z}_2 = \beta \cdot (\gamma - z_2) - \delta \cdot [x_2(t-\tau) - \Gamma]^+ \cdot z_2, \tag{6}$$

$$\dot{x}_3 = -\varepsilon \cdot x_3 + \zeta \cdot [x_1(t-\tau) - \Gamma]^+ \cdot z_1, \tag{7}$$

$$\dot{x}_4 = -\varepsilon \cdot x_4 + \zeta \cdot [x_2(t-\tau) - \Gamma]^+ \cdot z_2, \tag{8}$$

$$\dot{x}_5 = -\omega \cdot x_5 + \kappa \cdot [x_3(t-\sigma) - x_4(t-\sigma)]^+, \tag{9}$$

$$\dot{x}_6 = -\omega \cdot x_6 + \kappa \cdot [x_4(t-\sigma) - x_3(t-\sigma)]^+, \tag{10}$$

$$O_5 = \lambda \cdot [x_5 - \Omega]^+, \tag{11}$$

$$O_6 = \lambda \cdot [x_6 - \Omega]^+. \tag{12}$$

Equations (3) and (4) describes the node activities at first stage of input processing, whose response is linear to their inputs, bias (B) or tonic input and drive (D) or shock input, and bias (B) input alone respectively. Equations (7) and (8) describe node activities at the second stage of processing connected to the first stage nodes via elastic weights, given by (5) and (6) respectively. The weight formation follows the law described earlier. Node activity (Eqn. 9 & 10) at the third stage of processing receives competitive signal inputs generated by the preceding node activities. In other words, node-3 and node-4 outputs are processed by a subtractive on-off field yielding inputs to node-5 and node-6. Finally, output of the DN is given by equations (11) and (12) which are activation functions of respective third stage node activities.

The properties of the network leading to the rebound mechanism as described by Grossberg [Grossberg 1972b] can be summarized as follows:

- Termination of drive input unmasks the effects of an internally driven input to cause transient off-response (output from x_6 activity). This internal source is the level (γ) sought by the weight formation (z_2, Eqn. 6) when there is no preceding node activity. Hence this internal source or level is neither turned on nor off by the drive input.

- Internal source or level accumulates (summates) when drive input is on. That is, drive input summates with bias input.

- The transient off-response (O_6) shuts off soon after it is turned on because with just bias input, the equivalent x_3 and x_4 activity levels competing by mutual inhibition results in no input for nodes at third stage of the processing. Thus, there is no x_5 and x_6 activity.

The original dipole network by Grossberg did not present a long-term adaptive function. However, this thesis implements Grossberg's network with long-term adaptive capability. The adaptation occurs at the weights connecting the sensory inputs (from sensory representation, Fig. 1.3) to the dipole network. Adaptation of these weights is based on Grossberg's outstar rule [Grossberg 1978]. In psychological terms, adaption of the network implies that the conditioning (sensory) stimulus, by association with unconditioned (drive) stimulus, leads to a conditioned response for activities from the motor representation. A detailed qualitative and quantitative description of the adaptive capability of the network is given in the next chapter.

Eckhorn Neuron Model

Eckhorn and coworkers demonstrated in cat primary visual cortex that stimulus-evoked oscillations of local processing units representing local visual features get transiently locked into a common resonance state by appropriate global stimulus [Eckhorn et al. 1988a, 1988b, 1989a]. Activities of these neural groups become synchronized, representing feature linking via visual stimulus. The Eckhorn neuron model is the product of Eckhorn's et al. [Eckhorn et al. 1989b] search for physiological explanation (mechanism) of transient linking of local visual features into global coherent percepts. Based on the neuro-physiological findings, they designed a neural network model capable of performing feature linking via modulatory interactions. This neural network consisted of two one-dimensional layers of proxy neuron population models. We shall call these models Eckhorn Neural Units (ENUs) [Wells 2010, Ch8].

The ENU has two main parts. The first part receives external inputs and the second receives inputs from the first (Fig. 1.5). These components are named dendrite and soma, respectively. However, one should be warned that these two terms are not to be confused with the dendrites and soma of a biological neuron. The dendrite compartment can further be sub-divided with respect to the two functionally different inputs for soma it generates. These are the regular "feeding" inputs and modulatory "linking" inputs. Eckhorn et al. uses the term modulatory (as in amplitude modulation of a radio-frequency carrier) for linking signals due to its modulatory effect on the feeding signals. Within their network, the concept of the linking field was introduced as a correspondence to the association field of a local assembly of visual neurons providing the linking mechanism in perceptual feature linking [Eckhorn et al. 1990].

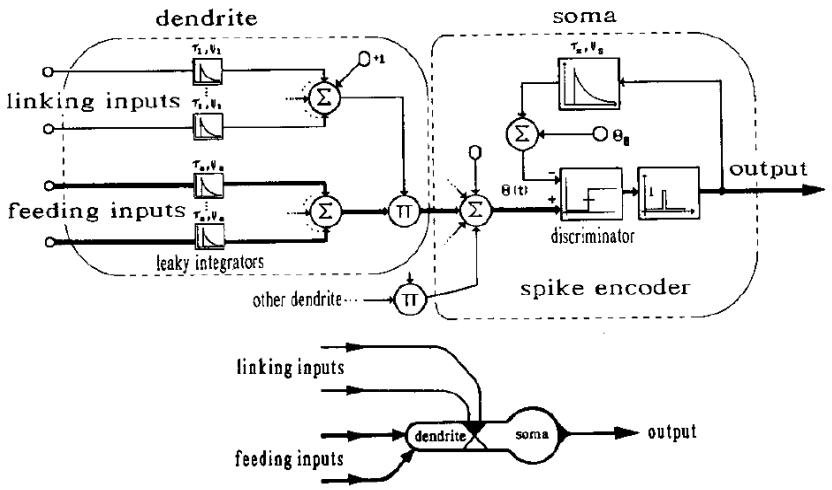

Figure 1.5. Basic Eckhorn neural unit (ENU) having two components (dendrite & soma). Inset shows internal workings in the components (adopted from [Eckhorn et al. 1990]).

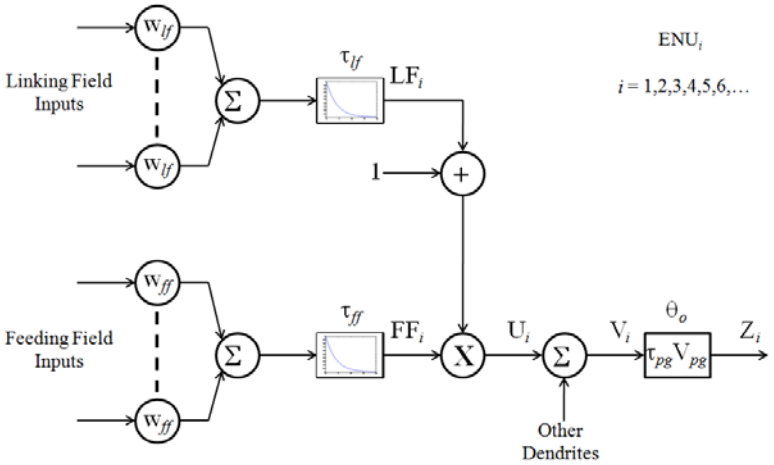

Figure 1.6. Another view of the above basic ENU architecture. Subscript of ENU$_i$ is such that i denotes one specific ENU. The feeding field input value is either 0 or 1.
Linking field: w_{lf} & τ_{lf} are parameters (weight & time constant) and LF_i the output.
Feeding field: w_{ff} & τ_{lf} are parameters (weight & time constant) and FF_i the output.
Soma/Neuromime Pulse Generator (NMPG): τ_{pg}, V_{pg} & θ_o (time constant, threshold amplitude & threshold offset) and Z_i (spike output).

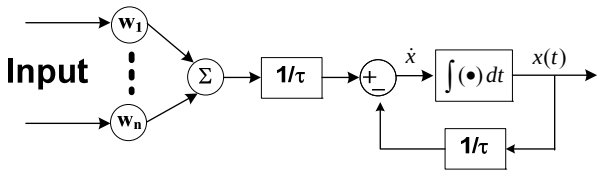

Figure 1.7. Block diagram of the leaky-integrator (LI). Feed-forward gain ($1/\tau$) is used to make the transfer function have unity gain for step function inputs. This implementation is shown in equations (13) and (14).

For a detailed description of the ENU one must consider the quantitative relationship within and between the components. Figure 1.6 shows a detailed representation of figure 1.5. The difference equations for the mathematical description [Eckhorn et al. 1990] are

$$FF_i(t) = FF_i(t-\Delta t)\cdot\exp(-\Delta t/\tau_{ff}) + (1/\tau_{ff})\cdot w_{ff}\cdot\sum_{\forall j} F_j^{inputs}, \quad (13)$$

$$LF_i(t) = LF_i(t-\Delta t)\cdot\exp(-\Delta t/\tau_{lf}) + (1/\tau_{lf})\cdot w_{lf}\cdot\sum_{\forall j} L_j^{inputs}, \quad (14)$$

$$U_i(t) = FF_i(t)\cdot(1 + LF_i(t)), \quad (15)$$

$$V_i(t) = \sum_{\forall i} U_i(t), \quad (16)$$

$$\Theta_{V_i}(t+\Delta t) = \begin{cases} V_{pg}, & V_i(t) \geq \Theta_i(t) \\ \Theta_{V_i}(t)\cdot\exp(-\Delta t/\tau_{pg}), & V_i(t) < \Theta_i(t) \end{cases}, \quad (17)$$

$$\Theta_i(t) = \Theta_O + \Theta_{V_i}(t), \quad (18)$$

$$Z_i(t+\Delta t) = \begin{cases} 1, & V_i(t) \geq \Theta_i(t) \\ 0, & V_i(t) < \Theta_i(t) \end{cases}. \quad (19)$$

The feeding and linking inputs for the soma are generated by their respective leaky-integrator functions (Eqn. 13 & 14). The leaky-integrators integrate the weighted afferent signals at respective rates given by their time constants, τ_{ff} and τ_{lf} . These integrated signals then leak exponentially at their rates. Eckhorn et al. used a time-step (Δt) of 1ms for their simulations [Eckhorn et al. 1990]. The LFLI together with a constant offset term (+1) interacts multiplicatively with the FFLI resulting in amplitude modulation of the FFLI output (Eqn. 15). Thus, the two parts of the dendrite components come together to form the dendrite output (U_i).

Depending upon the presence of other dendrite components, the respective dendrite outputs are summed to form the soma input (V_i) signal (Eqn. 16). The soma component as a neuromime is represented by the two-state variables (Θ_{V_i} & Z_i) to generate pulses from i^{th} ENU (Eqns. 17, 18, 19). Thus, equation (19) shows that if $V_i <$ neuromime threshold (Θ_i), there is no output from the soma. However if $V_i \geq \Theta_i$, the output is 1, resulting in pulse generation. In addition equation (17) shows that the $V_i \geq \Theta_i$ condition also resets the neuromime threshold ($\Theta_i = V_{pg}$) corresponding to an absolute refractory period. This is followed by an exponential decay at a rate given by the time constant τ_{pg} when soma input returns to the $V_i < \Theta_i$ case. This exponential decay of Θ_i to its resting level (Θ_O) corresponds to a relative refractory period.

Pulse-mode firing resulting from the above mechanisms can be classified into types: all-pass mode, high-pass mode, rate-multiplier mode and saturated mode (Fig. 1.8). The saturated mode is an original finding in this thesis. During all-pass firing mode (Fig. 1.8a), every input stimulus produces soma input exceeding the neuromime threshold, i.e., $V_i \geq \Theta_i$. All-pass mode occurs if the condition, $\frac{V_{ff}}{\tau_{ff}} \geq \Theta_o$ is satisfied ($V_{ff} = \sum_{\forall j} w_{ff_j} \cdot F_j^{inputs}$).

In high-pass mode (Fig. 1.8b), ENU spiking occurs such that the interval of the successful inputs are wider than the actual inter-input interval (Fig. 1.9). That is, ENU in this mode perform as a high-pass like filter as they filter out lower frequency inputs. For a long input tetanus at spike interval T, the FFLI output has a DC base, $\frac{1}{\mathrm{T}} \sum_{\forall j} w_{ff_j} \cdot F_j^{inputs}$.

Thus with increasing input rate, the FFLI output builds up a DC base and the *V* amplitude

gets higher eventually reaching Θ. This mode occurs if $\frac{V_{ff}}{\tau_{ff}} < \Theta_o$ is satisfied.

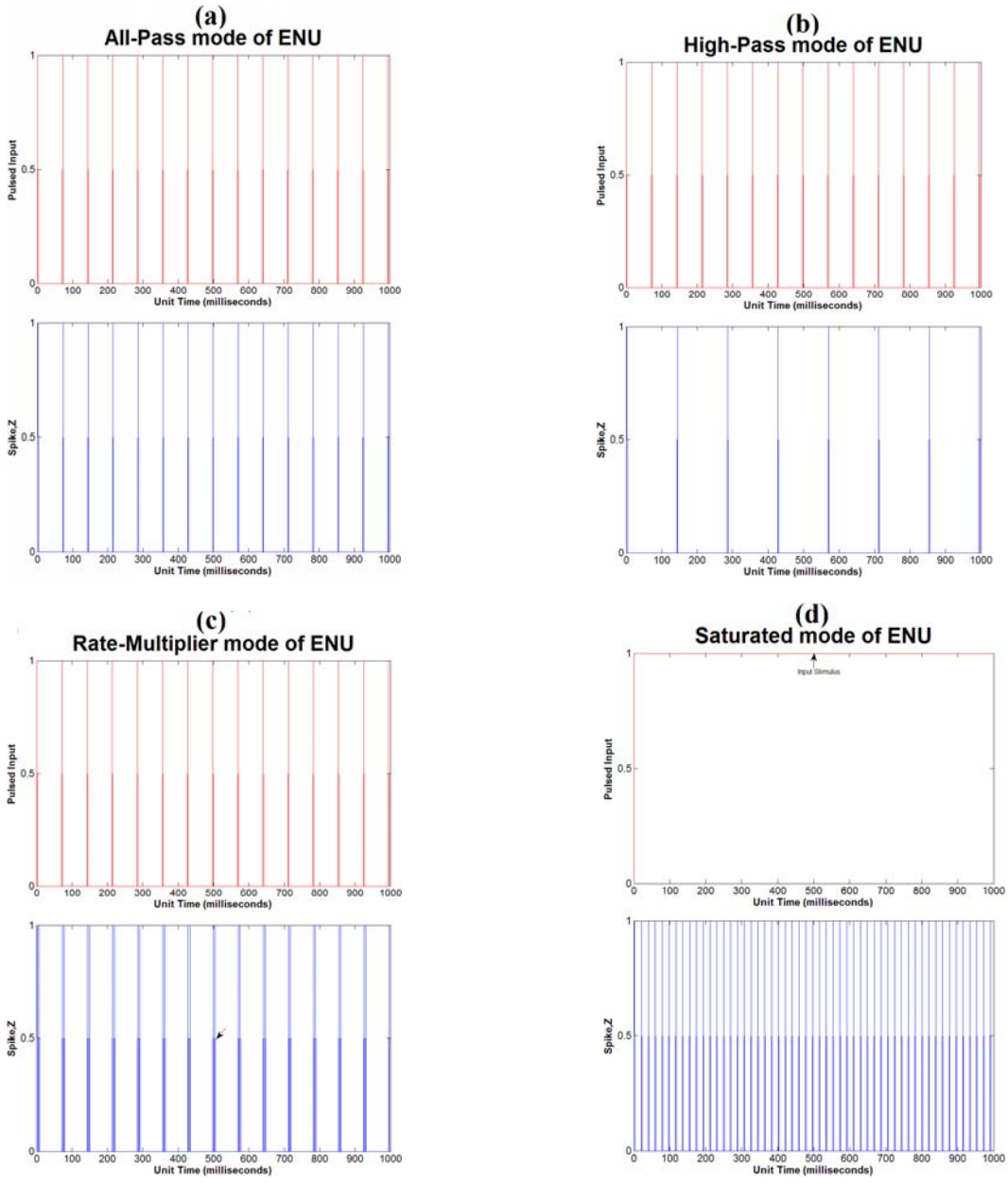

Figure 1.8. Different firing modes of an ENU. (a) All-pass mode: every input stimulus (red) results in ENU spiking (blue). (b) High-pass mode: ENU spiking occurs by skipping inputs (≥1, here just 1) between inputs that succeeded in causing spike. That is, it acts as a high-pass filter where inputs with low rates are filtered out. (c) Rate-multiplier mode: Single input stimulus causes more than one spike output (here 2, arrow). (d) Saturated mode: Input pulses with very short intervals produce a DC LI output and result in a maximum NMPG spiking rate decoupled from the input spiking rate.

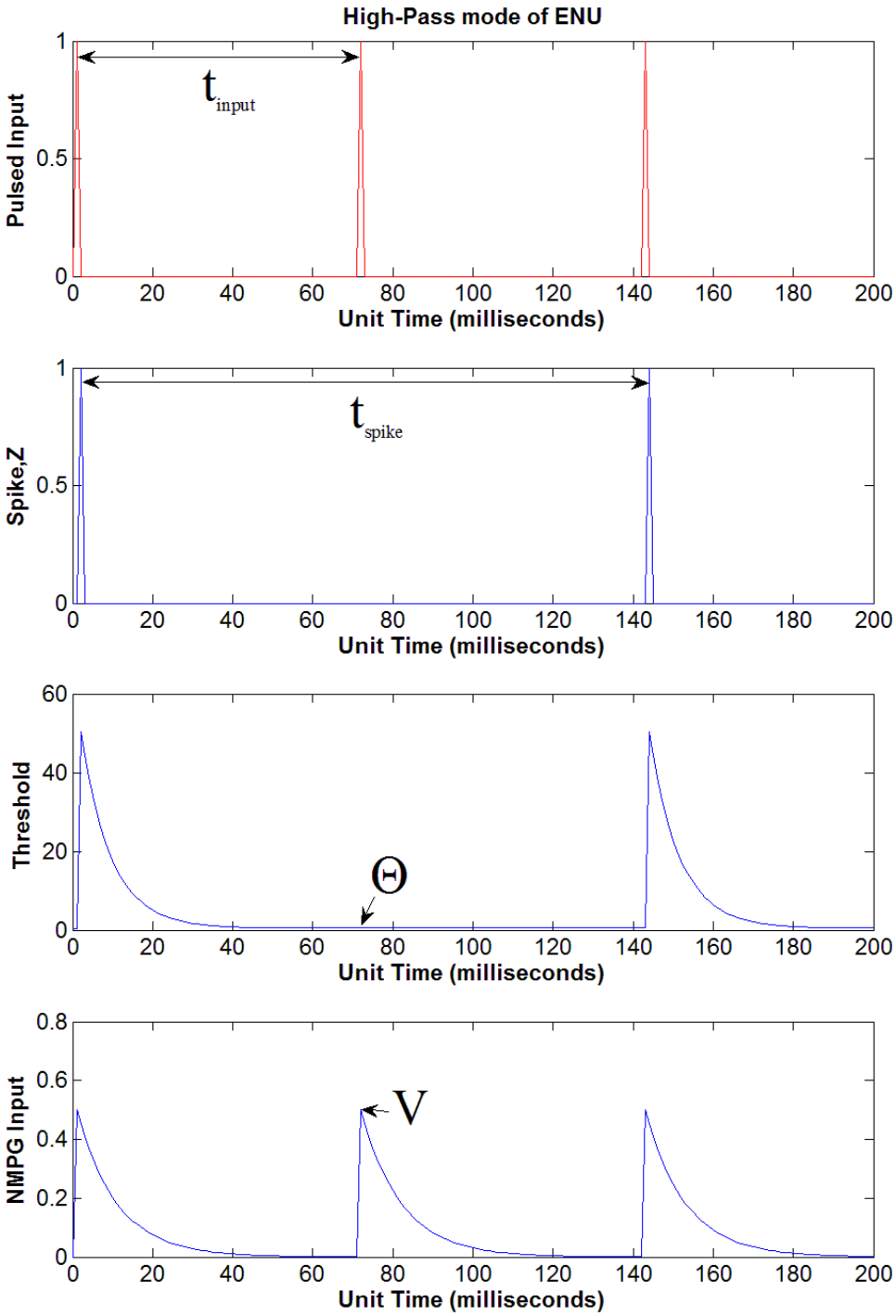

Figure 1.9. Snapshot of Figure 1.8b (High-Pass mode) demonstrating that the soma input (V, arrow of bottom plot) triggered by the second input (red, top plot) does not succeed in causing a spike because $V < \Theta$. Thus the inter-spike interval (t_{spike}) is wider than inter-input interval (t_{input}). That is, ENU at high-pass mode behaves like a high-pass filter as it filters out inputs with low rates.

Another mode the ENU can exhibit is the rate-multiplier mode (Fig. 1.8c). During this mode a single input can result in more than one spike (Fig. 1.8c arrow). This is because the soma input produced by the single input is strong enough that its decay still exceeds the threshold during the intra-spike interval (Fig. 1.10). Similar to all-pass firing mode, rate-multiplier modes can occur if $\frac{V_{ff}}{\tau_{ff}} \geq \Theta_o$ is satisfied. But in addition to this other conditions apply. That is, if $\tau_{ff} < \tau_{pg}$ and $V_{pg} > \frac{V_{ff}}{\tau_{ff}}$ then the ENU usually does not exhibit rate-multiplier mode. However this is not a sufficient condition because this mode may still be exhibited in at a later input impulse because, unlike soma threshold, the FFLI is not reset by soma firing. Rate-multiplier mode may also occur in cases when w_{ff} is adaptive and hence changing.

Finally, during saturated mode (Fig. 1.8d & 1.11) continuous spiking occurs within a particular total stimulus interval. The onset of this mode depends on the chosen parameters of the ENU. This mode occurs if the inter-input interval is very short, producing a large DC baseline. It results in soma threshold not able to reach its resting (Θ_o) level (Fig. 1.11). We shall call this Θ oscillation. This oscillation occurs around the plateau of the soma input (V) as shown in Figure 1.12a. The V plateau as the oscillatory baseline remains unchanged in cases with more than one ENU connected via the linking-field (Fig. 1.13a). In other words, Θ oscillates before V amplitude modulation (arrowhead, Fig. 1.13) by the linking field. The plateau level of V is determined by the FFLI output (Fig. 1.12b). Thus FFLI outputs can cause NMPG to oscillate.

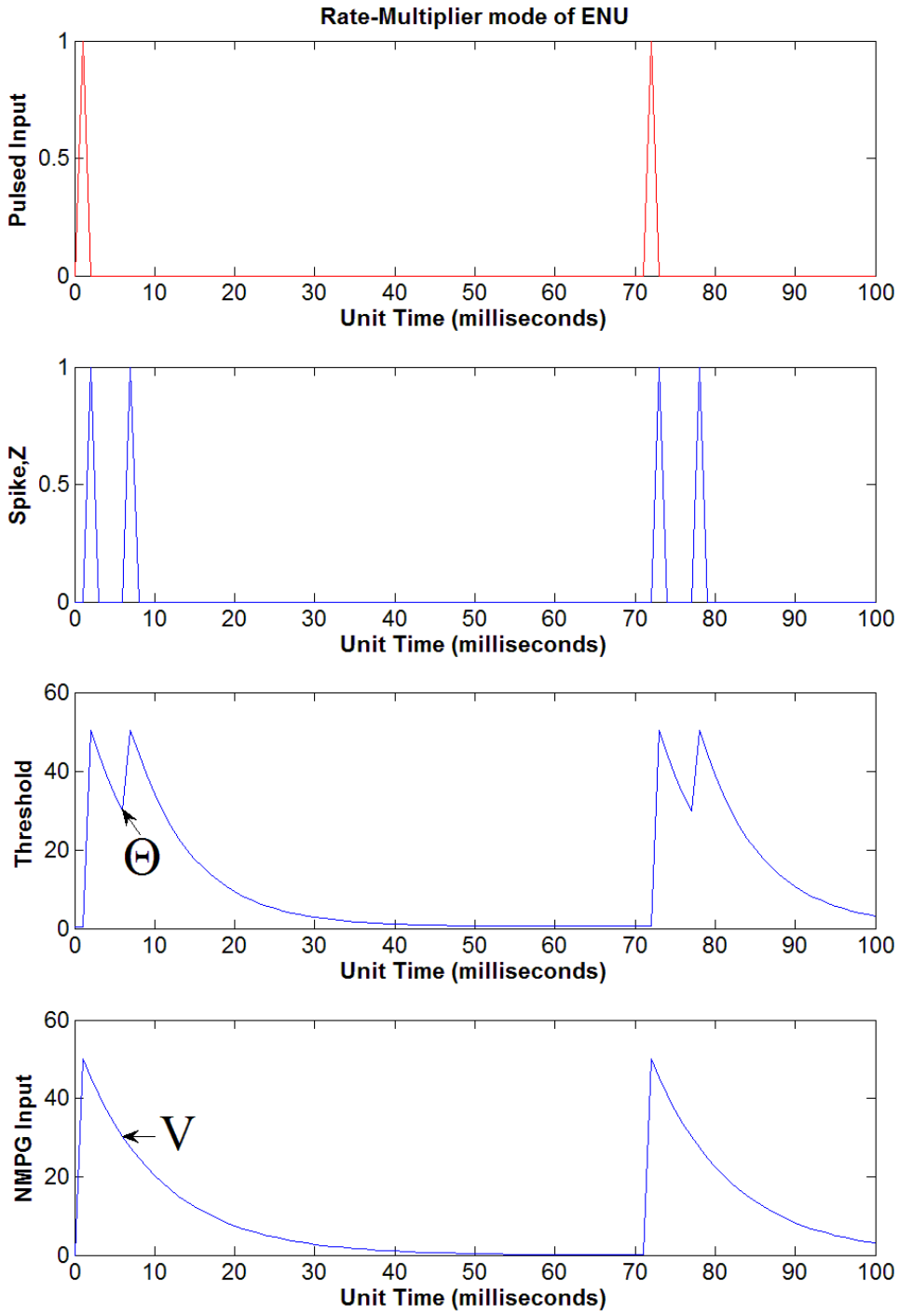

Figure 1.10. Snapshot of Figure 1.8c (Rate-Multiplier mode) demonstrating that the soma input (bottom plot) triggered by the input (red, top plot) succeeds ($V \geq \Theta$) in causing the first spike. Because of the success, the threshold is reset (to V_{pg}) and decays exponentially. Thus, $V < \Theta$. However at around 7ms magnitude of the decaying V (arrow of bottom plot) exceeds that of the decaying Θ (arrow of third plot). Thus, $V \geq \Theta$ results in a second spike caused by a single input. The second threshold reset and the already decaying soma input means that $V < \Theta$ at any given instant of time after the second spike.

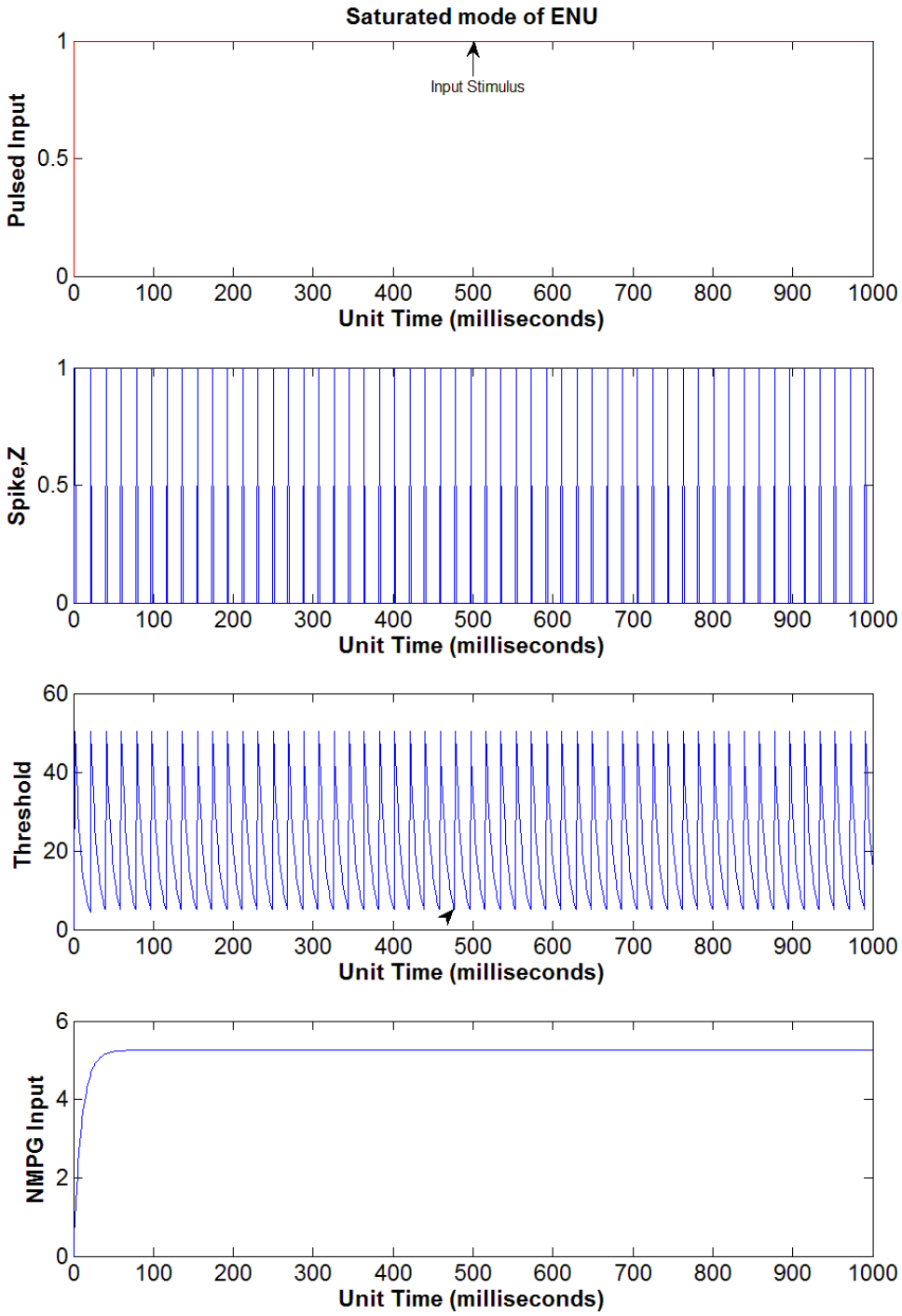

Figure 1.11. Snapshot of Figure 1.8d (Saturated mode) demonstrating that wide pulse inputs (top plot) cause the soma input (bottom plot) to have a DC-like feature. If this soma input satisfies the condition $V \geq \Theta$, then the soma threshold keeps oscillating (arrow head in third plot) above its resting (Θ_o) value. For a chosen set of parameters this means that the ENU produces a maximum number of spikes (second plot) during the total stimulus interval. In the case above, 53 spikes in 1 second of stimulus.

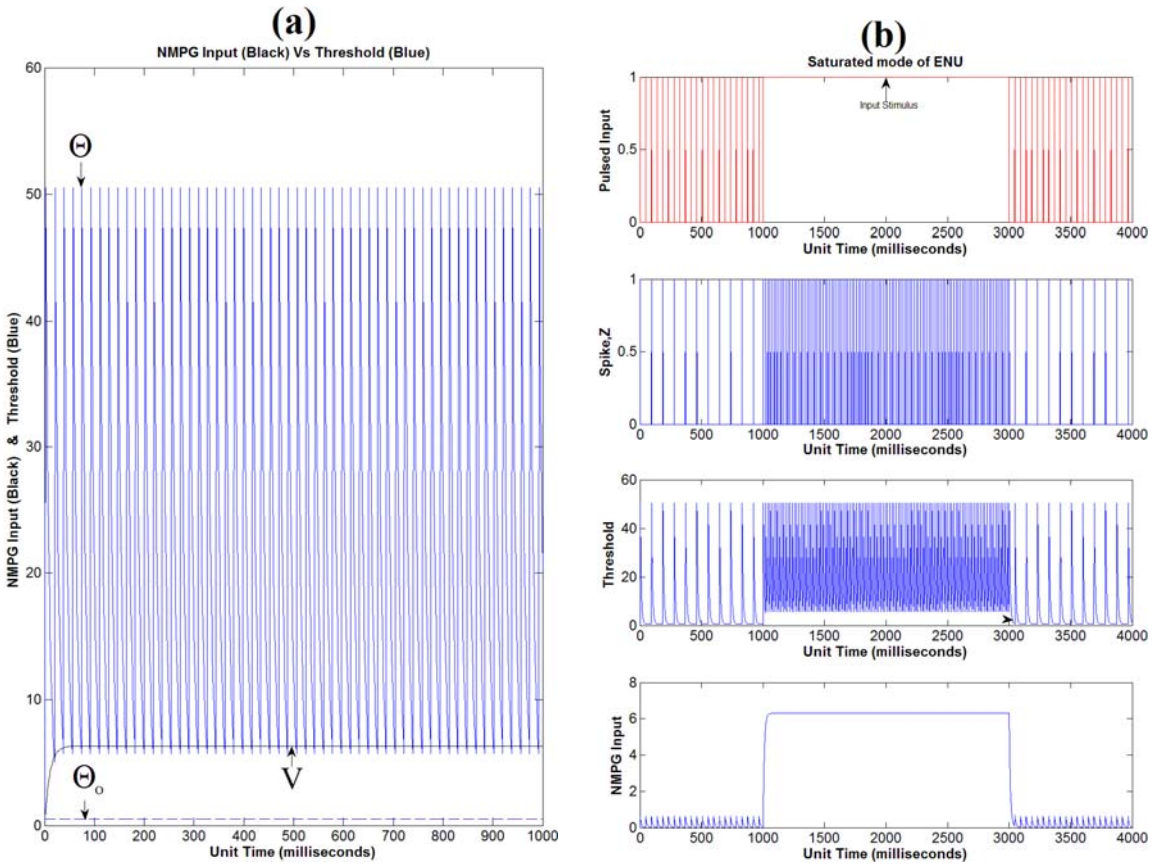

Figure 1.12. Plots for analysis of the saturated mode in a single ENU.

(a) Soma input and threshold (of Fig.1.11) in a single plot. This view demonstrates that the threshold (Θ) never reaches its resting value (Θ_o), rather Θ oscillates with its base as the V level.

(b) Plot for case when ENU receives standard input pulses (top) in the first and last seconds but a single pulsed input for the middle three seconds. During standard input pulses, the ENU is in high-pass mode but gets into saturated mode (second plot) as soon as the DC plateau is large enough (third plot). But as soon as the input reverts back to standard pulse the ENU goes back to high-pass mode. This is because the feeding field output and hence the soma input (bottom) decays back from the plateau. This means that the soma threshold (Θ) now has the opportunity to return to Θ_o (arrow, third plot). If the ENU instead receives impulsive volley inputs at inter-spike interval T, V will build up a DC plateau maximum equal to $\frac{1}{\mathrm{T}}\sum_{\forall j} w_{ff_j} \cdot F_j^{inputs}$. This figure mimics the effect of such a plateau. For biological ranges of T/τ, however, the plateau will be

$$\frac{\sum_{\forall j} w_{ff_j} \cdot F_j^{inputs}}{\mathrm{T}} \quad \frac{e^{-\mathrm{T}/\tau}}{1-e^{-\mathrm{T}/\tau}} \quad < \quad \frac{\sum_{\forall j} w_{ff_j} \cdot F_j^{inputs}}{\mathrm{T}} .$$

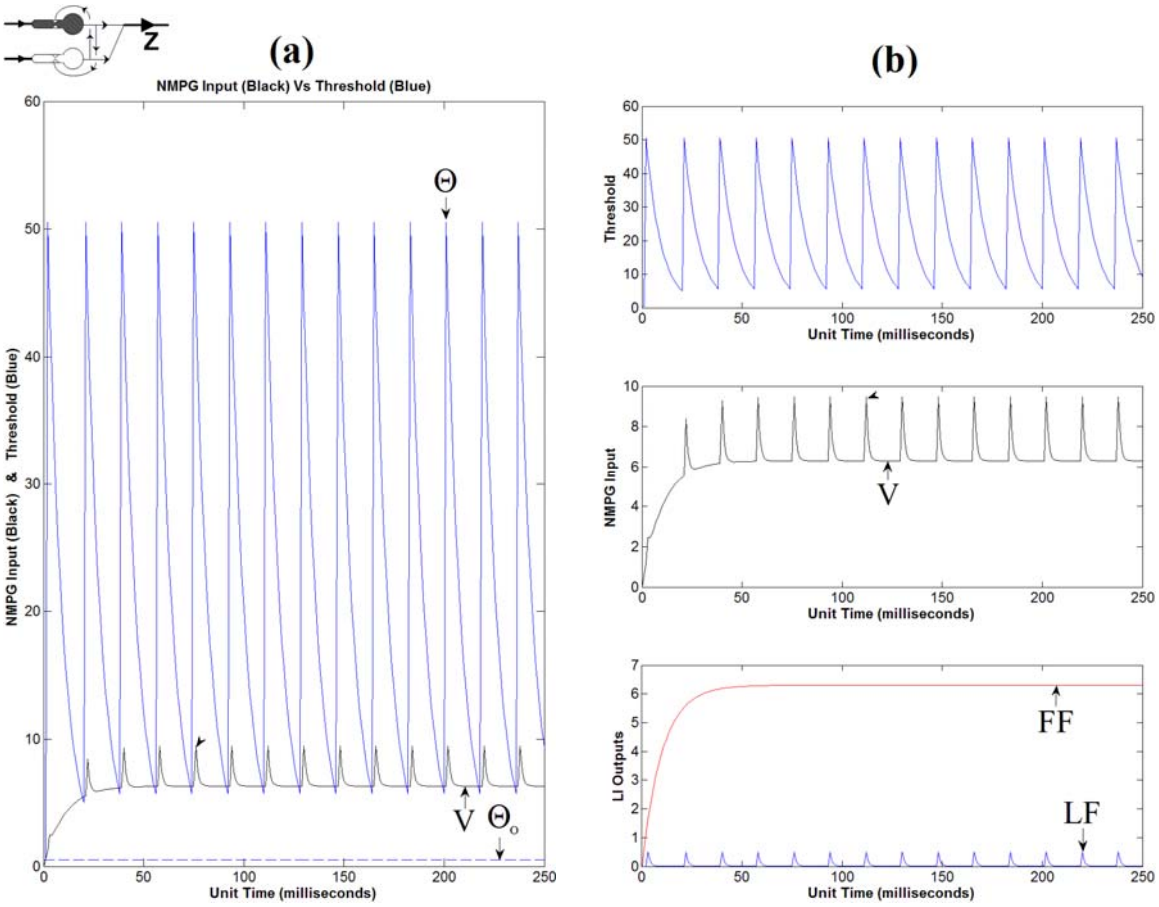

Figure 1.13. Plots for analysis of the saturated mode in a single ENU (shaded ENU, inset) when two ENU are connected via their linking fields.

(a) Soma input and threshold in a single plot. The soma input (V) unlike Figure 1.12a has a saw-tooth like feature (arrowhead). However the threshold (Θ) still never reaches its resting value (Θ_o) and oscillates around the base of the V saw-tooth.

(b) Plot shows the source of V seen in (a). The bottom figure shows that the saw-tooth feature of V (middle) is caused by the outputs (LF) from linking-field leaky-integrator (LFLI) and the plateau of V by the outputs (FF) from feeding-field leaky-integrator (FFLI).

With all these possible firing modes and the nonlinear behavior of the ENU one can see how this demonstrates the versatility of the ENU as a population neuron model. For instance, all-pass mode only ENU would be disadvantageous over other models, say I&F model due to the relatively complicated equations governing all-pass mode of an ENU

[Wells 2010, Ch.9]. However, high-pass mode ENU's in a network produce a phenomenon where the ENU spiking from each successive layer decreases resulting in an evanescent wave-like packet (Fig. 1.14). This phenomenon is consistent with brain signal processi-ng and hence can be implemented to test Malsburg's "binding" theory [Malsburg 1999].

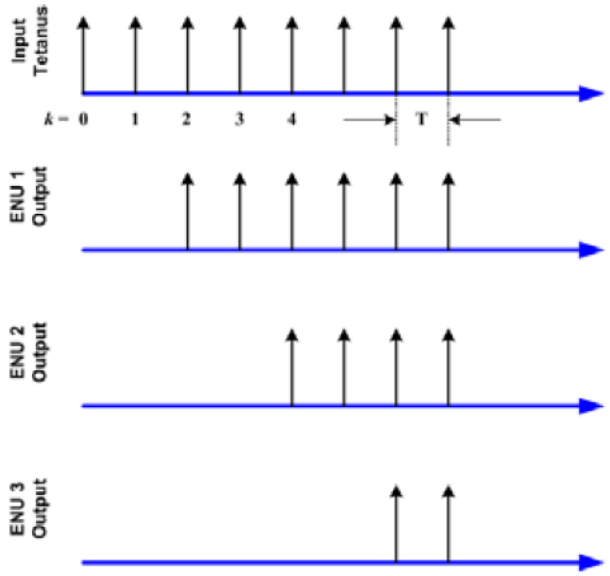

Figure 1.14. Illustration adopted from [Wells 2010, Ch.9] showing a simple ENU high-pass firing chain for a network consisting of three one-dimensional layers of neurons. The neural outputs from the end receiving stimulus to the third neural layer end demonstrate evanescent wave-like packets.

It was mentioned earlier that the terms "dendrite" and "soma" used for the ENU compartments do not correspond to those of biological neuron. There have been evidences to support the view that the ENU proxies for neuron pools [Wells et al. 2006]. Thus ENU outputs represent properties of a neuron pool or neuron population comprising hundreds to thousands of biological neurons. Freeman [Freeman 1972] defines "neuron population" as set of densely interconnected neurons with common input and same sign output. He further defines "aggregates" as neural mass with common input but zero

functional connection density even if anatomical connections exist within it.

In conclusion, the ENU differs from the integrate and fire (I&F) model [Burkitt 2006a, 2006b], another proxy neuron population model, primarily because the ENU incorporates refractory mechanisms and a variable threshold. However with respect to these general properties of the ENU, there are other model neurons/neuromimes [MacGregor & Lewis 1977]. What differentiates the ENU from these other models is the presence of linking-field part of the dendrite component modulating the feeding-field output.

Current APCNN's are designed for engineering applications, particularly image processing and hence these networks depart from biological plausibility. For instance, the PCNN's designed with ENUs produce wave-like firing action across the network (called auto-waves) via its linking-field connections, with each network representing a pixel [Johnson & Ritter 1993, Johnson 1994]. These networks are usually not connected with each other. Even some PCNNs that claim to be physiologically motivated [Broussard 1997] implement mathematical functions and techniques that diverge from biological plausibility. That is, it employs techniques or short-cuts to decrease the amount of computation for real-world engineering application. These arguments, in addition to the SR approach using model-reference principle employed here, let us to believe that the APCNN developed in this thesis is closer to biology than the current APCNNs.

CHAPTER 2

Approach to the problem

The principal approach to the problem is to compare and hence match the performances of a pulse-coded neuron (PCN) based network (PCNN, pulse-coded neural network) with an adaptive network. There is currently no physiologically plausible algorithm for an adaptive pulse-coded neural network (APCNN). Hence two models of different representations (phenomenological and physiological) were taken. A model developed by Grossberg was chosen for the phenomenological representation. For the physiological representation, a network comprised of PCN's was developed using Grossberg's method of minimal anatomies [Grossberg 1971, 1972a]. Grossberg's network is inherently adaptive while the PCNN is not. Comparing performances of the two networks using Grossberg's network as the reference, parameters within the PCNN may be tuned to achieve an APCN. This approach belongs to the class of adaptation methods known as model reference adaptation. It is conjectured that success in achieving a model reference APCNN could lay the groundwork for future development of PCNN adaptation by actor-critic methods [Werbos 1992].

Grossberg's Dipole Network

The phenomenological representation of brain function developed by Grossberg (Fig. 2.1) grossly models the scale of functional magnetic resonance imaging (fMRI) activity. This model was first introduced by Grossberg in a 1972 paper [Grossberg 1972b]. The model, due to its ability to either exhibit excitatory or inhibitory signal output depending upon the input can be considered a dipole network (G-DN, Grossberg's Dipole Network).

It should be noted that though the G-DN has nodes with connections resembling neuron to neuron connectivity, the activities from each node and synaptic weights represent a collective/population outcome. Figure 2.2 shows the G-DN implemented in this thesis. The G-DN used in the thesis is the same but with some change in notation and language. For instance, tonic and shock inputs are called bias and drive input respectively for a more general application of the input terminology, i.e., bias and drive inputs for both G-DN and PCNN.

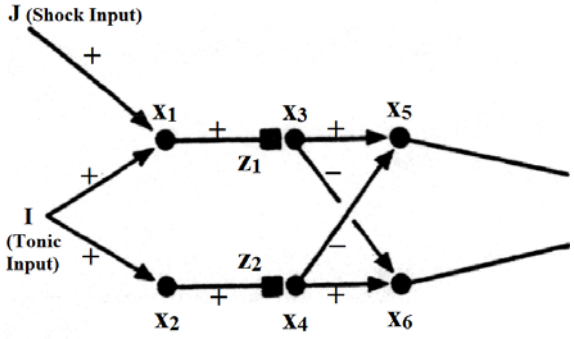

Figure 2.1. Dipole network of 6 nodes adopted from Grossberg's 1972 paper [Grossberg 1972b] receiving tonic (I) and shock (J) inputs. All the arrows represent excitatory (+) connection except for cross-inhibitory connection arrows from 3rd to 6th node and 4th to 5th node. x_i represents the activity of i^{th} node while z_i represent weights (elastic weights) for the respective elastic connections (x_1 to x_3 & x_2 to x_4). Note that for the elastic connection the arrow-heads are replaced by boxes. For the network to be a dipole network one of the last two node outputs (either x_5 or x_6) is excitatory while the other is inhibitory.

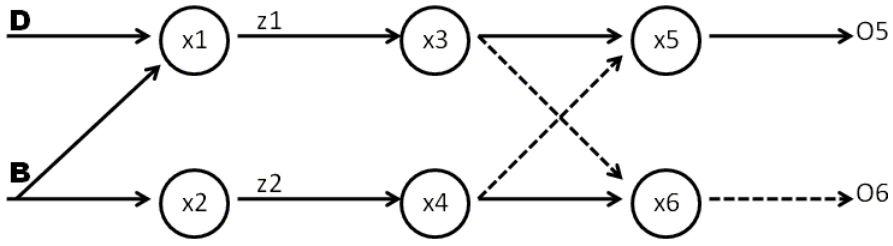

Figure 2.2. Dipole network used. The network remains same as in Figure 2.1 with minor change in description convention. Tonic input (I) is replaced by bias (B) and shock input (J) by drive (D). Solid lines represent excitatory connection while dashed lines represent inhibition. For the G-DN used in the thesis, node five activity (x5) leads to excitatory output (O5) while x_6 leads to inhibitory output (O6).

The equations for the G-DN (Fig. 2.2) are,

$$\dot{x}_1 = -\alpha \cdot x_1 + B + D, \quad (1)$$

$$\dot{x}_2 = -\alpha \cdot x_2 + B, \quad (2)$$

$$\dot{z}_1 = \beta \cdot (\gamma - z_1) - \delta \cdot [x_1(t-\tau) - \Gamma]^+ \cdot z_1, \quad (3)$$

$$\dot{z}_2 = \beta \cdot (\gamma - z_2) - \delta \cdot [x_2(t-\tau) - \Gamma]^+ \cdot z_2, \quad (4)$$

$$\dot{x}_3 = -\varepsilon \cdot x_3 + \zeta \cdot [x_1(t-\tau) - \Gamma]^+ \cdot z_1, \quad (5)$$

$$\dot{x}_4 = -\varepsilon \cdot x_4 + \zeta \cdot [x_2(t-\tau) - \Gamma]^+ \cdot z_2, \quad (6)$$

$$\dot{x}_5 = -\omega \cdot x_5 + \kappa \cdot [x_3(t-\sigma) - x_4(t-\sigma)]^+, \quad (7)$$

$$\dot{x}_6 = -\omega \cdot x_6 + \kappa \cdot [x_4(t-\sigma) - x_3(t-\sigma)]^+, \quad (8)$$

$$O_5 = \lambda \cdot [x_5 - \Omega]^+, \quad (9)$$

$$O_6 = \lambda \cdot [x_6 - \Omega]^+. \quad (10)$$

with parameters; $\alpha = 3$, $\beta = 1$, $\delta = 2/3$, $\gamma = 3$, $\varepsilon = \omega = 4$, $\zeta = 4/3$, $\kappa = 1$, $\lambda = 32$, $\Gamma = 1/2$ and $\Omega = 0$. Stimulus B (bias) is either 2 or 0 and D (drive) either 1 or 0. The model was simulated (Matlab®) using Euler's method for the difference equation given above with an increment Δt of 0.01, hence $\Delta t = t - \tau = t - \sigma$. The Heaviside extractor activation function $[H]^+$ is given by, $[H]^+ = \begin{cases} H, \text{ if } H > 0 \\ 0, \text{ if } H \le 0. \end{cases}$

The network G-DN receiving only bias (B) input (tonic input) gives no output due to the equal strength of excitatory and inhibitory (cross-inhibition) inputs into the last two

nodes, five and six (Eqns. 7 & 8). However with the addition of drive (D) input into one of the first two nodes (node-1 in Fig. 2.2) this balance is altered. That is, node-4 with lesser activity (than node-3) sends an inhibitory output into node-5 that is weaker than the excitatory input from node-3. This is reversed for node-6. Hence node-5 shows activities during dual (B & D) stimuli while there is no activity in node-6. But as soon as the D-stimulus is removed and the network reverts back to receiving only B-stimulus, activity in node-6 occurs for a short duration before the last two nodes (node-5 & node-6) have no activities due to above reasons (mutual inhibition). This is known as rebound phenomenon caused by the elastic z_i weights (Eqns. 3 & 4), a short-term memory-like effect. The above described behavior of the dipole network is shown in Figures 2.3 and 2.4.

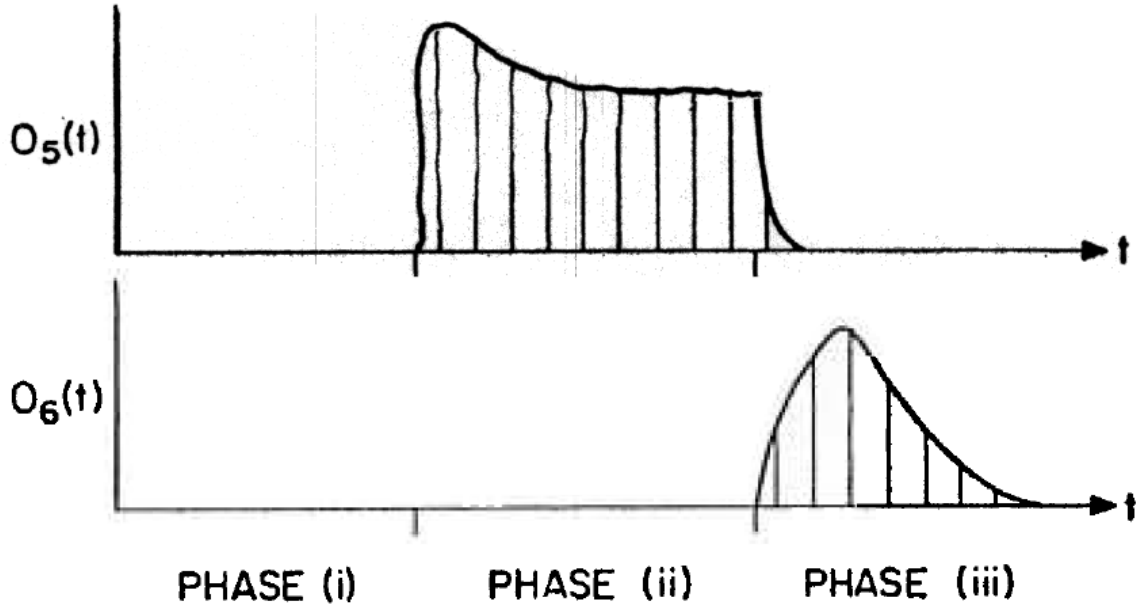

Figure 2.3. Persistent suppression and transient positive/rebound response to shock as seen in O_6 activity trace, following Grossberg's analysis of equations (1 to 10). Phase (i) & (iii) are when network receives only tonic (or bias) input while phase (ii) has the addition shock (or drive) input. The figure is taken from Grossberg's 1972 paper [Grossberg 1972b].

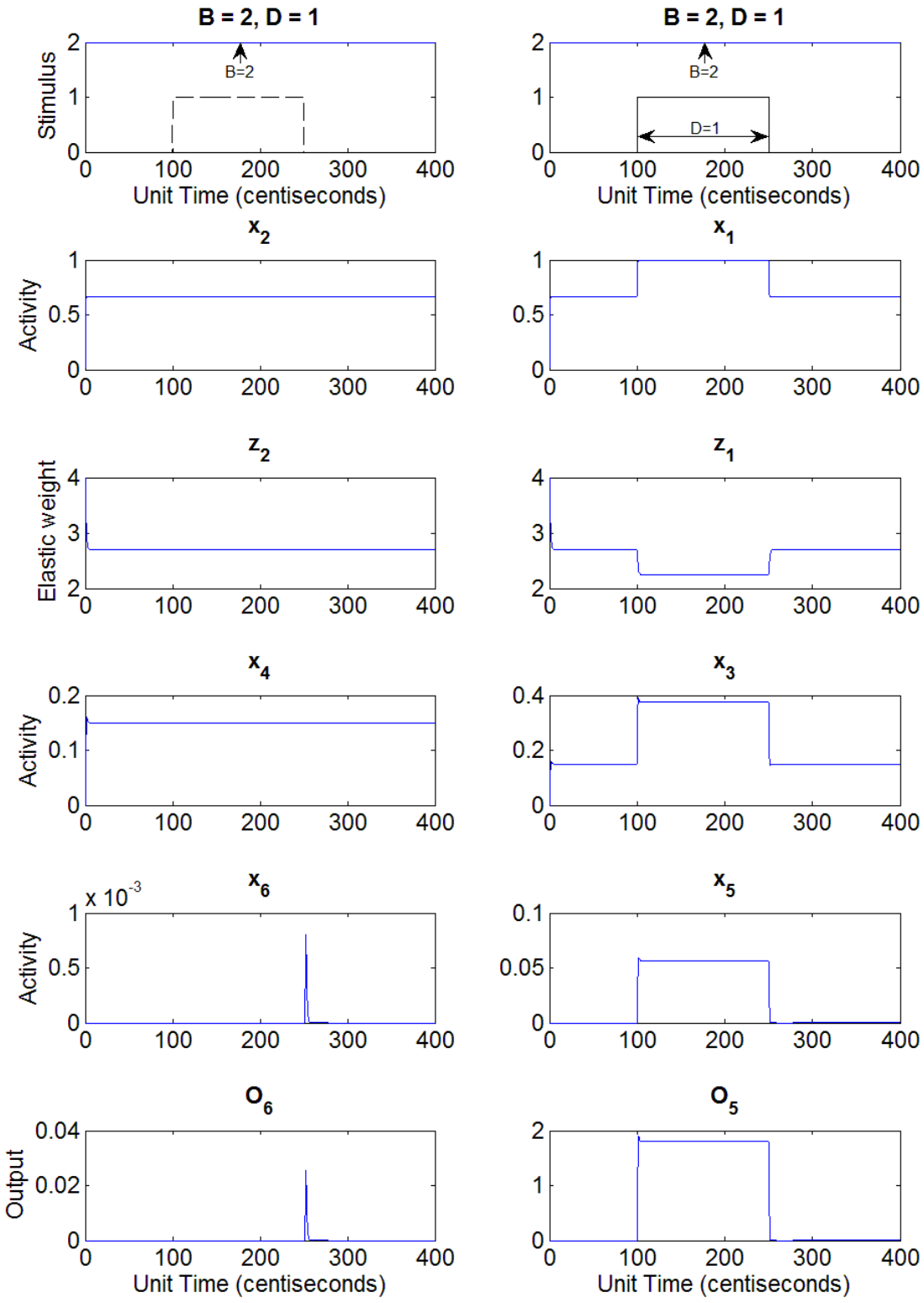

Figure 2.4. Simulation (time-step, $\Delta t = 0.01$) of G-DN from equations (1 to 10) shows the persistent suppression & rebound response seen in Figure 2.3.

Adaptation in Grossberg's Network

The dipole network (G-DN) with an additional sensory input sends outputs to the motor (M) node. This constitutes the Grossberg network (G-N) as shown in Figure 2.5. The adaptation of the network (G-N) takes place by adjusting the connection strengths (weights) between sensory input and nodes within the G-DN.

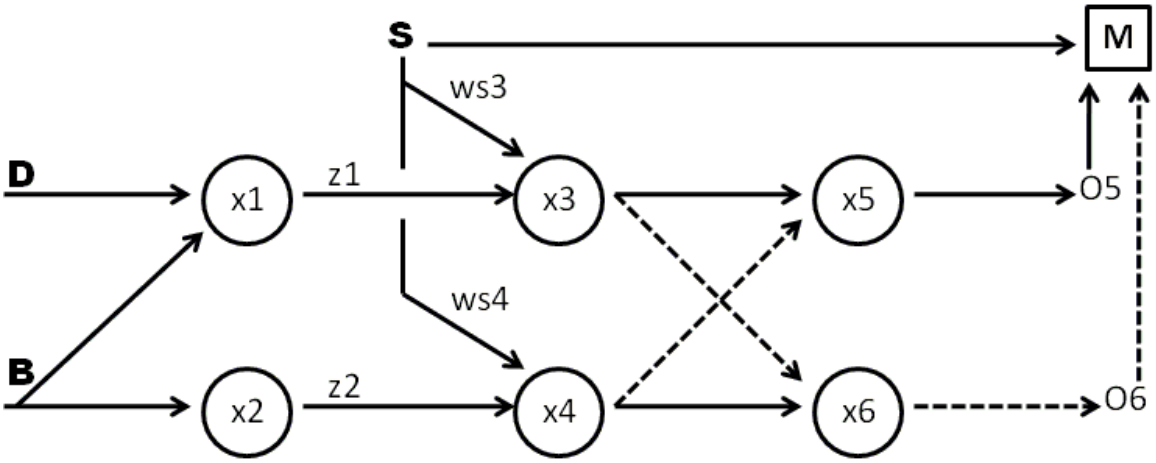

Figure 2.5. G-DN with sensory (S)/conditioning stimulus connected to x3 & x4 by respective synaptic weights (w_{s3} & w_{s4}) which are adaptive. The outputs from the dipole network in addition to the sensory stimulus are the inputs for the motor node (M). This configuration is called the Grossberg network, G-N. (Solid line: excitatory & Dashed line: inhibitory connection).

Activity of the M-node is a reflection of unconditioned response (UR) with unconditioned stimulus (US, Drive: D) and conditioned responses (CR) with conditioned stimulus (CS, post-learned Sensory: S).

The mathematical description of the G-DN was based on functionals [Grossberg 1972c] rather than functions. That is, the original G-DN did not present a long-term adaptive function. However, recent works by Hill and Wells [Hill et al. 2009] have shown that incorporating Grossberg's outstar rule based on Hebb's principle [Hebb 1949] can make the G-DN stably adaptive. However their rule required some alterations for the network used in the thesis. The modified version of the rule implemented in G-N is

$$\dot{w}_{ji} = -\upsilon_{ji} \cdot w_{ji} + \eta \cdot [s_j - \Gamma_s]^+ \cdot [x_i - \Gamma_o]^+, \qquad (11)$$

$$\dot{\upsilon}_{ji} = -\varphi \cdot \upsilon_{ji} + \rho \cdot [s_j - \Gamma_\upsilon]^+ + \rho' \cdot [x_h - \Gamma_{\upsilon'}]^+ \cdot (s_j - \Gamma_\upsilon)_0^1, \qquad (12)$$

with parameters; $\eta = 4.4$, $\Gamma_s = 1/2$, $\Gamma_o = 0.35$, $\Gamma_\upsilon = 0.79$ and $\Gamma_{\upsilon'} = 0.67$. The notation is such that x_i is the activity of the node whose synaptic connection with the sensory node is being adapted and x_h is the activity of the preceding node within the G-DN elastically connected to i^{th} node. Sensory input s_j is either 0.8 or 0 and the weight values w_{ji} are constrained such that $0 \leq w_{ji} \leq 0.5$. Note that presence of the very fast function, $\dot{\upsilon}_{ji}$ causes $\dot{w}_{ji}$ to retain its values (i.e., learns). For reasons of computation, υ_{ji} being a very fast function simulation was done by considering $\dot{\upsilon}_{ji} = 0$, i.e., υ_{ji} reaches steady-state very fast. The equation used in the simulation instead of equation (12) is,

$$\upsilon_{ji} = c \cdot [s_j - \Gamma_\upsilon]^+ + c' \cdot [x_h - \Gamma_{\upsilon'}]^+ \cdot (s_j - \Gamma_\upsilon)_0^1 \qquad (13)$$

with parameters, $c = 0.03$ and $c' = 1$ with Heaviside step function, $(S)_0^1 = \begin{cases} 1, \text{ if } S > 0 \\ 0, \text{ if } S \leq 0 \end{cases}$.

In the Grossberg's network implemented for the thesis, the middle nodes (node-3 & node-4) receive sensory inputs (Fig. 2.5) whose synaptic connections are determined by equations (11) and (13). Thus, $j = s$ and $i \in \{3, 4\}$, implying each node (node-3 & node-4) have equations (11) and (13). This means that equations (5) and (6) are replaced by

$$\dot{x}_3 = -\varepsilon \cdot x_3 + \zeta \cdot [x_1(t - \tau) - \Gamma]^+ \cdot z_1 + \sum_{j=1}^{n} w_{j3} \cdot s_j, \qquad (5')$$

$$\dot{x}_4 = -\varepsilon \cdot x_4 + \zeta \cdot [x_2(t - \tau) - \Gamma]^+ \cdot z_2 + \sum_{j=1}^{n} w_{j4} \cdot s_j. \qquad (6')$$

Finally, the motor (M) node receives inputs from the sensory and dipole network outputs. This is expressed as,

$$M = \mu \cdot [(s_j + O_5 - O_6) - \Xi]^+, \qquad (14)$$

with parameters; $\mu = 1$ and $\Xi = 1$. Note that the overall behavior of the G-N network is defined by the M-node activity. That is, M-node activity occurring during B and D-stimulus is called the unconditioned response to unconditioned stimulus (D-stimulus) while M-node activity during B and S-stimulus after conditioning (learning) is called conditioned response to condition stimulus (S-stimulus).

Simulation of the G-N shows the long-term adaptive property (or just adaptive property) of the network (Fig. 2.6, 2.7 & 2.8). Immediately after the learning phase (when all B, D and S-stimulus are given) the network remains learned, although there is a small decrease in adapted weight value (≈ 0.3 % of peak). It should be noted that learning occurs during simultaneous conditioning and delay conditioning paradigms [Balkenius 1995] but not with trace or backward conditioning. This is because the connection assumed in the G-N follows Hebbs's cell-assembly theory [Hebb 1949].

Finally, Figure 2.9 shows that the behavior produced (M-node activity to S-stimulus) and the association between condition and unconditioned stimulus eventually gets extinguished. This overall adaptive property of the G-D network can then be taken as a reference to achieve an adaptive PCNN (APCNN) that is psycho-neurologically feasible.

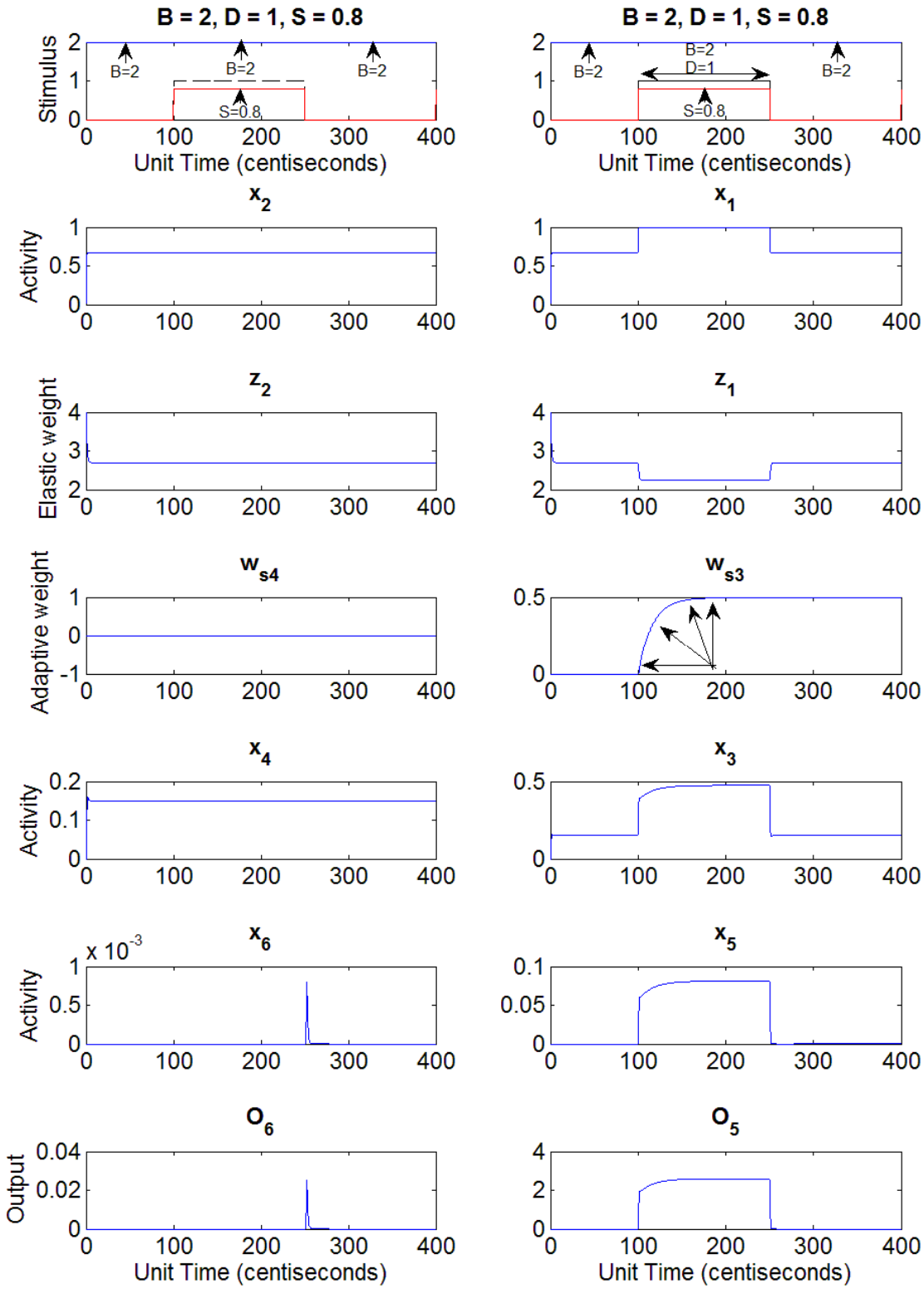

Figure 2.6. Simulation (time-step, $\Delta t = 0.01$) of G-N (Eqns:1 to 4, 5', 6', 7 to 11 & 13) shows learning (cartwheel arrows) in the network, i.e., rise of w_{s3} strengthening the connection in part of network during association of S to D stimulus.

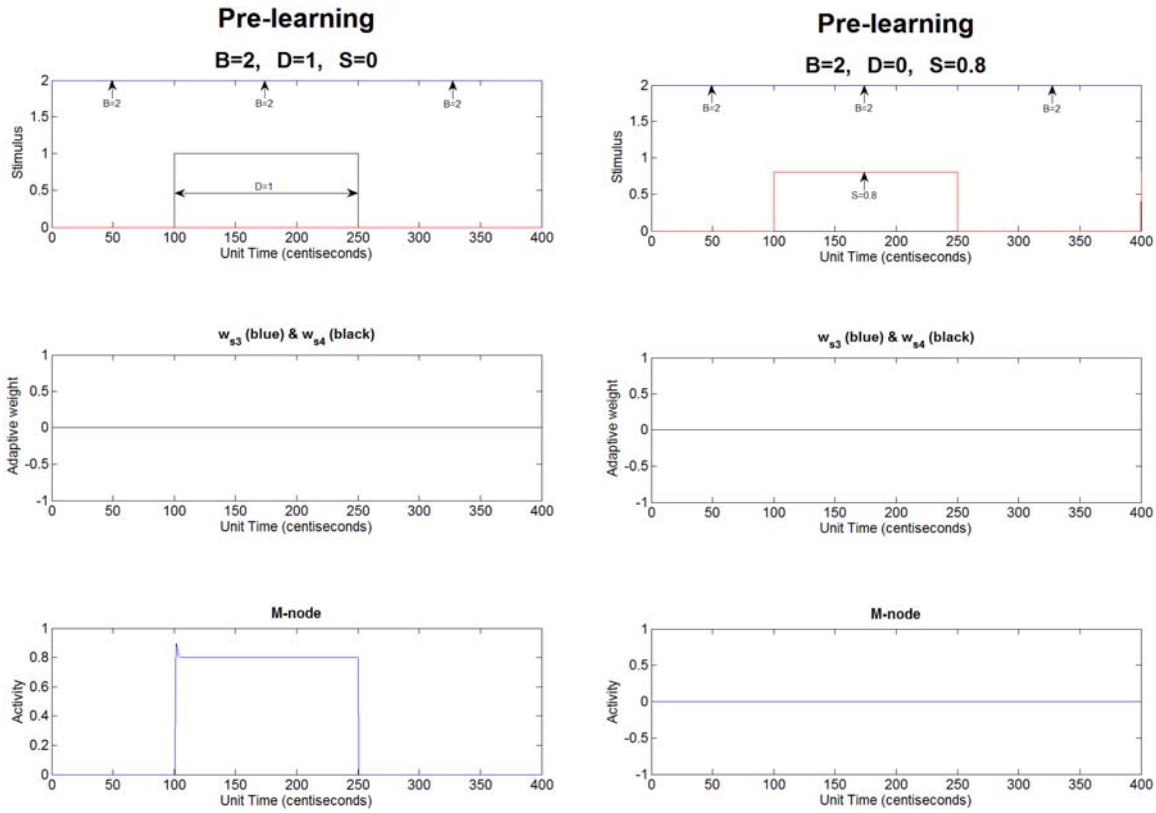

Figure 2.7. Simulation (time-step, $\Delta t = 0.01$) of G-N (Eqns: 1 to 4, 5', 6', 7 to 11 & 13) shows network behavior prior to learning/conditioning.

Left: M-node activity (bottom) during B & D stimulus (top) representing unconditioned response to D-stimulus. No learning takes place (middle).

Right: prior to conditioning and hence before association process between conditioning (S) stimulus and unconditioned (D) stimulus there is no M-node activity (bottom) with S-stimulus.

In both cases w_{s3} and w_{s4} remains zero, i.e., no learning takes place and hence blue (w_{s3}) and black (w_{s4}) values are overlapping.

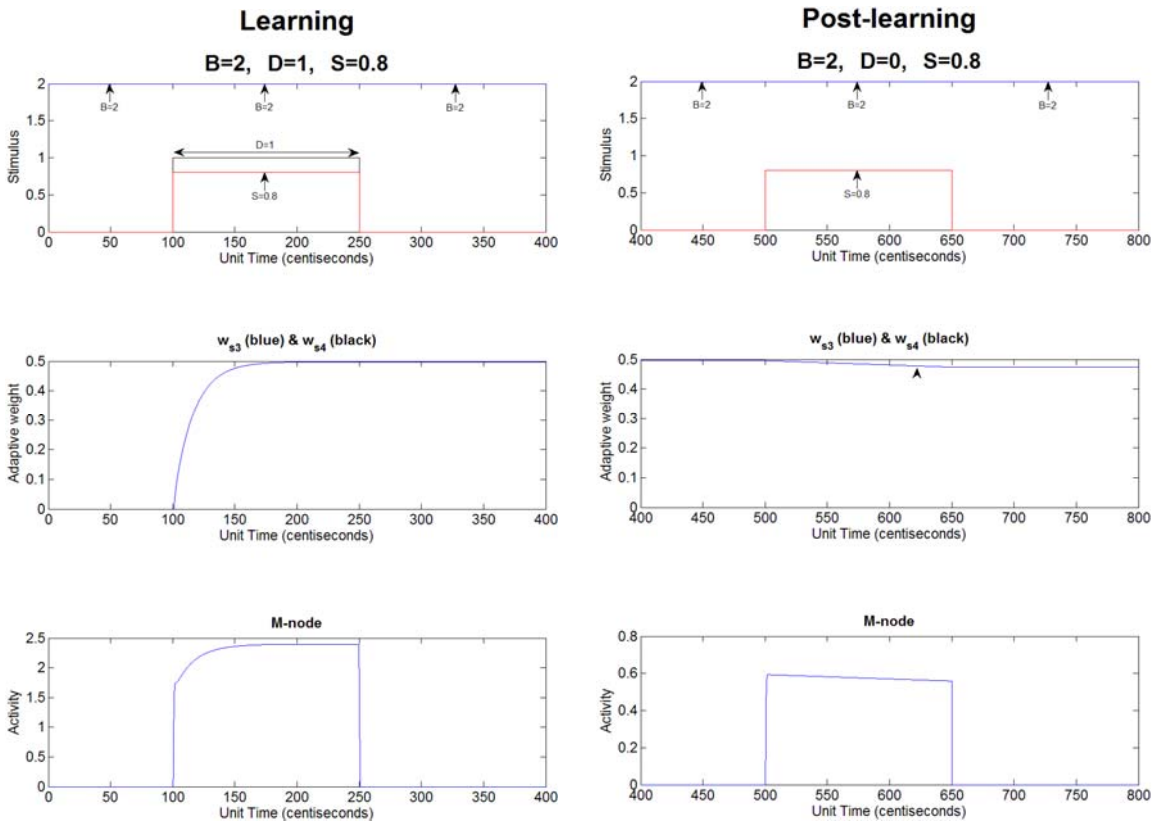

Figure 2.8. Simulation (time-step, $\Delta t = 0.01$) of G-N (Eqns: 1 to 4, 5', 6', 7 to 11 & 13) shows network behavior after learning/conditioning.

Left: M-node activity (bottom) during B, D & S stimulus (top) representing response during the association process of conditioning (S) stimulus to unconditioned (D) stimulus. Learning occurs during conditioning (middle).

Right: after conditioning the conditioned (S) stimulus is capable to inducing a conditioned response (bottom).

During learning (left), w_{s4} remains zero while w_{s3} (blue) connected with the G-DN node (node-3) at the receiving end of all three stimuli (B, D & S) rises.

Post-learning (right) during the duration of condition stimulus (S), w_{s3} (blue) has a very small decrease (arrowhead, middle) from its plateau achieved during learning. This is the consequence of the G-N's use of a Hebbian-class learning rule.

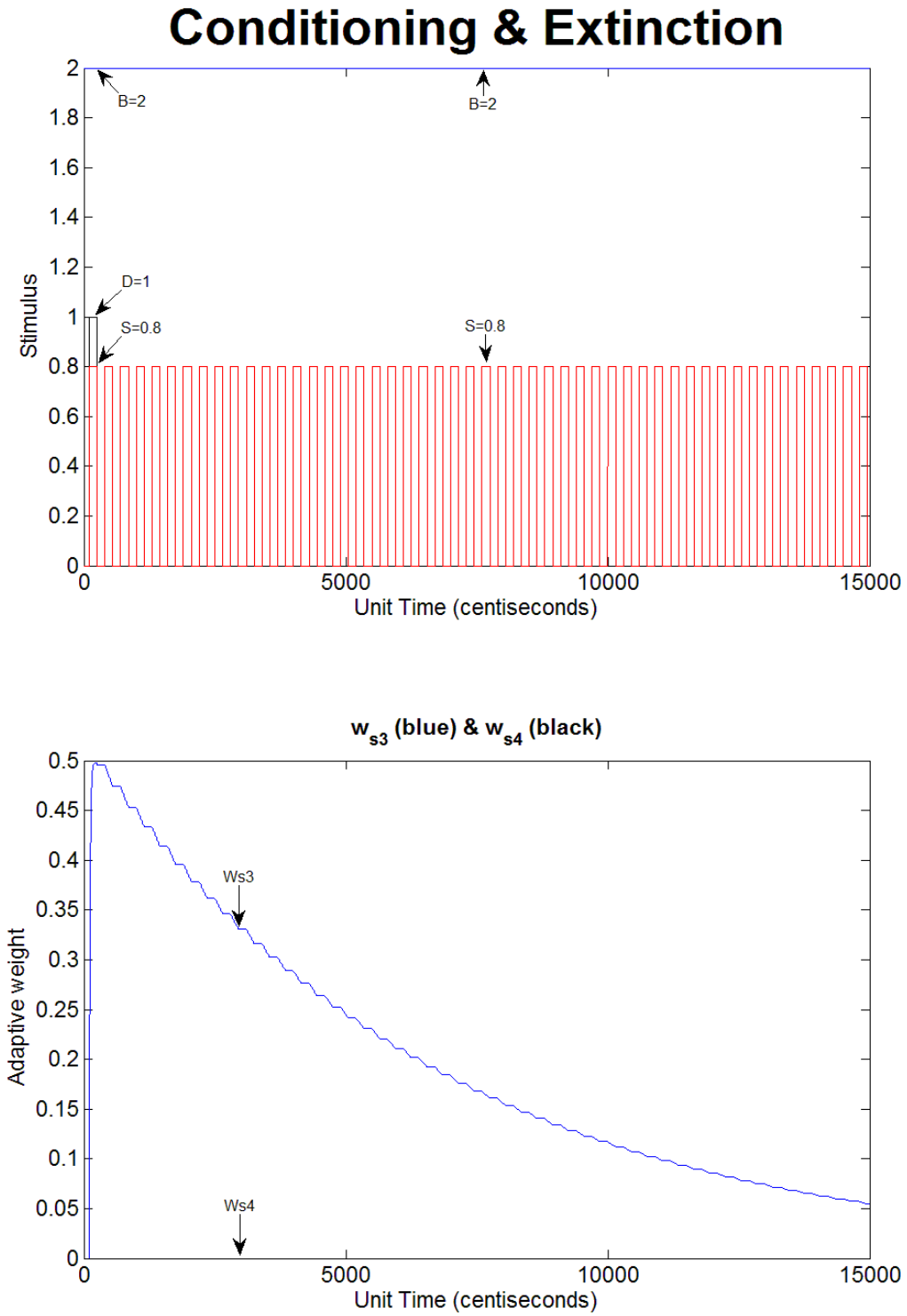

Figure 2.9. Simulation (time-step, $\Delta t = 0.01$) of G-N (Eqns:1 to 4, 5', 6', 7 to 11 & 13) during extinction experiment. First phase (B = 2, D = 1, S = 0.8): establishment of association or learning or conditioning as seen in Figure 2.8 (left). Second phase (intervals of B = 2, S = 0.8): only S (conditioned) stimulus is applied (without unconditioned D-stimulus) extinguishing the developed association ($\downarrow w_{s3}$) with each successive S-stimulus.

Building a PCNN using Eckhorn's model (ENU)

The functional unit used for the PCNN analogue of the G-N is the Eckhorn neuron unit (ENU). The ENU model introduced by Eckhorn et al. [Eckhorn et al. 1990] has been shown to be a population neuron model [Wells et al. 2006]. Figures 1.5, 1.6 and 1.7 show the components of a (i^{th}) basic ENU whose equations are

$$FF_i(t) = FF_i(t-\Delta t)\cdot\exp(-\Delta t/\tau_{ff}) + (1/\tau_{ff})\cdot w_{ff}\cdot\sum_{\forall j} F_j^{inputs}, \quad (15)$$

$$LF_i(t) = LF_i(t-\Delta t)\cdot\exp(-\Delta t/\tau_{lf}) + (1/\tau_{lf})\cdot w_{lf}\cdot\sum_{\forall j} L_j^{inputs}, \quad (16)$$

$$U_i(t) = FF_i(t)\cdot(1 + LF_i(t)), \quad (17)$$

$$V_i(t) = \sum_{\forall i} U_i(t), \quad (18)$$

$$\Theta_{V_i}(t+\Delta t) = \begin{cases} V_{pg}, & V_i(t) \geq \Theta_i(t) \\ \Theta_{V_i}(t)\cdot\exp(-\Delta t/\tau_{pg}), & V_i(t) < \Theta_i(t) \end{cases}, \quad (19)$$

$$\Theta_i(t) = \Theta_O + \Theta_{V_i}(t), \quad (20)$$

$$Z_i(t+\Delta t) = \begin{cases} 1, & V_i(t) \geq \Theta_i(t) \\ 0, & V_i(t) < \Theta_i(t) \end{cases}. \quad (21)$$

Equations (15), (16) and (17) represents dendrite component. The dendrite outputs are summed to become soma input (Eqn. 18). The remaining equations (Eqn. 19, 20 & 21) represent the soma component. The time-step ($\Delta t = 1$) for simulation of PCNN and parameter value are given in the next chapter.

The Eckhorn model (ENU) was chosen over other proxy neuron models particularly the integrate and fire (I&F) model [Burkitt 2006a, 2006b], because it overcomes the

shortcomings of a basic I&F model namely, presence of refractory period (Eqns. 19 & 20), ability to generate bursting response due to the absence of reset functions in an ENU and the capability for synchronous firing without being in all-pass mode (Eqns. 16 & 17). Other models such as Rulkov's model [Rulkov 2002] and the Hodgkin-Huxley model [Hodgkin & Huxley 1952] though biologically more realistic than the ENU were not chosen for developing the PCNN because of the complications in choosing the parametric values or because of greater computational cost. The design process for developing the ENU based network analogue of a G-DN is discussed first and then it's behavior in the following two chapters.

Incorporation of the adaptive property of G-N to achieve APCNN

The property of an adaptive G-N can be incorporated into the E-N using the adaptation scheme called performance feedback adaptation [Widrow & Stearns 1985]. In this schema the M-node activity of G-N is taken as the reference performance for the M-node spikes of E-N to achieve (match). That is, the performance reference or desired response is compared with the output of the E-N such that the adjustable variables within the E-N are tuned to achieve an output that closely (minimum error) resembles the desired output (figure 2.10).

Bridging of the two networks (G-N & E-N) requires one of the network outputs to be transformed before comparison between performances. This is because M-node outputs (activities) from G-N represent functional Magnetic Resolution imaging (fMRI) while M-node outputs (spikes) from E-N mimic electro-encephalogram (EEG) readings. Hence different signal types, real signals for G-N and spikes for E-N. With regard to signal analysis the major area where fMRI's and EEG's differ is their temporal resolution.

Temporal resolutions of fMRI's are in seconds while EEG's are in milliseconds [Gazzaniga et al. 2006].

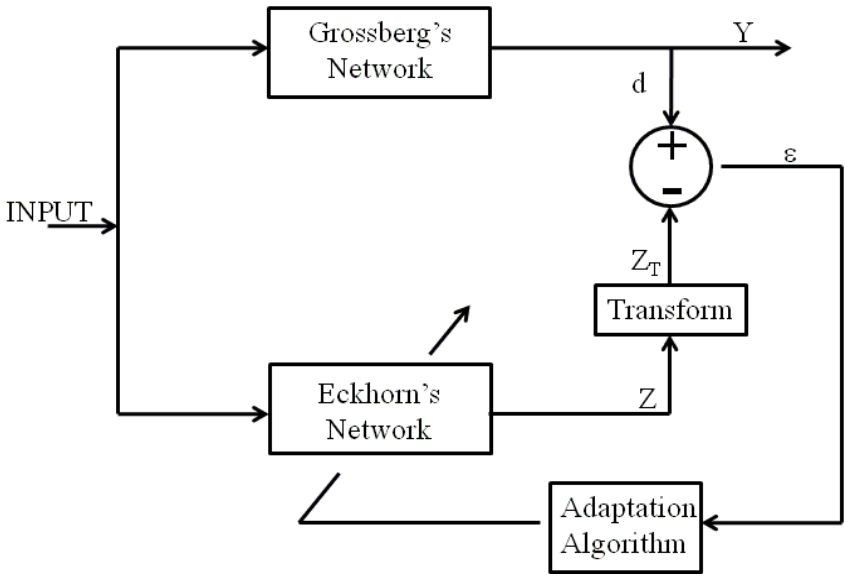

Figure 2.10. Principle approach to the problem. The desired response (d) is the output from Grossberg's network while Z_T is the transformed spike outputs from Eckhorn's. The error between these outputs (ε) is then used by the algorithm to adapt the weights.

Since M-node activity of the G-N is the reference or desired output (d), the M-node spikes of E-N are transformed as shown in Figure 2.11. This transformation is based on the method of moving point averages (MPA) [Whittaker & Robinson 1967]. For performance evaluation the E-N spike signal is transformed as a product of MPA, an arbitrary constant (k=0.5) and the number of basic ENU's (n) within the M-node of E-N (i.e., $Z_T = k \bullet n \bullet MPA$). Hence the transformed E-N outputs (Z_T) can be directly compared with "d".

To our best knowledge, the use of model-reference performance feedback to tune a pulse-coded neural network has not been previously reported. This method is therefore an original contribution of this thesis.

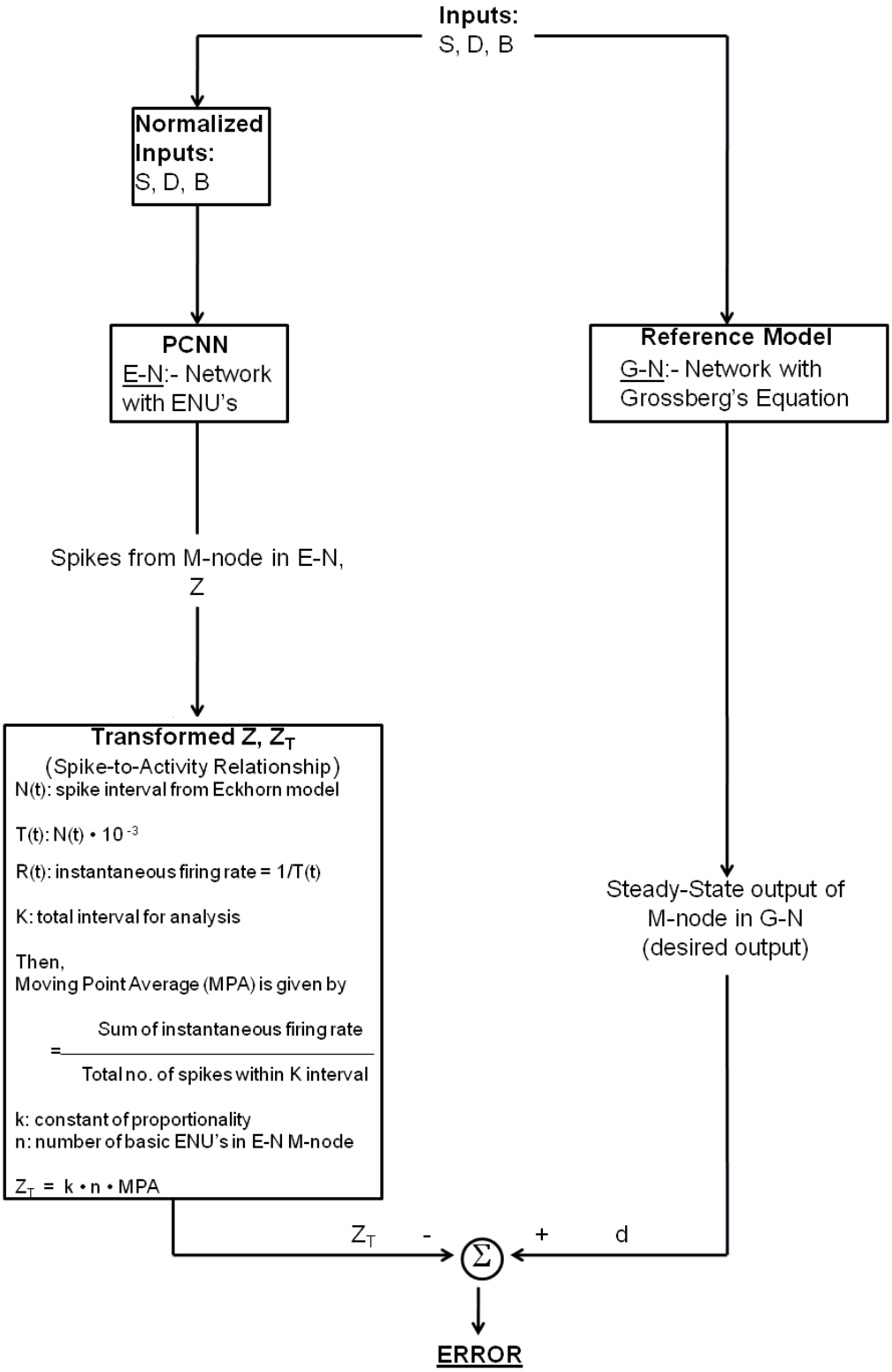

Figure2.11. Approach implemented for obtaining the error needed for measuring the performance. The desired output (d) is taken as the steady-state (single sample) M-node output of G-N. This is then compared with the transformed spike output (Z_T) derived by taking the moving point average (MPA).

CHAPTER 3

Architecture considerations for G-N like network based on ENU's

Chapter Introduction

Almost the entire corpus of current literature on pulse-coded neural networks (PCNN) uses arguments and analyses based on the presumption of steady-state tetanus inputs in which activity level is coded by firing rate. This has a tendency to promote a presumption that PCNN analogs to non-pulsing networks based on level-coding can be obtained by a simple mapping and scaling process of some sort. This assumption can be traced all the way back to Von Neumann [von Neumann 1958].

As this chapter demonstrates, this presupposition is wholly unwarranted. The actual "in vivo" environment of PCNN systems produces a much more diverse set of firing patterns. The function of the network is strongly affected by surprisingly small variations in the firing pattern. This makes functional mapping from traditional neural network systems to PCNN systems much more challenging than has been presumed. The findings reported in this chapter reveal that PCNN functional architecture is a new topic within neural network theory for which there is much yet to be learned.

This chapter presents the detailed step-by-step process through which the final Eckhorn dipole network was achieved. The methodology employed here was first established by Grossberg in 1978 for level-coded neural networks [Grossberg 1978]. Perhaps the most significant lesson learned from this study is: the non-linear effects in PCNN signaling belong to a class of non-linear system theory so unlike older neural network analysis that functional design of PCNN systems should be approached in a two-

step process. First, the functional capabilities should be developed at the G-N network level. Second, the functioning G-N should be mapped to a functionally equivalent PCNN. This chapter illustrates how this was accomplished for dipole network using Grossberg's methodology.

The Direct Network

Before outputs from Grossberg's network (G-N) can be used for performance reference a working Eckhorn dipole network (E-DN) is required. The first goal in the design process will therefore be to achieve an E-DN whose network properties resemble G-DN (Grossberg dipole network). This means G-DN will be the functional model for designing the E-DN.

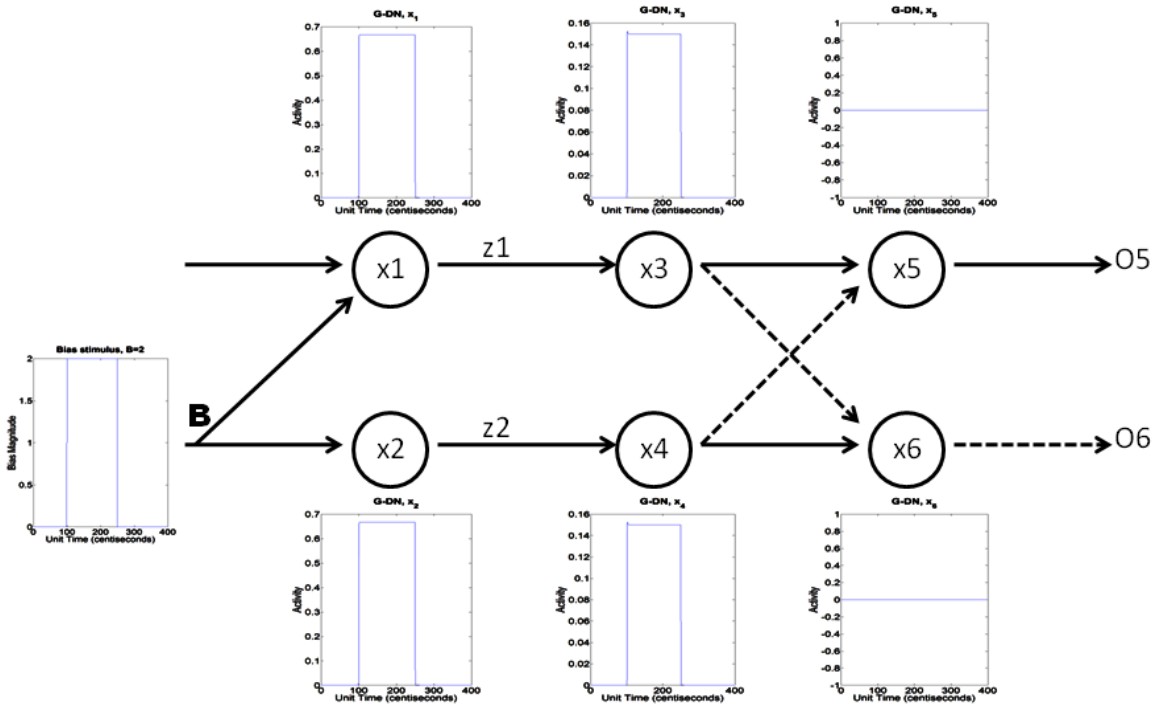

Figure 3.1. G-DN (Grossberg's Dipole Network) receiving just bias (B) stimulus.

We start with G-DN (Fig. 2.2) but with the simplest input-output relationship, i.e., with only bias input (B-input), as shown in Figure 3.1. The initial nodes (x1 & x2) receiving the same stimulus causes excitation of the succeeding nodes, x3 and x4 respectively with equal strength. This leads to cancellation of equal input strengths during cross-inhibition resulting in no activities at x5 and x6 nodes (Fig. 3.2).

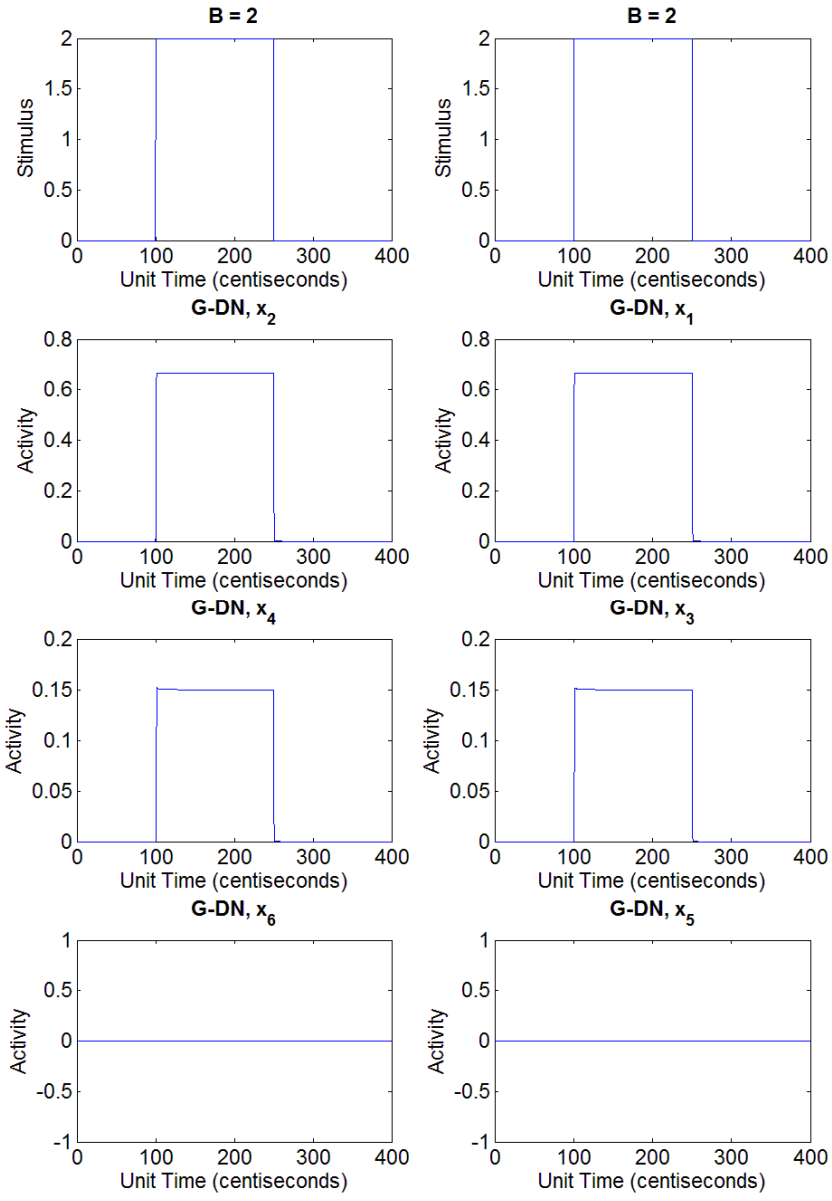

Figure 3.2. Output traces of G-DN in Figure 3.1 (inset) with just B-stimulus showing no activities in x5 & x6 nodes due to cancellation of incoming activities from x3 & x4 of equal strength.

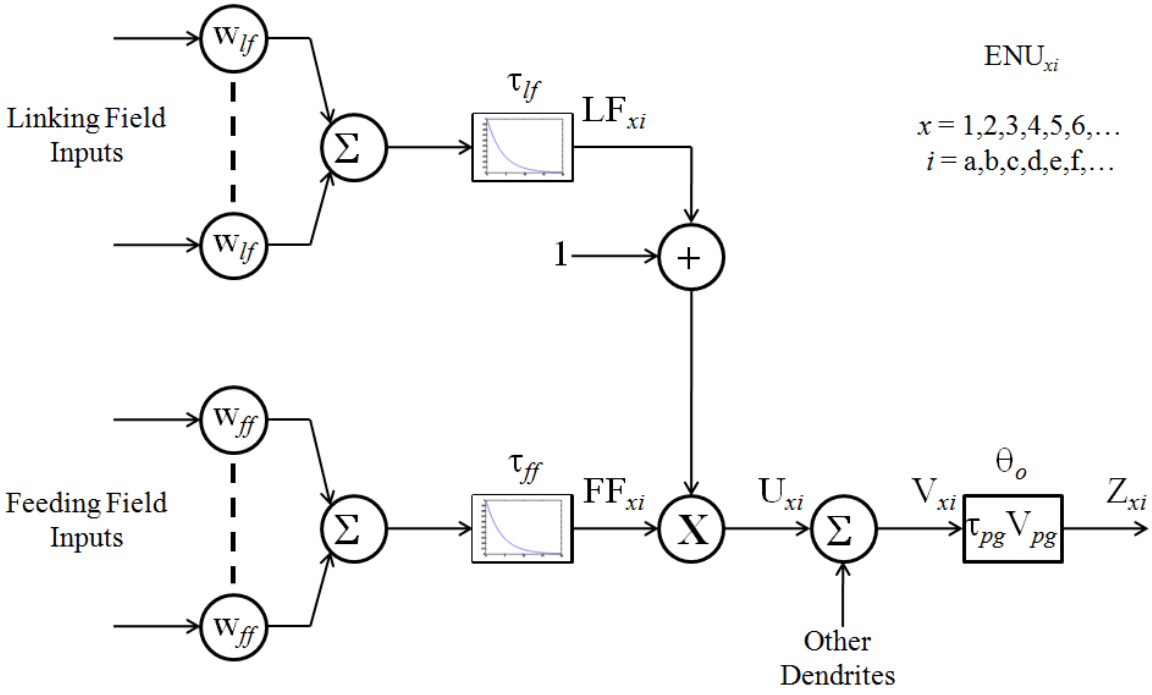

Figure 3.3. Another view of the ENU architecture showing the basic ENU (as seen in Fig. 2.11). Subscript of ENU_{xi} is such that *i* denote one of the basic ENU shown above while *x* denotes the ENU group composed of the basic ENU's. The feeding field input value is either 0 or 1.
Linking field: w_{lf} & τ_{lf} are parameters (weight & time constant) and LF_{xi} the output.
Feeding field: w_{ff} & τ_{lf} are parameters (weight & time constant) and FF_{xi} the output.
Soma/Neuromime Pulse Generator (NMPG): τ_{pg}, V_{pg} & θ_o (time constant, voltage amplitude & threshold offset) and Z_{xi} spike output.

The ENU with basic configuration as shown in Figure 3.3 and with set parameters is required for constructing an E-DN analogue that would have the property as shown in Figure 3.1. The inhibitory input of a basic ENU includes an inhibitory dendrite with just the feeding field (without linking field) whose output is connected to the soma/NMPG by summation with other dendrites outputs. It should also be noted that the basic ENU implemented in the E-DN has a uniform weight value (either w_{lf} or w_{ff}) within the linking field or feeding field of the respective ENU_x group. A node within E-DN may comprise more than one ENU_x group.

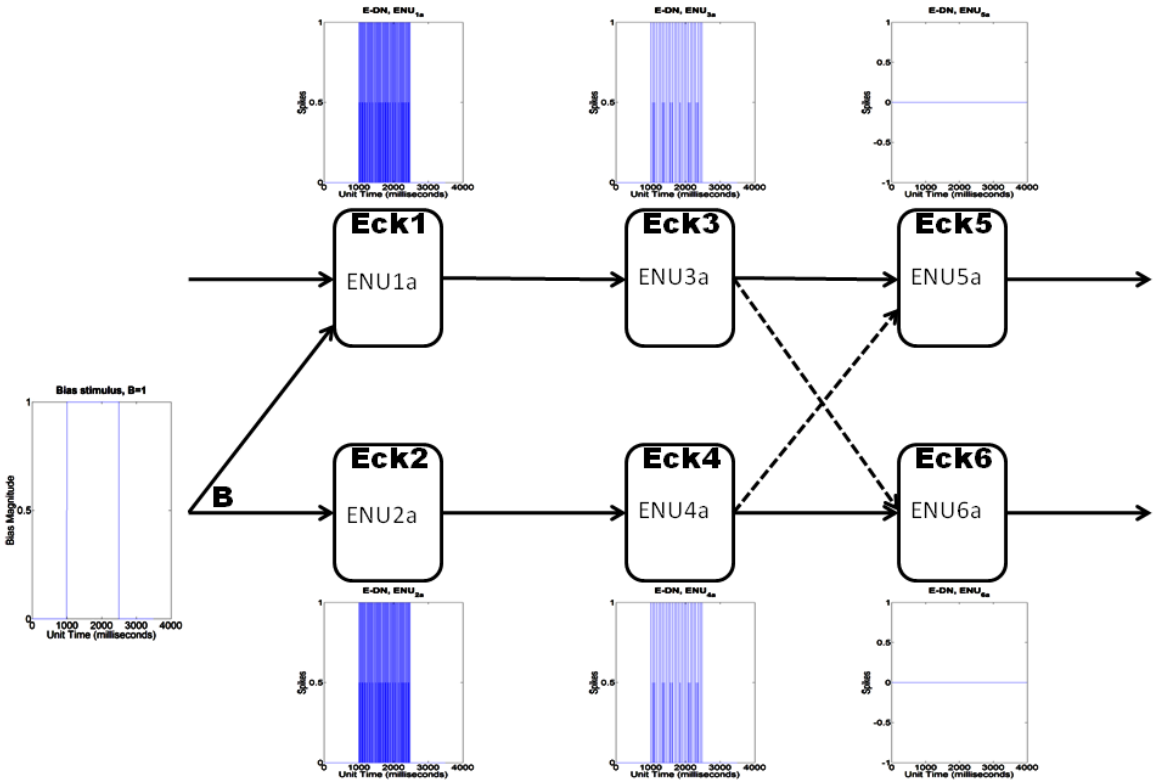

Figure 3.4. E-DN receiving just bias (B) stimulus as an Eckhorn analogue of Figure 3.1. Each node (Eck1 to Eck6) is made up of a single ENU. The figure shows outputs from respective ENU's following simulation with B-stimulus (as DC/constant) during a particular interval (1 to 2.5 seconds). A larger view of these outputs is shown in Figure 3.5. The parameter values of the simulation are shown in table 3.1.

To achieve an Eckhorn analogue of G-DN shown in Figure 3.1, the E-DN constructed (Fig. 3.4) is composed of six nodes each containing 1 ENU group and each group formed by a single basic ENU. Simulation with just B-input results in similar outcome as seen with G-DN where ENU in the node-5 (Eck5) and node-6 (Eck6) do not produce any spikes (outputs in Fig. 3.4 or Fig. 3.5 for larger view). Note that though the neuronal population are PCN's (pulse-coded neurons), to achieve an initial working model of E-DN DC (constant) input stimulus was chosen for simplicity. However, later all bias and drive inputs will be implemented as pulse trains.

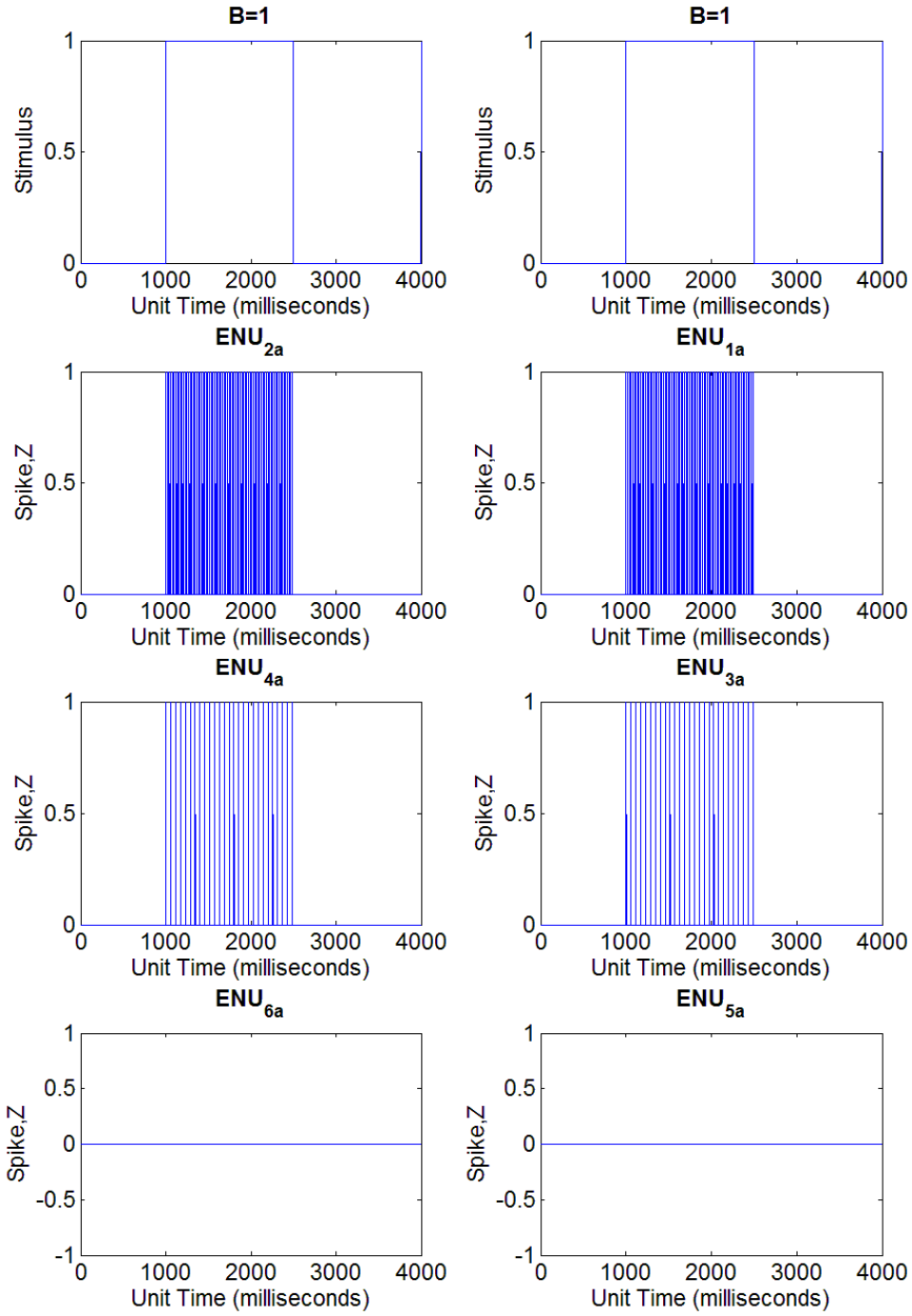

Figure 3.5. Output traces of E-DN in Figure 3.4 (inset) with just B-stimulus showing no spikes in corresponding ENU of fifth and sixth nodes (Eck5 & Eck6).

ENU PART			E-DN Node			
			1 or 2	3 or 4	5 or 6	
			ENU Group			
			ENU_1 or ENU_2	ENU_3 or ENU_4	ENU_5 or ENU_6	
			Basic ENU			
			ENU_{1a} or ENU_{2a}	ENU_{3a} or ENU_{4a}	ENU_{5a} or ENU_{6a}	
Dendrite	Linking Field	w_{lf}	No linking field			
		τ_{lf}				
	Feeding Field	w_{ff}	5	5	$5^{(+)}$	$5^{(-)}$
		τ_{ff}	10	10	$10^{(+)}$	$10^{(-)}$
Soma		τ_{pg}	7.5	7.5	7.5	
		V_{pg}	50	50	50	
		θ_o	0.5	0.5	0.5	

Table 3.1. Parameters used for the simulation (Fig. 3.5) of E-DN architecture shown in Figure 3.4. Parameter values with superscript (+) and (-) indicate values for excitatory and inhibitory connections respectively. Connections for parameter values without any superscript are excitatory by default.

The next step is to replicate the property of G-DN during both drive (D) and bias (B) inputs as shown in Figure 3.6. Unlike the case with just B-input (Fig. 3.1 & 3.2) node x1 receives stronger input stimulus due to the additional D-input and hence stronger stimulus is applied from x3 to x5 (than x4 to x6) with stronger inhibition from x3 to x6 (than x4 to x5) resulting in activity in x5 node but not in x6 (Fig. 3.7). In addition as soon as the network does not get D-input (but continues to receive B-input) there is activity in x6 node for a very short duration before the equally strong inputs from x3 and x4 cancel each other causing no activity in x5 and x6 nodes. Due to the elastic phenomenon of x6 node just described this property of G-DN is also called rebound/elastic property. The mechanics behind the cause is the short-term memory (psychological moment) property of G-DN given by the equation of z1 and z2 described earlier (Chapter-2, p22-26).

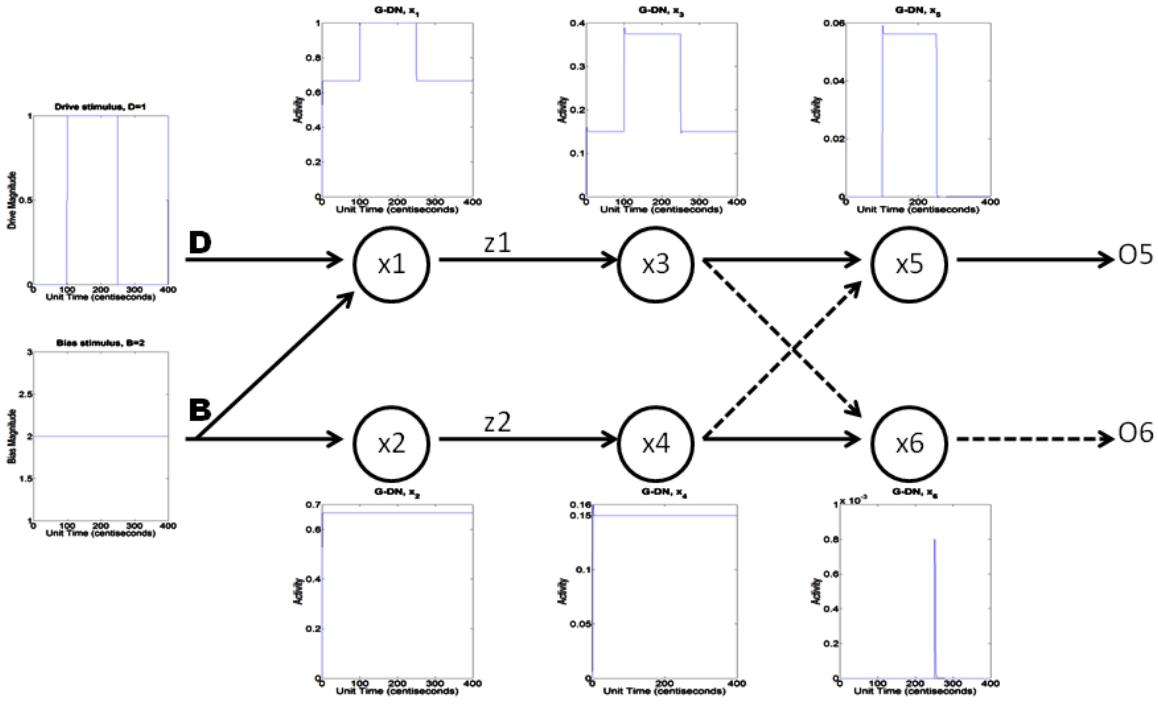

Figure 3.6. G-DN receiving both bias (B) and drive (D) stimulus.

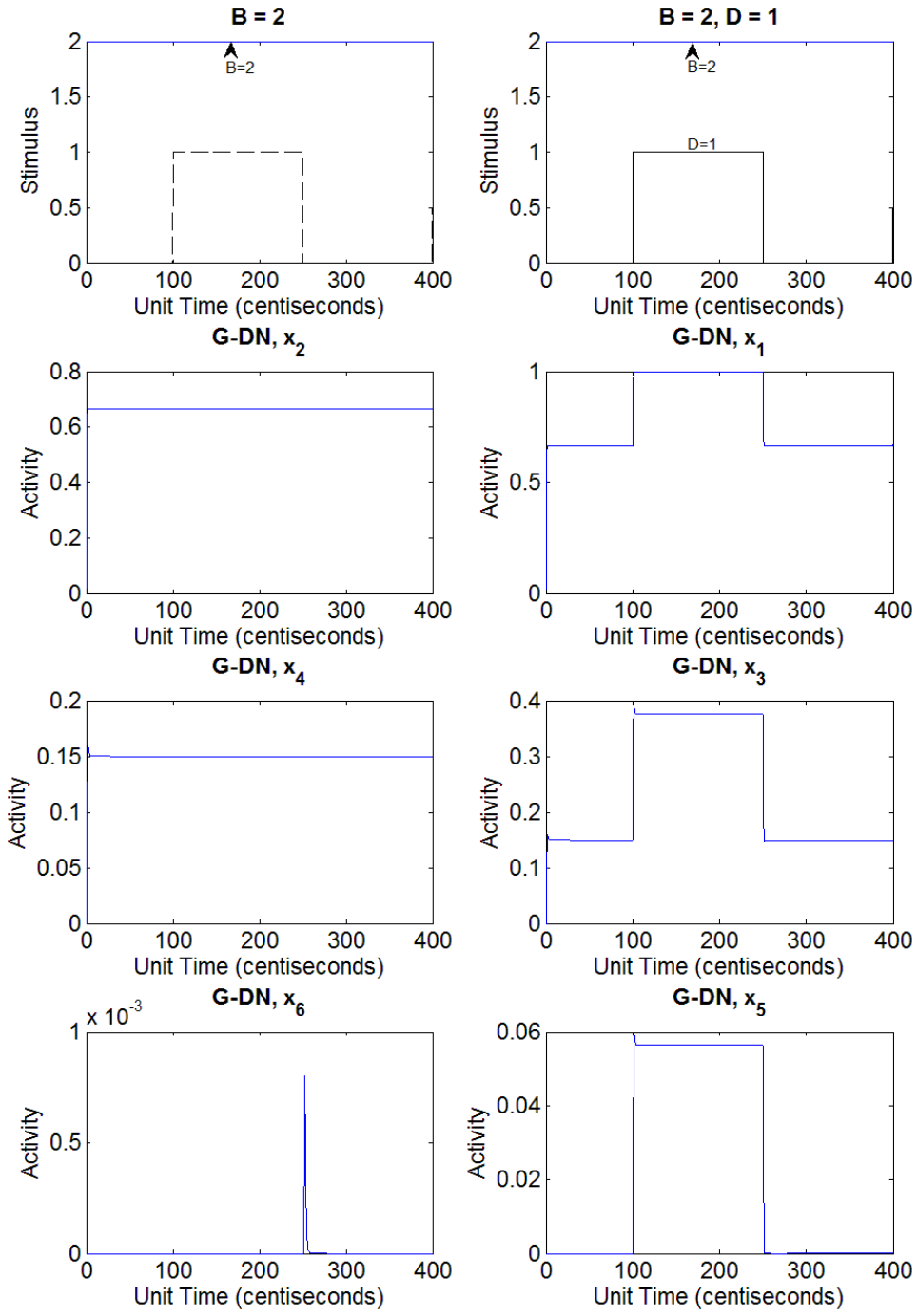

Figure 3.7. Output traces of G-DN in Figure 3.6 (inset) receiving both B and D-stimulus showing activity in node-5 (x_5) during B & D interval and activity in node-6 (x_6) for very short duration just after D-stimulus is turned off. Note that the dashed line (left stimulus/top plot) indicates absence of D-stimulus for node-2 during the interval node-1 receives D-stimulus.

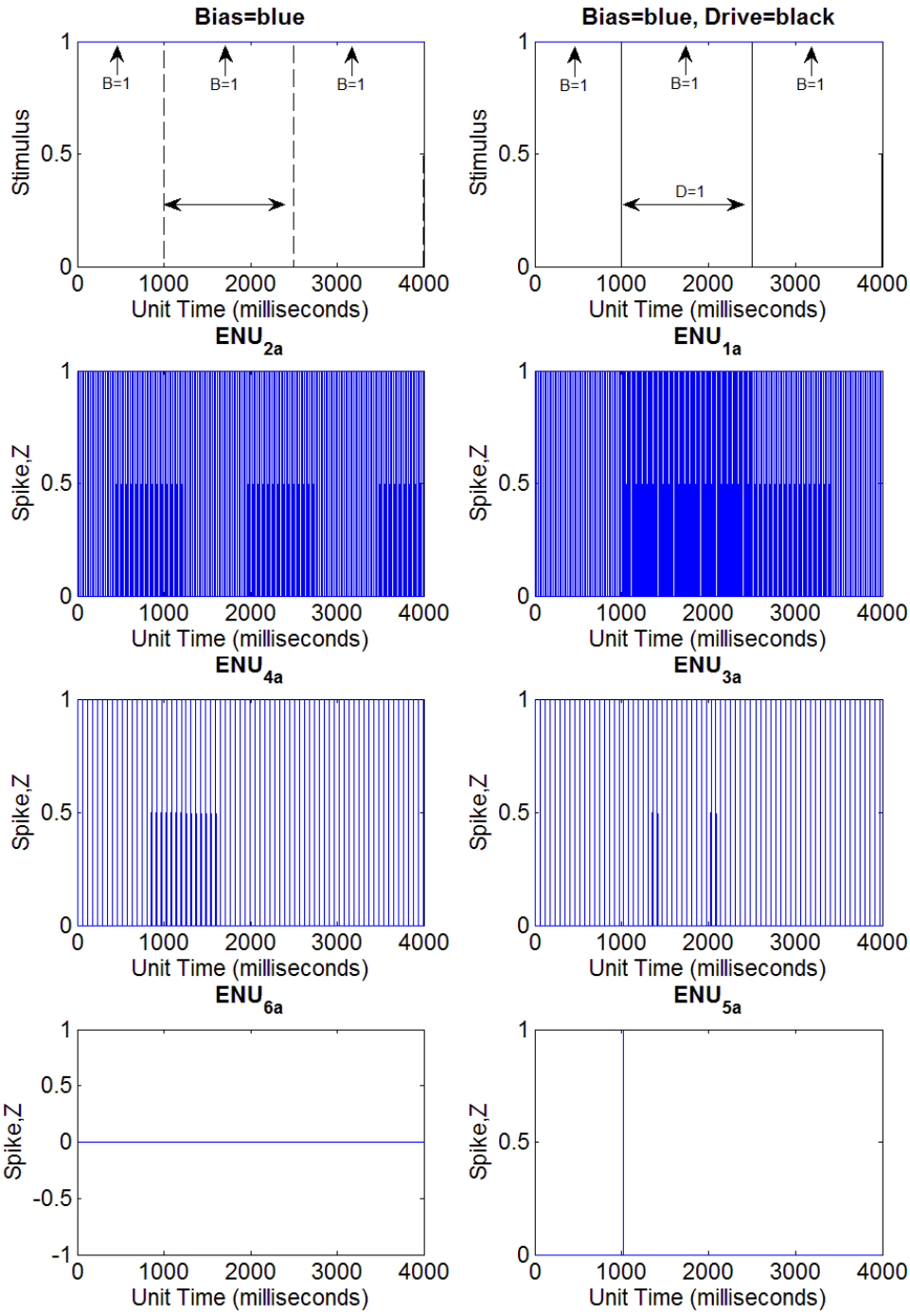

Figure 3.8. Output traces of E-DN architecture in Figure 3.4 but with both B and D-stimulus. Note that the dashed line (left stimulus/top plot) indicates absence of D-stimulus for node-2 (Eck2) during the interval node-1 (Eck1) receives D-stimulus.

Putting the E-DN seen in Figure 3.4 with the same parameters (table 3.1) through both B and D-stimulus produces the spike output traces shown in Figure 3.8. The

designed E-DN does not replicate the property of G-DN (Fig. 3.6 & 3.7). Apart for one spike in node-5 (Eck5) during the B & D interval there is no spiking even though node-1 (Eck1) clearly has more spiking during this interval. The increased spiking in the node-1 (Eck1) does not seem sufficient to considerably increase the spiking in node-3 (Eck3) relative to those during just B-stimulus. Hence the outcome is similar to the output trace with just B-stimulus (Fig. 3.5).

Adding more basic ENU's

The lack of change (Fig. 3.8) in node-3 (Eck3) even after receiving greater spiking input relative to node-4 (Eck4) could either be due to insufficient number of basic ENU's implemented in the E-DN or different to the parameter values or to the nature of PCNN dynamics. This section investigates the failure mechanism.

Using the same parameter values (table 3.1 with additional linking field parameters; $w_{lf} = 0.5$ & $\tau_{lf} = 1$), the basic ENU's in each node were increased by one, i.e., ENU_{xi} where i = a & b (Fig. 3.9). Running the simulation of the E-DN with increased number of basic ENU receiving both B and D-stimulus, the output trace of Figure 3.12 was obtained. With this network spikes now occur in both node-5 (Eck5) and node-6 (Eck6) during the B & D interval after which node-5 (Eck5) continues spiking. However this is not the behavior replicating G-DN (Fig. 3.6 & 3.7). Output trace of node-3 (Eck3) shows that though it is now receiving more input stimulus spikes (than E-DN in Fig. 3.8) spike output from this node does not increase proportionately. However the spiking pattern of node-3 (Eck3) is changed relative to node-4 (Eck4) causing successful inhibition (no spike) by either of the nodes (on respective Eck5 or Eck6) only at certain intervals.

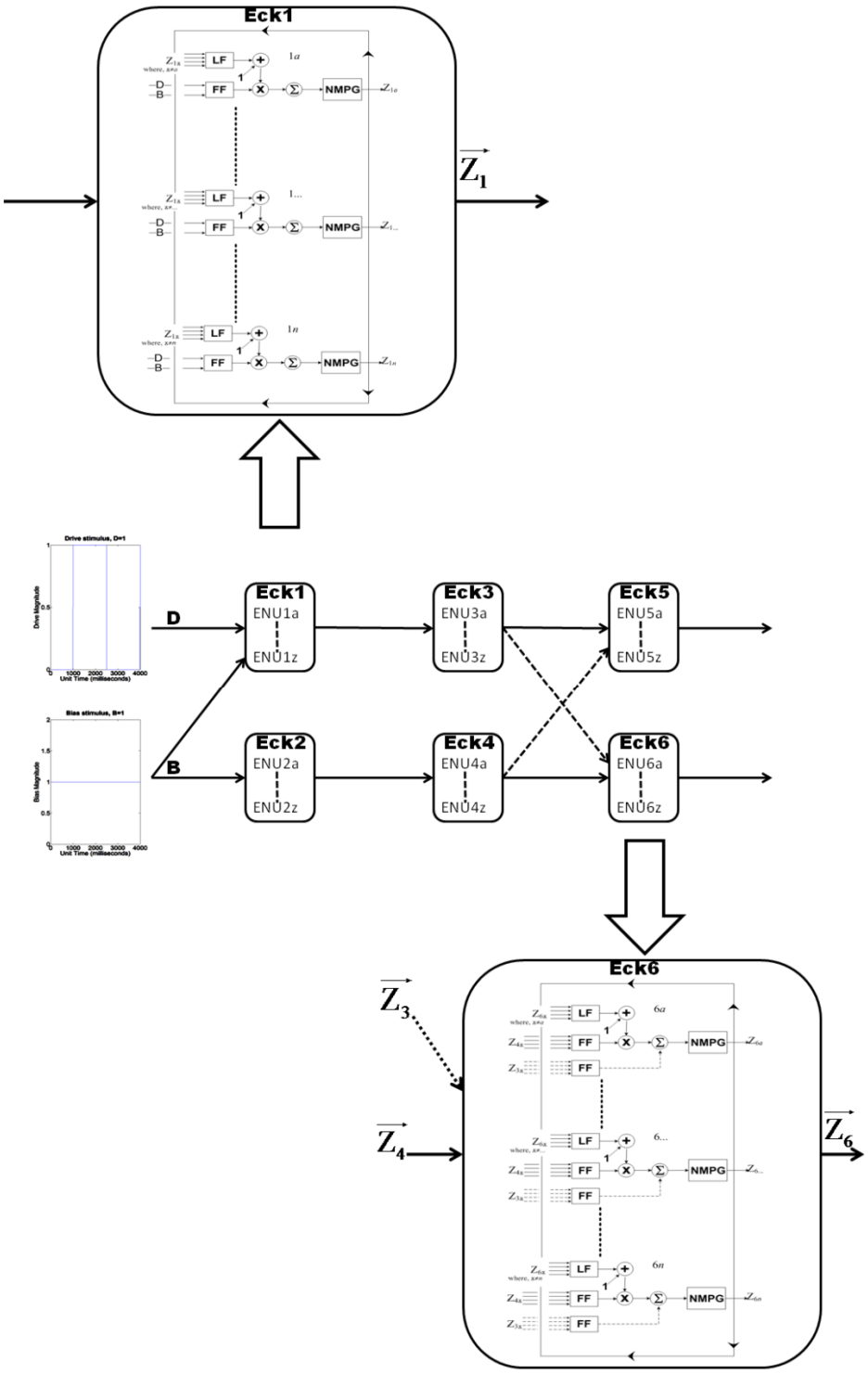

Figure 3.9. General scheme of E-DN for Figures 3.12, 3.13 and 3.15. This E-DN is similar to Figure 3.4 but with increased number of basic ENU's (a,…,z per ENU group, i.e., a to z basic ENU's) receiving both B & D-stimulus. The inset shows connection amongst basic ENU's within respective ENU group (ENU_1 & ENU_6 shown of nodes-1(Eck1) and node-6 (Eck6) respectively). Figures 3.10 and 3.11 provide enlarged views of the inset.

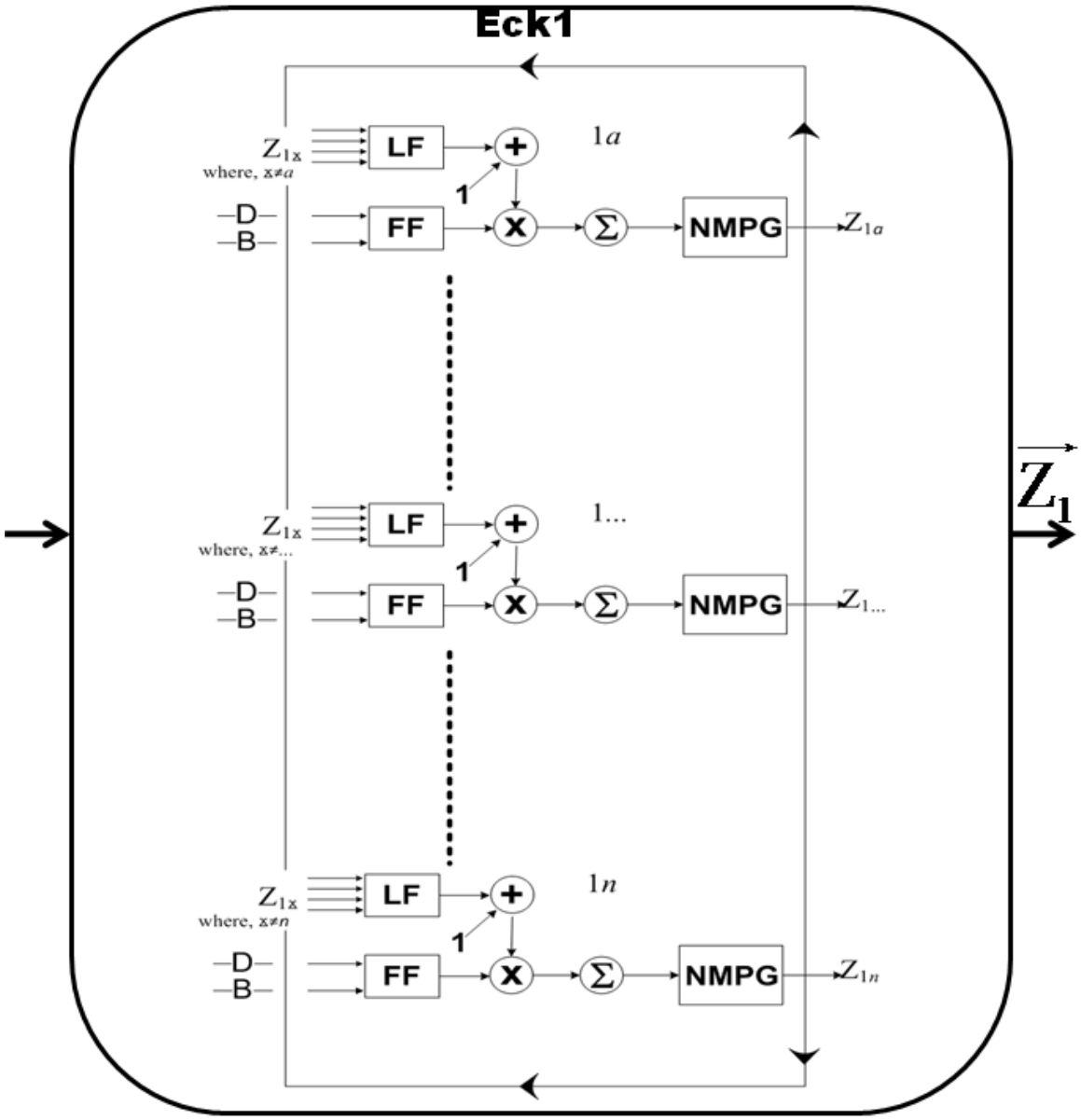

Figure 3.10. Enlarged view of the top inset seen in Figure 3.9 showing the configuration of *n*-basic ENU's within node-1 (Eck1). For i^{th} basic ENU its linking field (LF) receives output from neighboring basic ENU's apart from its own Z_{1i}, that is, elements of the LF input vector are the NMPG outputs excluding its own NMPG output it feeds into. But feeding field (FF) for all basic ENU's receives input stimulus which in the case of node-1 (Eck1) is the drive (D) and bias (B) stimulus as DC.

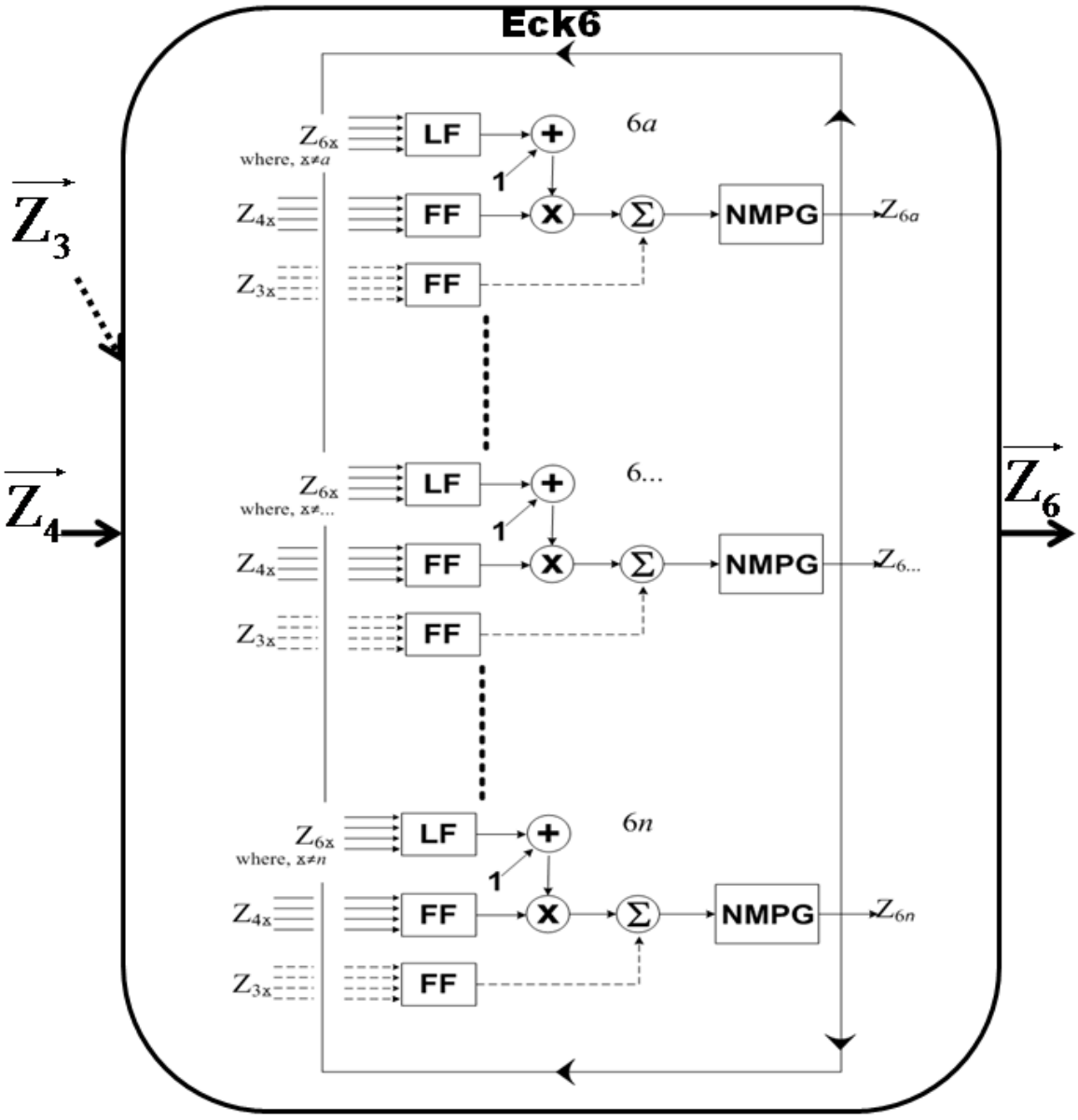

Figure 3.11. Enlarged view of the bottom inset (Fig. 3.9), showing the configuration of *n*-basic ENU's within node-6 (Eck6). Feeding fields (FF) for basic ENU's within Eck6 receives excitatory input (solid line) from Eck4 outputs ($\vec{Z}_4$) and inhibitory input (dashed line) from Eck3 outputs ($\vec{Z}_3$) via respective dendrites. Note that this is reversed for Eck5.

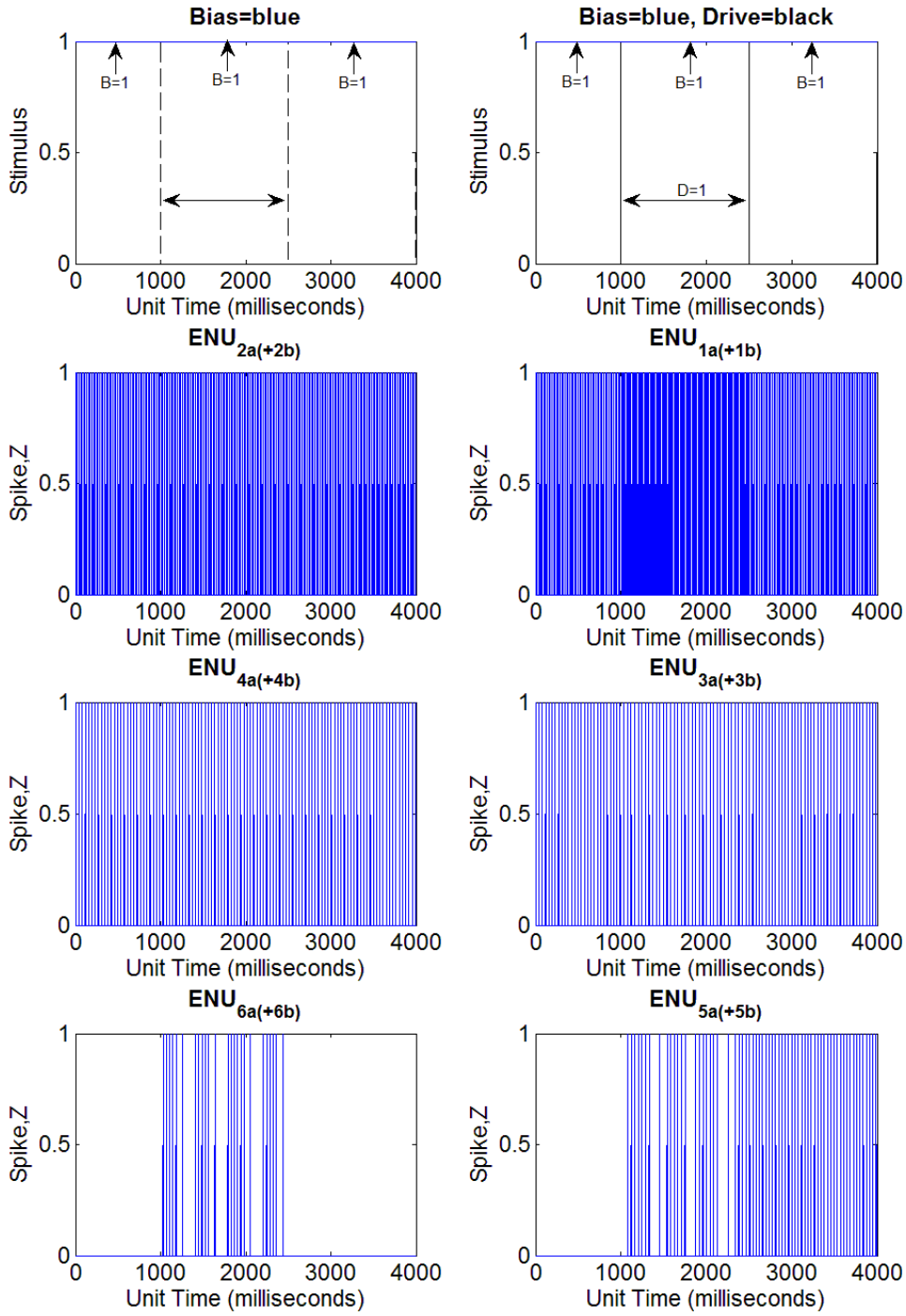

Figure 3.12. Output traces of just one basic ENU (ENU_{xa}) implemented (out of two per ENU group) in E-DN architecture of Figure 3.9 receiving both B and D-stimulus using parameters (table 3.1 with additional linking field parameters; $w_{lf} = 0.5$ & $\tau_{lf} = 1$).

Comparing Figure 3.12 to 3.8, spiking from Eck3 and Eck4 has increased which has resulted in Eck5 spiking during dual-stimuli, but so does Eck6. After the dual-stimuli, Eck5 continues to spike and not spiking from Eck6. Due to the lack of apparent increase in Eck3 spiking relative to Eck4 (Fig. 3.12) during dual-stimuli, the number of basic ENU's was increased using the same E-DN architecture (Fig. 3.9). The number of basic ENU's per group in E-DN (Fig. 3.12) was increased such that there are12 basic ENU's each in ENU_1 & ENU_2, 9 each in ENU_3 & ENU_4 and 3 each in ENU_5 & ENU_6 group. In addition, linking field parameter values were changed (from table 3.1) as shown in table 3.2. Output traces of this E-DN when run under simulation with both B and D-stimulus is shown in Figure 3.13.

ENU PART			**E-DN Node**		
			1 or 2	3 or 4	5 or 6
			ENU Group		
			ENU_1 or ENU_2	ENU_3 or ENU_4	ENU_5 or ENU_6
			Basic ENU		
			$ENU_{1a(b,\ldots,l)}$ or $ENU_{2a(b,\ldots,l)}$	$ENU_{3a(b,\ldots,i)}$ or $ENU_{4a(b,\ldots,i)}$	$ENU_{5a(b,c)}$ or $ENU_{6a(b,c)}$
Dendrite	Linking Field	w_{lf}	0.5	0.05	0.005
		τ_{lf}	1	1	1

Table 3.2. Parameters used for the simulation (Fig. 3.13) of E-DN architecture shown in Figure 3.9. All other parameter values (soma parameters) are same as in table 3.1.

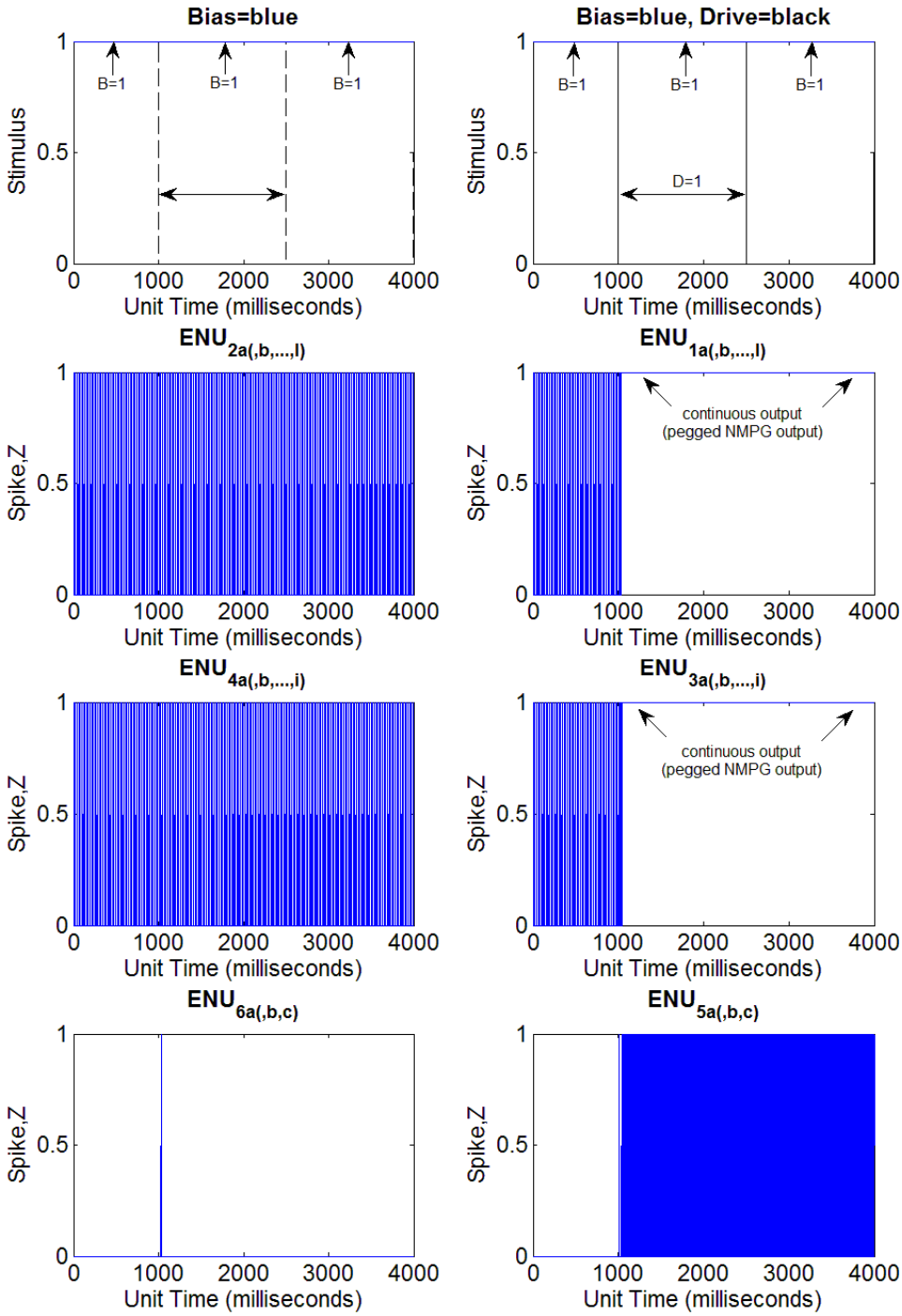

Figure 3.13. Output traces of just one basic ENU (ENU_{xa}) implemented (out of 12 each in ENU_1 & ENU_2, 9 each in ENU_3 & ENU_4 and 3 each in ENU_5 & ENU_6 group) in E-DN architecture of Figure 3.9 receiving both B and D-stimulus using parameters (table 3.2).

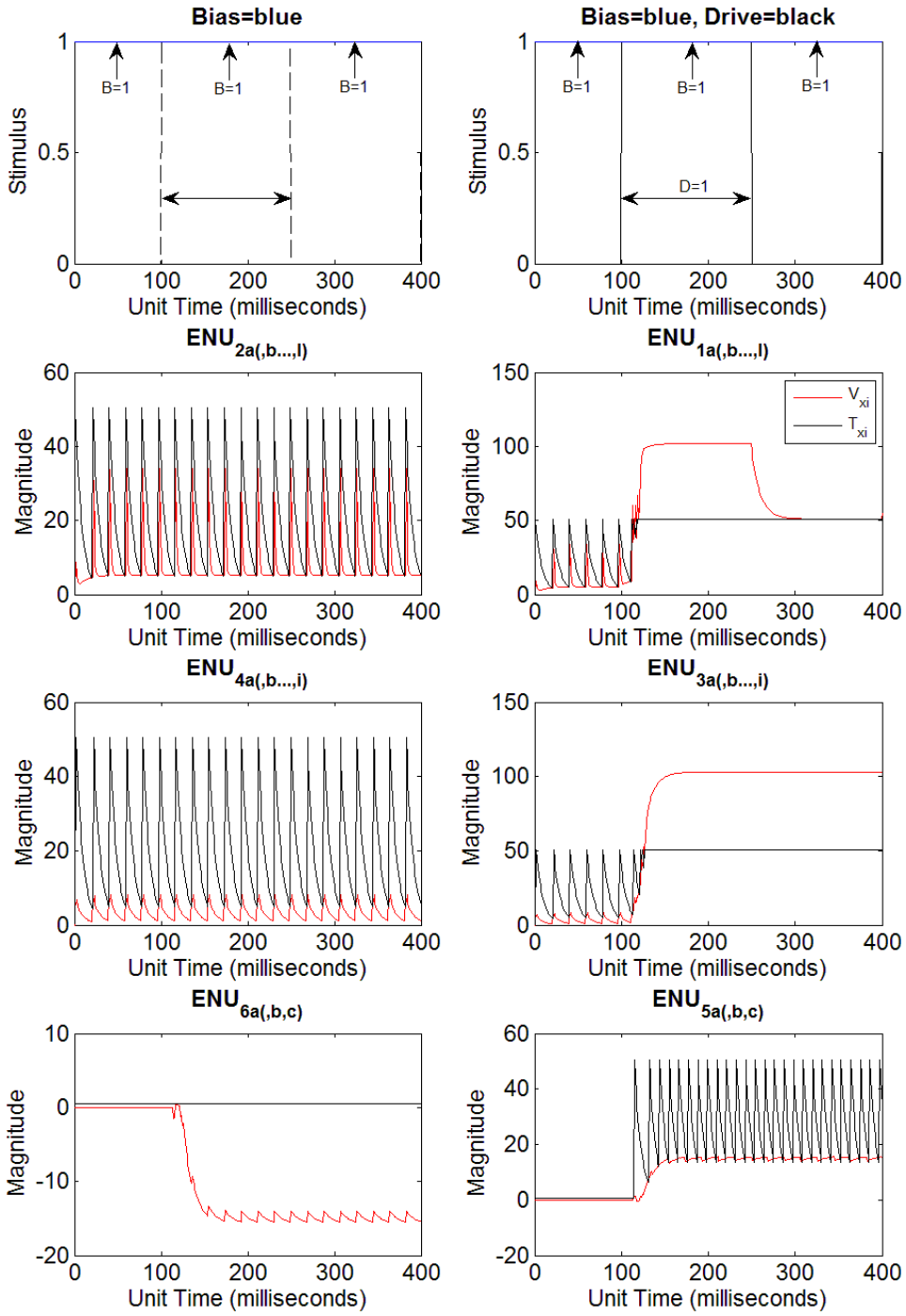

Figure 3.14. Soma inputs compared with soma threshold for the traces seen in Figure 3.13. V_{xi} (red) soma input and T_{xi} (black) soma threshold (or θ_{xi}). Notations as used in Figure 3.3. Note that after initiating dual stimuli (B & D), the T_{xi} (or θ_{xi}) for Eck1, Eck3 and Eck5 never reaches its resting baseline ($\theta_o = 0.5$, from table 3.1) unlike their counterparts (Eck2, Eck4 and Eck6). Thus ENU's in the former three nodes are firing in saturated mode.

Output traces (Fig. 3.13) of the current E-DN shows spiking in Eck5 while spiking in Eck6 is inhibited during B & D-stimulus interval. This should be the case (unlike those seen in Fig. 3.8 & 3.12) since Eck5 receives pulsed inputs from nodes receiving B & D-stimulus while preceding nodes for Eck6 receives only B-stimulus. But after the B & D-stimulus interval there is no spiking from Eck6 (that is, no elasticity) and instead Eck5 spiking persists.

The outputs from Eck1, Eck3 and Eck4 indicate that their respective ENU's are firing in saturated mode as shown in Figure 3.14. Apart from the linking field parameters (whose purpose is synchronization) all other parameters are the same as table 3.1. Hence increased spiking is due to considerable increase in basic ENU numbers particularly in first four nodes of E-DN. ENU's in saturated mode is not desired for E-DN because the network cannot replicate G-DN as one connection of nodes (those receiving B & D-stimulus) will uniformly be having an upper hand, incapable of producing any dipole property.

Next the number of basic ENU's per group in E-DN architecture (Fig. 3.9) is changed (decreased relative to Fig. 3.13), such that there are12 basic ENU's each in ENU_1 & ENU_2, 3 each in ENU_3 & ENU_4 and 3 each in ENU_5 & ENU_6 groups. In addition, different parameter values are used for this E-DN (table 3.3). A major change in parameter value is the time constant of inhibitory feeding field which is set larger than the corresponding value of the excitatory dendrite within respective ENU_x group. Output traces of this E-DN when run under simulation with both B and D-stimulus are shown in Figure 3.15.

ENU PART			E-DN Node			
			1 or 2	3 or 4	5 or 6	
			ENU Group			
			ENU_1 or ENU_2	ENU_3 or ENU_4	ENU_5 or ENU_6	
			Basic ENU			
			$ENU_{1a(b,\ldots,l)}$ or $ENU_{2a(b,\ldots,l)}$	$ENU_{3a(b,c)}$ or $ENU_{4a(b,c)}$	$ENU_{5a(b,c)}$ or $ENU_{6a(b,c)}$	
Dendrite	Linking Field	w_{lf}	0.5	0.05	0.005	
		τ_{lf}	1	1	1	
	Feeding Field	w_{ff}	0.5	1	$5^{(+)}$	$5^{(-)}$
		τ_{ff}	10	10	$10^{(+)}$	$12.5^{(-)}$

Table 3.3. Parameters used for the simulation (Fig. 3.15) of E-DN architecture shown in Figure 3.9. Notice that the linking field parameter used for simulation in Figure 3.15 remains unchanged (compared to table 3.2 for Fig. 3.13 simulation) but the feeding field weight (w_{ff}) for nodes receiving the first line of stimulus (nodes 1 & 2) has changed (reduced to 0.5). Also the time constant for inhibitory feeding field is increased (12.5). The parameters for soma/neuromime remain the same as in table 3.1.

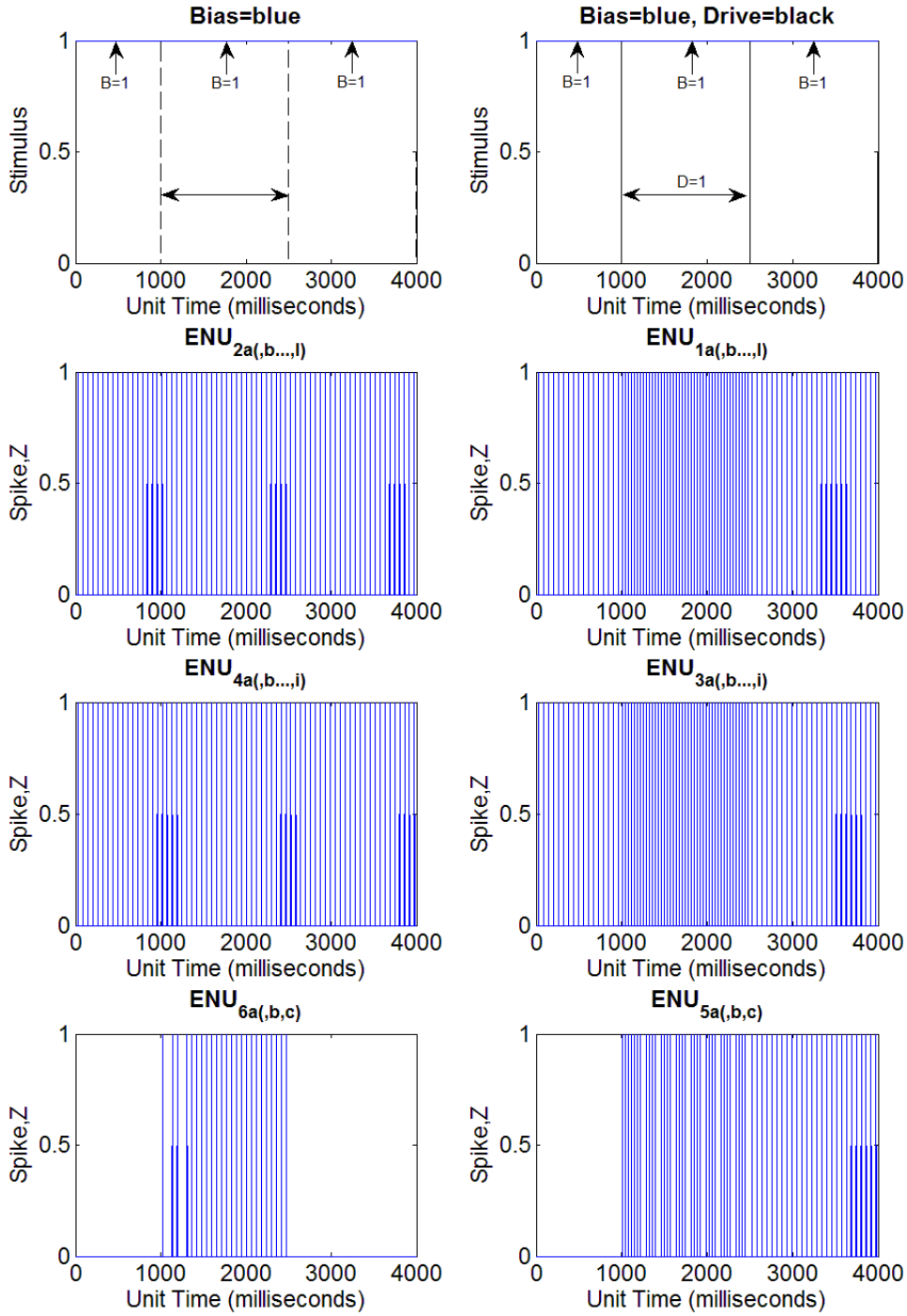

Figure 3.15. Output traces of one basic ENU (ENU_{xa}) implemented (out of 12 each in ENU_1 & ENU_2, 3 each in ENU_3 & ENU_4 and 3 each in ENU_5 & ENU_6 group) in E-DN architecture of figure 3.9 receiving both B and D-stimulus using parameters given in table 3.3.

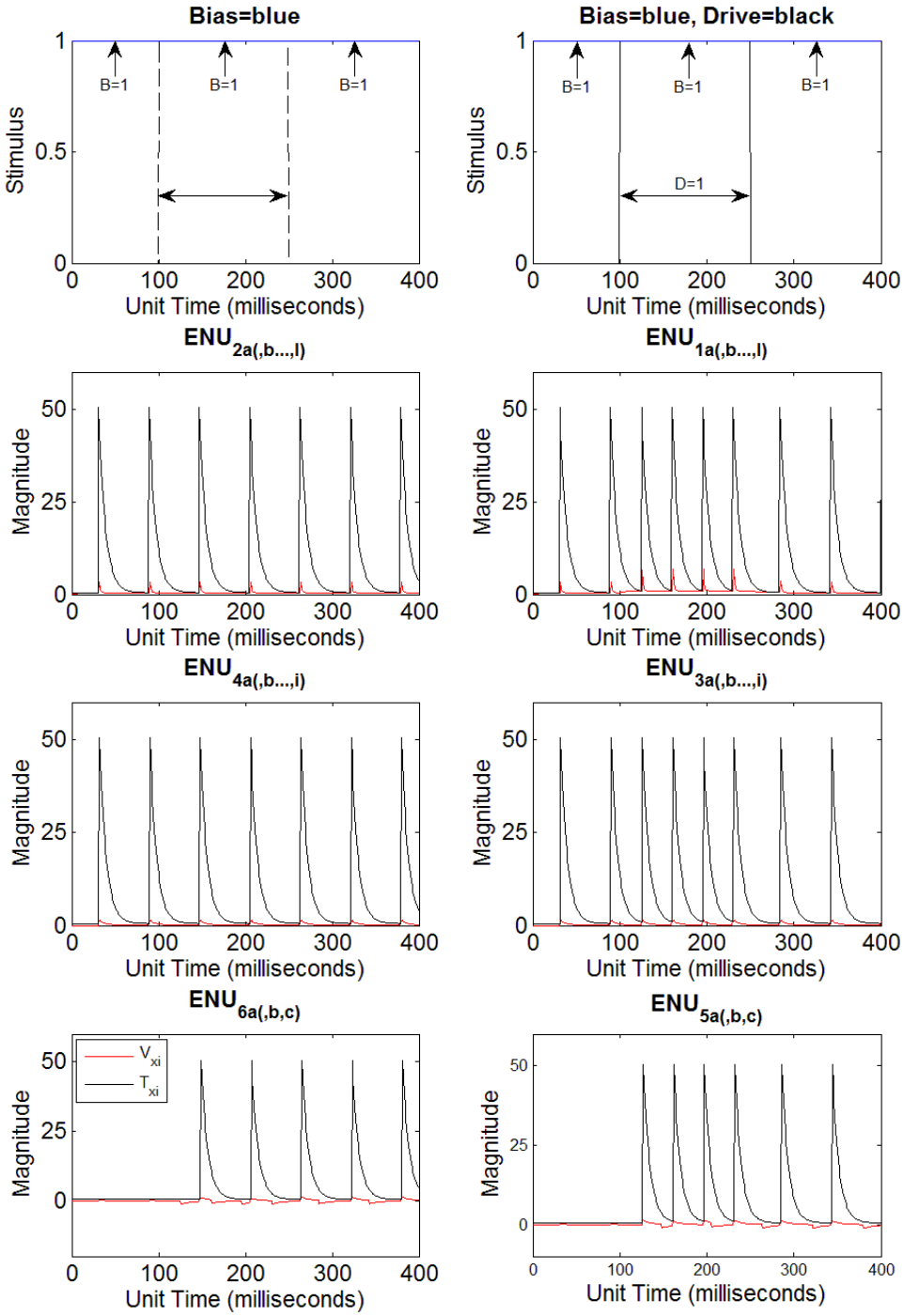

Figure 3.16. Soma inputs (V_{xi}, red) compared with soma threshold (T_{xi} or θ_{xi}, black) for the traces seen in Figure 3.15. V_{xi}, soma input and T_{xi}, soma threshold (or θ_{xi}). Notice that T_{xi} (or θ_{xi}) of all the ENU's in all six nodes reach their resting baseline ($\theta_o = 0.5$, from table 3.1).

The output traces in Figure 3.15 are qualitatively similar to those already seen in Figure 3.12 with respect to spiking from node-5 (Eck5) and node-6 (Eck6) of E-DN. However unlike Figure 3.12 there is a noticeable increase in node-3 (Eck3) spiking. The spiking behavior in the first four nodes (Eck1 to Eck4) corresponds intuitively with the initial stimulus node-1 (Eck1) and node-2 (Eck2) receives. To check the mode of the ENU's, soma inputs were compared with threshold as seen in Figure 3.16. The figure shows that the ENU's are no longer in saturated mode as was the case for earlier E-DN (Fig. 3.13).

Till now the network architecture of E-DN has been identical to G-DN, but the goal is to replicate the property of G-DN. While using G-DN as the roadmap network the E-DN architecture can be changed or modified to achieve the goal. The results just shown indicate that PCNN dynamics differ significantly enough to require this.

Two ENU groups within initial nodes (node-1 or Eck1 & node-2 or Eck2) with reciprocal inhibition (Eck3↔Eck6 & Eck4↔Eck5)

The previous E-DN (Fig. 3.15) has spikes from Eck6 during B and D-stimulus though Eck3 is spiking more than Eck4. Increasing just the basic ENU's can lead them into saturated mode but this particular problem of insufficient inhibition can be tackled by adding reciprocal inhibition between the nodes (Eck3 & Eck6 and Eck4 & Eck5). In addition, during B-stimulus (post dual stimuli) both Eck5 and Eck6 are at the end of network receiving the same B-stimulus but Eck5 continues spiking. To solve this issue two ENU groups (ENU_{1syn} & ENU_{2syn}) are introduced such that they receive pulsed inputs from ENU_1 & ENU_2 groups respectively with the intention to achieve certain

amount of synchrony in inputs, particularly during B-stimulus. The ENU_1 and ENU_{1syn} constitute Eck1 (similarly for Eck2). The new E-DN is shown in Figures 3.17 and 3.18.

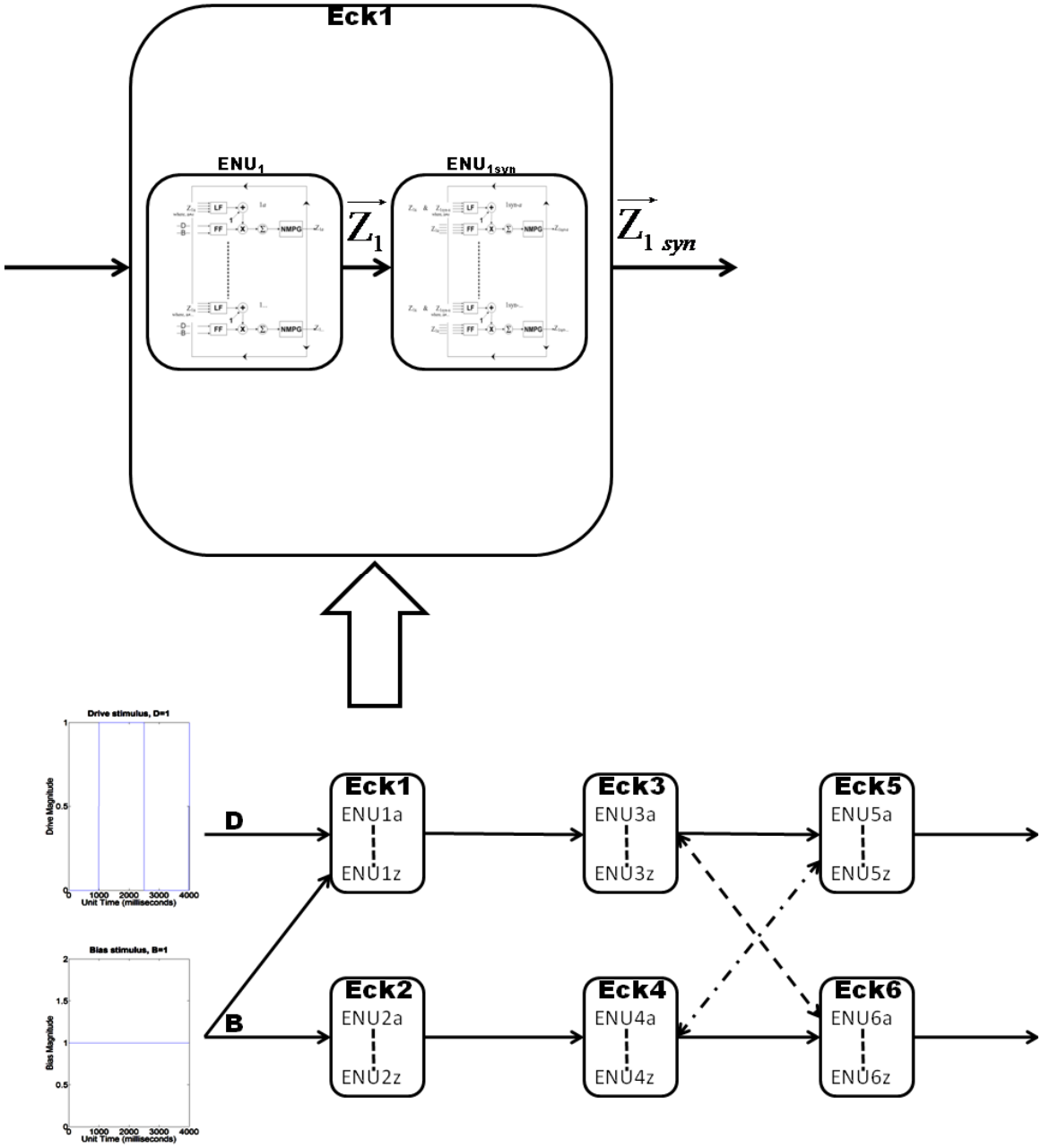

Figure 3.17. E-DN with reciprocal inhibition between nodes 3↔6 (Eck3↔Eck6) & 4↔5 (Eck4↔Eck5) with two ENU groups each in node-1 (ENU_1 & ENU_{1syn} in Eck1) & node-2 (ENU_2 & ENU_{2syn} in Eck2). Number of basic ENU's per ENU groups: 12 each in ENU_1 & ENU_2, 12 each in ENU_{1syn} & ENU_{2syn}; 9 each in ENU_3 & ENU_4, 3 each in ENU_5 & ENU_6.

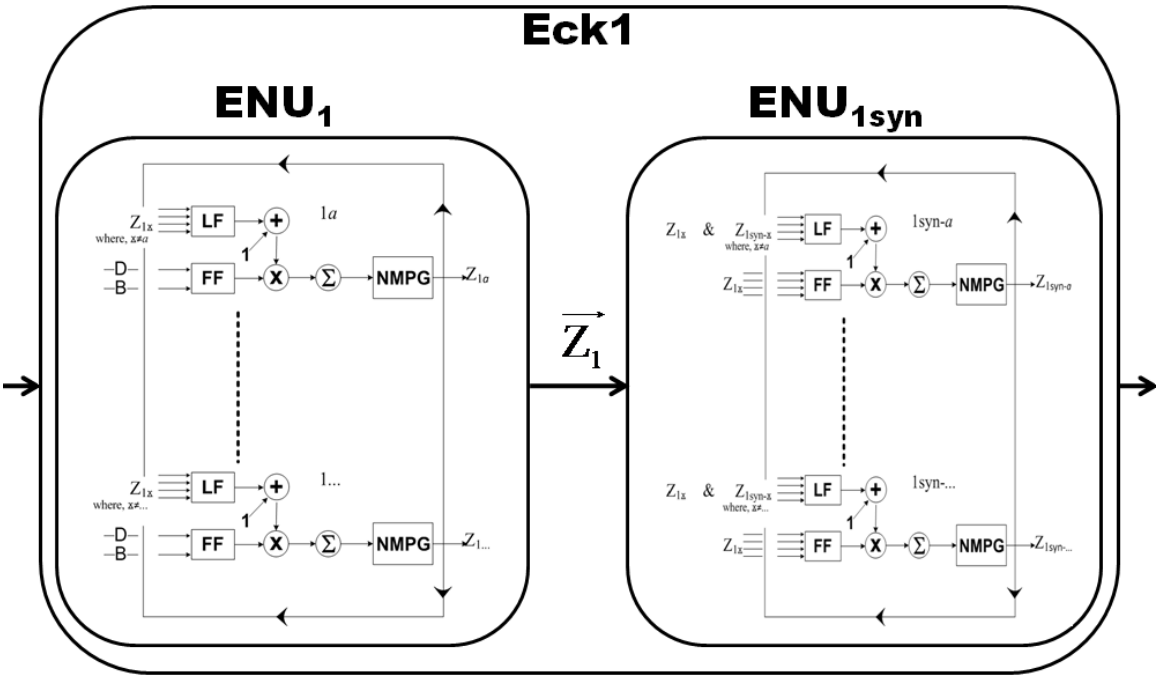

Figure 3.18. Enlarged view of the inset seen in Figure 3.17 showing the configuration of *n*-basic ENU's amongst the two ENU groups (ENU_1 & ENU_{1syn}) within Eck1. Feeding field (FF) for all basic ENU's within ENU_1 group receives input stimulus which in the case of Eck1 is the drive (D) and bias (B) stimulus as DC. However, outputs of ENU_1 group ($\vec{Z}_1$) are the inputs for the FF of basic ENU's within ENU_{1syn} group. Finally, inputs for Eck3 and Eck4 are from ENU_{1syn} ($\vec{Z}_{1syn}$) of Eck1 and ENU_{2syn} ($\vec{Z}_{2syn}$) of Eck2 respectively. Notice that LF's in ENU_{1syn} and ENU_{2syn} receives $\vec{Z}_1$ and $\vec{Z}_2$ respectively in addition to receiving NMPG outputs within ENU_{1syn} and ENU_{2syn}.

Output traces following simulation using parameters given in table 3.4 for E-DN (Fig. 3.17) are shown in Figure 3.19. The spiking from Eck5 and Eck6 resembles those seen in Figure 3.15. However amount of spiking from Eck6 during B and D-stimuli has decreased. Hence increasing the strength of inhibitory connections from basic ENU's of the preceding nodes (Eck3 for Eck6 and Eck4 for Eck5) could inhibit the Eck6 spiking. This was done by changing the inhibitory feeding field weight parameter for basic ENU's in Eck5 and Eck6 ($w_{ff} = 5^{(-)}$, increased from $w_{ff} = 2^{(-)}$). The output traces with increased inhibition is shown in Figure 3.20.

ENU PART			**E-DN Node**					
			1 or 2		3 or 4		5 or 6	
			ENU Group					
			ENU_1 or ENU_2	ENU_{1syn} or ENU_{2syn}	ENU_3 or ENU_4		ENU_5 or ENU_6	
			Basic ENU					
			$ENU_{1a(b,\ldots,l)}$ or $ENU_{2a(b,\ldots,l)}$	$ENU_{1syn\text{-}a(b,\ldots,l)}$ or $ENU_{2syn\text{-}a(b,\ldots,l)}$	$ENU_{3a(b,\ldots,i)}$ or $ENU_{4a(b,\ldots,i)}$		$ENU_{5a(b,\ldots,c)}$ or $ENU_{6a(b,\ldots,c)}$	
Dendrite	linking field	w_{lf}	0.5	0.5 (amongst ENU1syn-…) 1 (with ENU1…) (similarly for ENU2syn-…)	0.5		0.5	
		τ_{lf}	1	1	1		1	
	feeding field	w_{ff}	0.5	1	$1^{(+)}$	$5^{(-)}$	$2^{(+)}$	$2^{(-)}$
		τ_{ff}	10	10	$10^{(+)}$	$30^{(-)}$	$20^{(+)}$	$20^{(-)}$

Table 3.4. Parameters used for the simulation (Figure 3.19) of E-DN architecture shown in Figure 3.17. Notice that the linking field parameter weight (w_{lf}) for ENU_{1syn} & ENU_{2syn} is such that $w_{lf} = 0.5$ between $ENU_{1syn\text{-}\ldots}$'s & between $ENU_{2syn\text{-}\ldots}$'s while $w_{lf} = 1$ between $ENU_{1\ldots}$'s & between $ENU_{2\ldots}$'s. The parameters for soma/neuromime remain the same as in table 3.1.

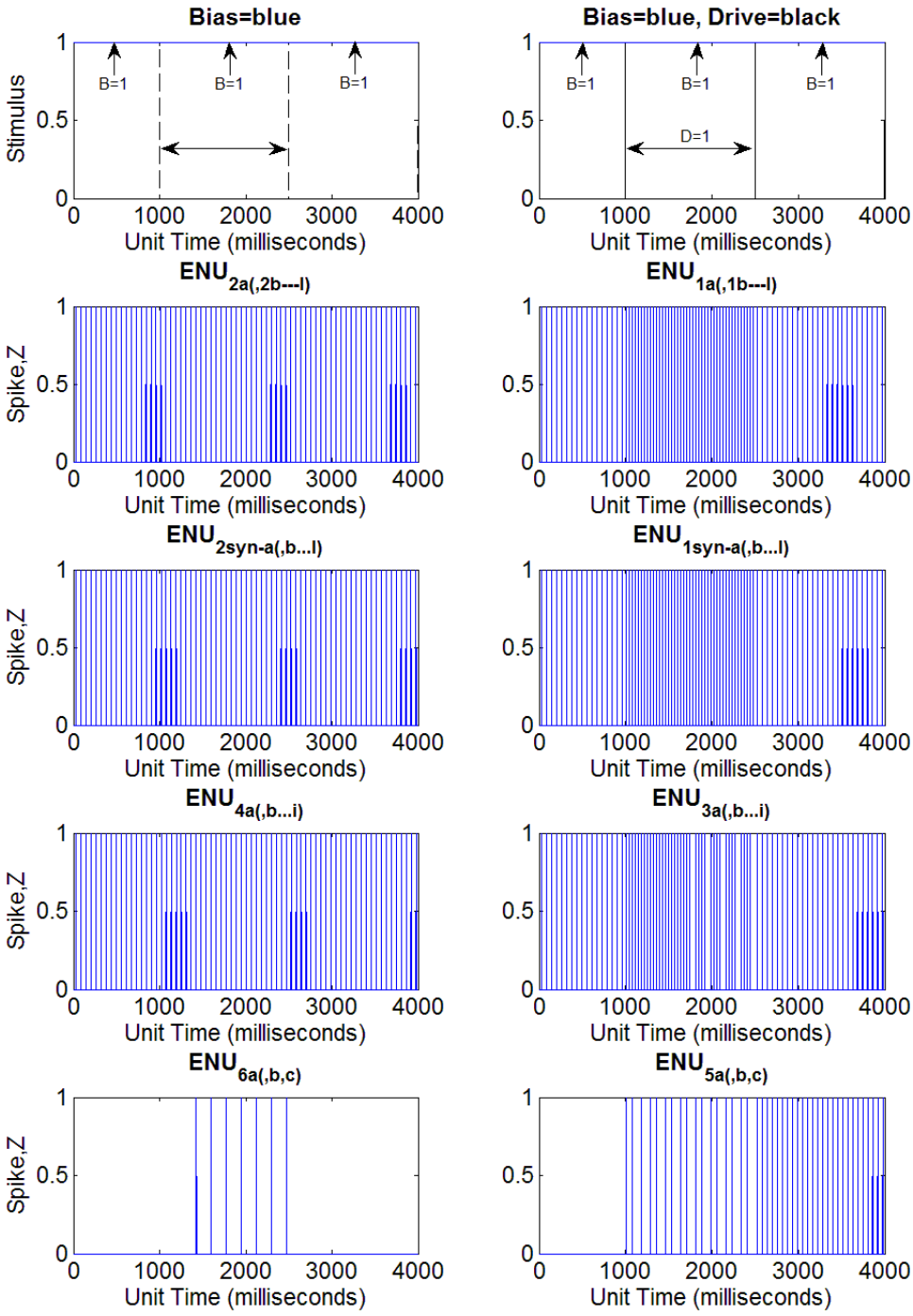

Figure 3.19. Output traces of one basic ENU (ENU_{xa}) implemented (out of 12 each in ENU_1 & ENU_2, 12 each in ENU_{1syn} & ENU_{2syn}, 9 each in ENU_3 & ENU_4 and 3 each in ENU_5 & ENU_6 group) in E-DN architecture of Figure 3.17 receiving both B and D-stimulus using parameters given in table 3.4.

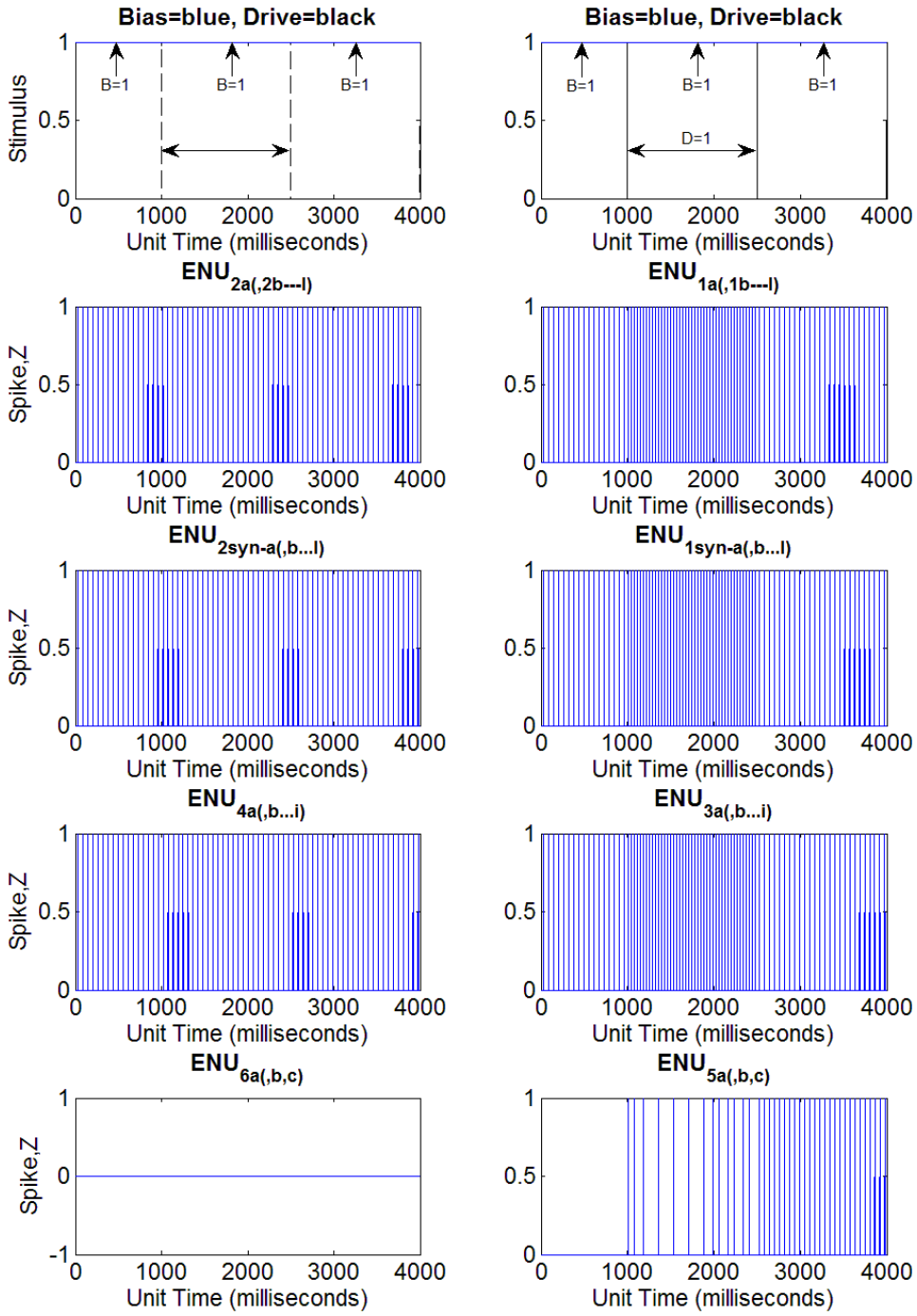

Figure 3.20. Output traces of just basic ENU (ENU_{xa}) implemented (out of 12 each in ENU_1 & ENU_2, 12 each in ENU_{1syn} & ENU_{2syn}, 9 each in ENU_3 & ENU_4 and 3 each in ENU_5 & ENU_6 group) in E-DN architecture of Figure 3.17 receiving both B and D-stimulus using same parameters as in table 3.4 with the exception that $w_{ff} = 5^{(-)}$ for basic $ENU_{5a(b,c)}$ or $ENU_{6a(b,c)}$,i.e., feeding field weights for incoming cross-inhibitions.

The reciprocal inhibition with forward and backward component in the E-DN is not successful in reproducing the property of G-DN (Fig. 3.19 & 3.20). During initial B-stimulus the forward inhibition (Eck3→$^{(-)}$Eck6 & Eck4→$^{(-)}$Eck5) is strong enough to prevent spiking. With B & D-stimulus, Eck6 receives stronger inhibition leading to no backward inhibition of Eck3 which in turn makes Eck3 stimulate Eck5 consistently (Fig. 3.20). However spiking in Eck5 continues after the dual stimuli and no elastic property is obtained.

Three ENU groups within initial nodes (node-1 or Eck1 & node-2 or Eck2) without reciprocal inhibition

The architecture of E-DN in Figure 3.17 was next modified by removing the backward inhibition (Eck3$^{(-)}$←Eck6 and Eck4$^{(-)}$←Eck5). Spiking from the middle two nodes (Eck3 & Eck4) is to be reduced while still maintaining the desired relation with B, D-stimulus. That is, Eck3 is to have relatively more spiking than Eck4. To achieve this, two more ENU groups (ENU_{1elas} & ENU_{2elas}) are introduced into the first two nodes (Eck1 & Eck2) such that they receive pulsed inputs from ENU_{1syn} & ENU_{2syn} respectively but project lateral inhibition to these groups (Fig. 3.21 & 3.22).

Simulation results (Fig. 3.23) show that the E-DN of Figure 3.21 has achieved one property of G-DN, i.e., during B & D-stimulus Eck3 is able to excite Eck5 despite receiving inhibition from Eck4, whereas during B-stimulus (pre- or post-dual stimuli) the equal strength of excitation and inhibition causes no spiking in either Eck5 or Eck6. However unlike G-DN (Fig. 3.6 & 3.7) no spiking occurs in Eck6 just after the removal of D-stimulus. In other words, rebound/elastic property of G-DN is still not represented

by the current E-DN.

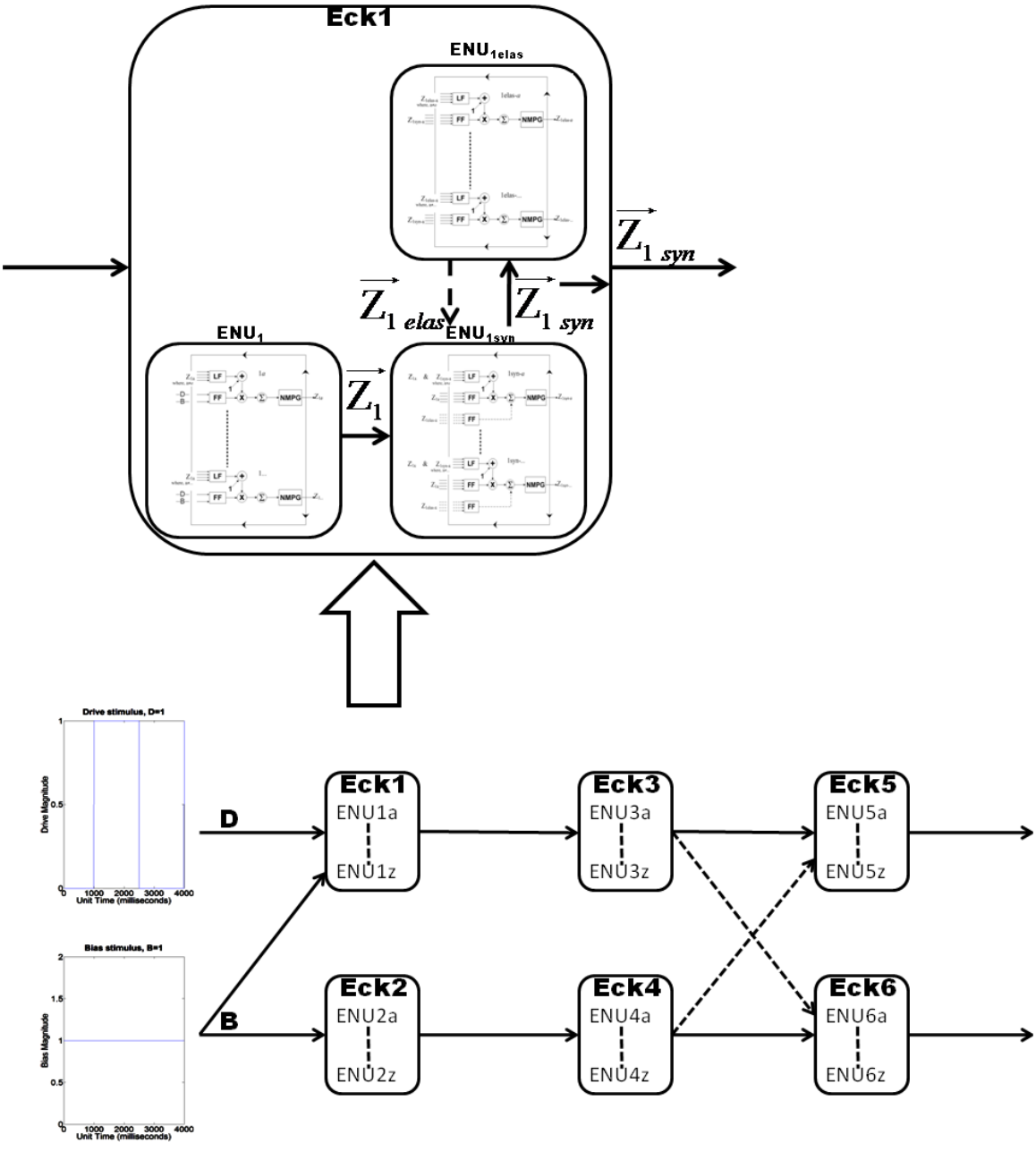

Figure 3.21. E-DN with three ENU groups (ENU_1, ENU_{1syn} & ENU_{1elas}) in Eck1 (and Eck2) such that ENU_{1elas} receives pulsed inputs and sends inhibitory pulses back to ENU_{1syn}. Number of basic ENU's per ENU groups: 12 each in ENU_1 & ENU_2, 6 each in ENU_{1syn} & ENU_{2syn}, 12 each in ENU_{1elas} & ENU_{2elas}; 12 each in ENU_3 & ENU_4 and 12 each in ENU_5 & ENU_6.

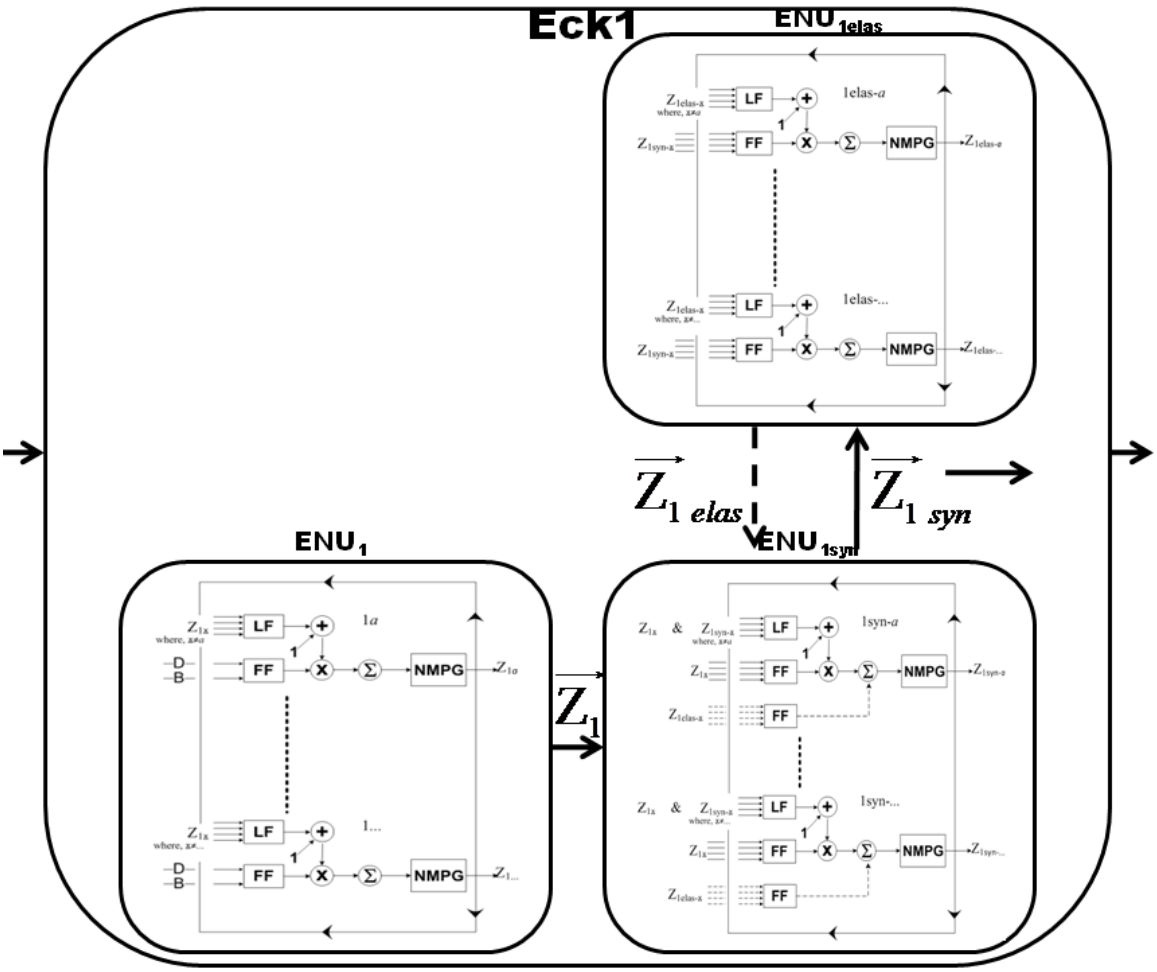

Figure 3.22. Enlarged view of the inset seen in Figure 3.21 showing the configuration of *n*-basic ENU's amongst the three ENU groups (ENU_1, ENU_{1syn} & ENU_{1elas}) within Eck1.

Feeding field (FF) for all basic ENU's within ENU_1 group receives input stimulus which in the case of Eck1 is the drive (D) and bias (B) stimulus as DC. However, outputs of ENU_1 group ($\vec{Z}_1$) are the inputs for the FF (excitatory) of basic ENU's within ENU_{1syn} group whose outputs ($\vec{Z}_{1syn}$) in turn are the inputs for the FF of basic ENU's within ENU_{1elas} group. The ENU_{1elas} outputs ($\vec{Z}_{1elas}$) are then inputs for the FF of inhibitory dendrite of ENU_{1syn} (i.e., lateral inhibition).

Finally, inputs for Eck3 and Eck4 are from ENU_{1syn} ($\vec{Z}_{1syn}$) of Eck1 and ENU_{2syn} ($\vec{Z}_{2syn}$) of Eck2 respectively.

		E-DN Node						
		1 or 2				3 or 4	5 or 6	
		ENU Group						
ENU Part		ENU_1 or ENU_2	ENU_{1syn} or ENU_{2syn}		ENU_{1elas} or ENU_{2elas}	ENU_3 or ENU_4	ENU_5 or ENU_6	
		Basic ENU						
Dend.		$ENU_{1a(b,\ldots,l)}$ or $ENU_{2a(b,\ldots,l)}$	$ENU_{1syn\text{-}a(b,\ldots,f)}$ or $ENU_{2syn\text{-}a(b,\ldots,f)}$		$ENU_{1elas\text{-}a(b,\ldots,l)}$ or $ENU_{2elas\text{-}a(b,\ldots,l)}$	$ENU_{3a(b,\ldots,l)}$ or $ENU_{4a(b,\ldots,l)}$	$ENU_{5a(b,\ldots,l)}$ or $ENU_{6a(b,\ldots,l)}$	
LF	w_{lf}	0.5	0.5		0.5	0.5	0.5	
	τ_{lf}	1	1		1	1	1	
FF	w_{ff}	0.5	$1^{(+)}$	$125^{(-)}$	1	$1^{(+)}$	$0.5^{(+)}$	$2^{(-)}$
	τ_{ff}	10	$10^{(+)}$	$30^{(-)}$	10	$10^{(+)}$	$10^{(+)}$	$40^{(-)}$

Table 3.5. Parameters used for simulation (Fig. 3.23) of E-DN architecture shown in Figure 3.21. Notice that the linking field parameter weight for ENU_{1syn} & ENU_{2syn}, w_{lf} = 0.5 between $ENU_{1syn\text{-}\ldots}$'s (& also between $ENU_{2syn\text{-}\ldots}$'s) and also with $ENU_{1\ldots}$'s (& with $ENU_{2\ldots}$'s). The parameters for soma/neuromime remain same as in table 3.1.

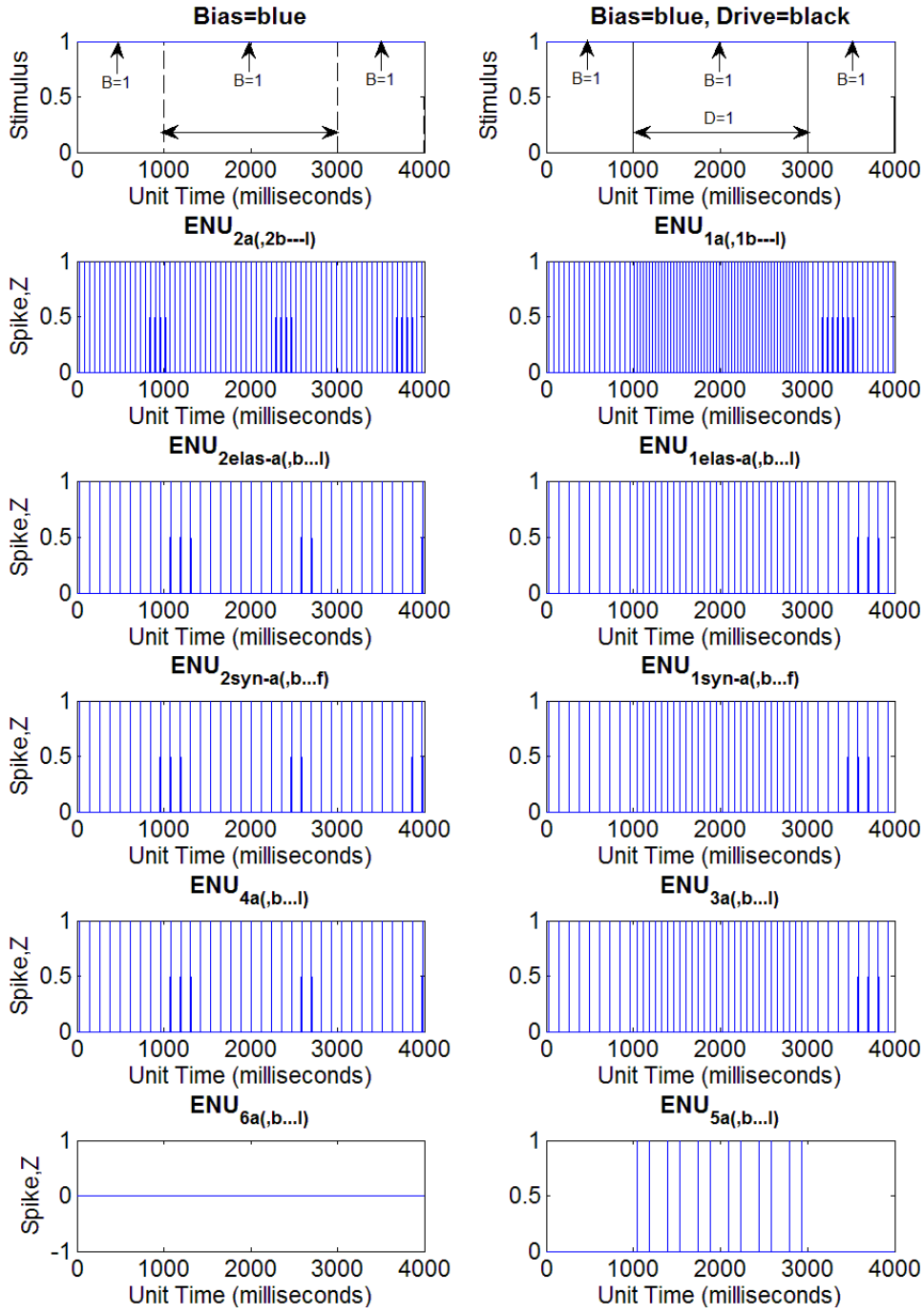

Figure 3.23. Output traces of one basic ENU (ENU_{xa}) implemented (out of 12 each in ENU_1 & ENU_2, 6 each in ENU_{1syn} & ENU_{2syn}, 12 each in ENU_{1elas} & ENU_{2elas}, 12 each in ENU_3 & ENU_4 and 12 each in ENU_5 & ENU_6 group) in E-DN architecture of Figure 3.21 receiving both B and D-stimulus using same parameters (table 3.5).

This outcome for the current E-DN (Fig. 3.23) shows slowing of spiking rates in ENU groups (ENU_{1elas} & ENU_{1syn} also ENU_{2elas} & ENU_{2syn}) within the first two nodes (Eck1 & Eck2) which do not receive the B or D-stimulus directly. During just B-stimulus equally strong inputs from Eck3 and Eck4 cancel each other out resulting in desired output traces (G-DN property) of Eck5 and Eck6. However the netlet within first two nodes might still be modified such that it is effective only during dual-stimuli (during B & D) thus retaining the achieved G-DN property but altering the amount of spiking during dual stimuli (causing elastic property). This was studied next.

Four ENU groups within initial nodes (node-1 or Eck1 & node-2 or Eck2)

The E-DN architecture in Figure 3.21 was modified based on the intuition that the network behavior may differ from Figure 3.23 if there is a decrease in inhibition from ENU_{1elas} to ENU_{1syn} (ENU groups in nodes receiving the additional D-stimulus) during dual-stimuli. That is, the additional D-stimulus during dual-stimuli causes decreased output from ENU_{1elas} group. Therefore, during just B-stimulus there are no outputs from the network ends (Eck5 & Eck6) due to the equally active initial nodes (Eck1 & Eck3 for Eck5 and Eck2 & Eck4 for Eck6). But during dual-stimuli Eck3 has more activity relative to Eck4 causing inhibition Eck6 but excitation of Eck5.

For reduced inhibition of ENU_{1syn} only during dual stimuli another ENU group (ENU_{1modu} & ENU_{2modu}) is added in the first two nodes (Eck1 & Eck2 respectively) such that they respond/spike only during dual-stimuli as shown in Figures 3.24 and 3.25. To observe the behavior of this E-DN, simulation was done using parameters given in table 3.6. Results are shown in Figure 3.26.

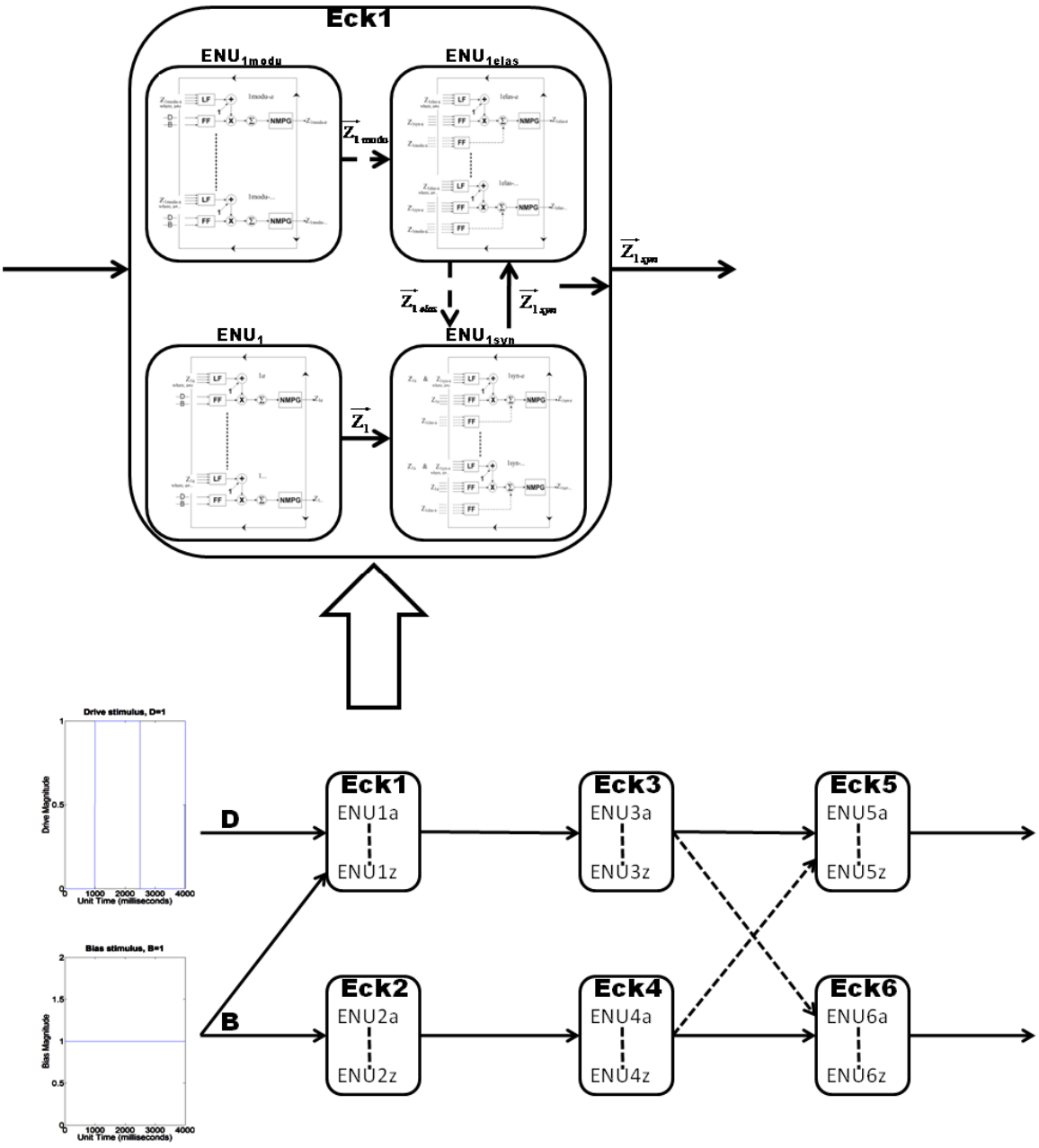

Figure 3.24. E-DN with four ENU groups (ENU_1, ENU_{1syn}, ENU_{1elas} & ENU_{1modu}) in Eck1 (and Eck2) such that ENU_{1elas} receives inhibitory pulsed inputs from ENU_{1modu} and also excitatory inputs from ENU_{1syn}. Number of basic ENU's per ENU groups: 12 each in ENU_1 & ENU_2, 6 each in ENU_{1syn} & ENU_{2syn}, , 12 each in ENU_{1modu} & ENU_{2modu}, 12 each in ENU_{1elas} & ENU_{2elas}; 12 each in ENU_3 & ENU_4 and 12 each in ENU_5 & ENU_6.

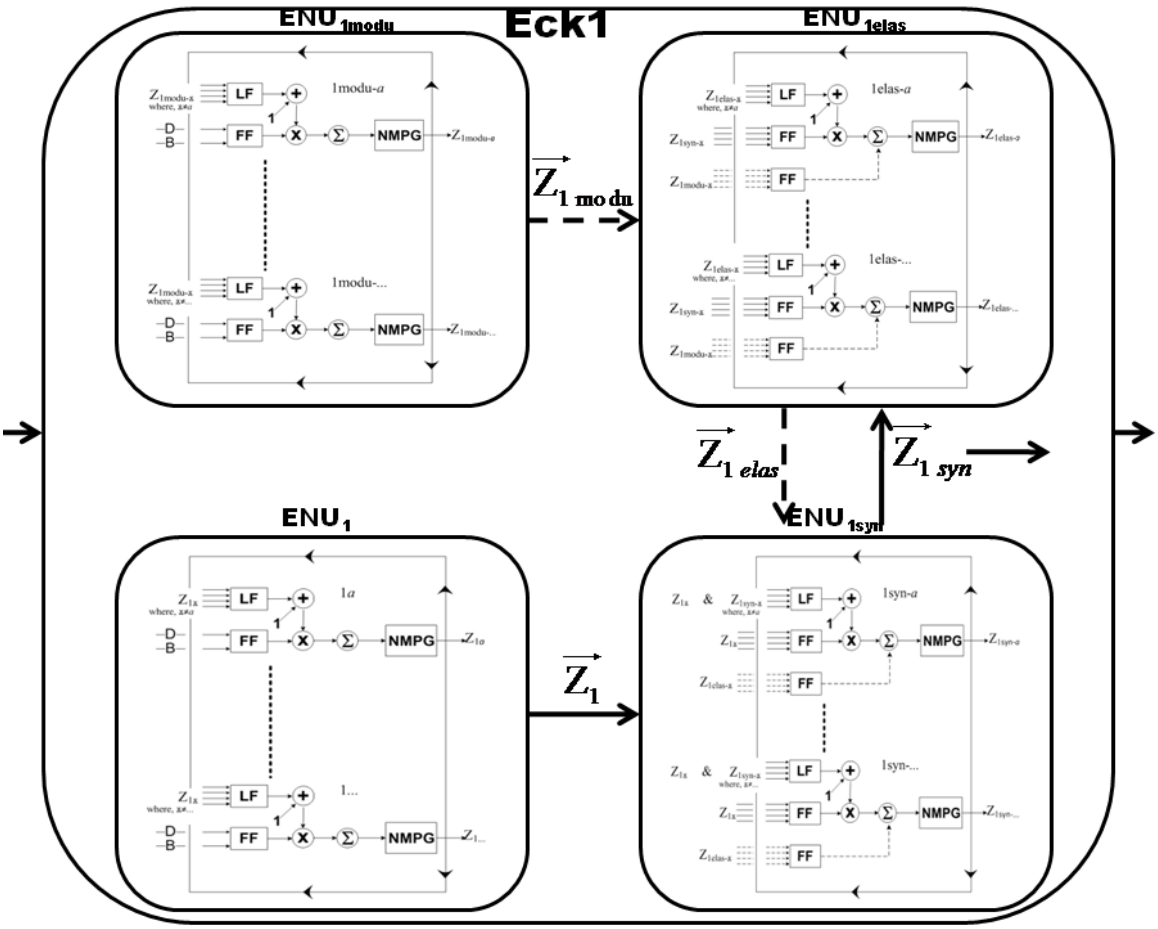

Figure 3.25. Enlarged view of the inset seen in Figure 3.24 showing the configuration of *n*-basic ENU's amongst the four ENU groups (ENU_1, ENU_{1syn}, ENU_{1elas} & ENU_{1modu}) within Eck1.

Feeding field (FF) for all basic ENU's within ENU_1 and ENU_{1modu} group receives input stimulus which in the case of node-1 (Eck1) is the drive (D) and bias (B) stimulus as DC. Outputs of ENU_1 group ($\vec{Z}_1$) are the inputs for the FF of basic ENU's within ENU_{1syn} group. However, outputs of ENU_{1modu} group ($\vec{Z}_{1modu}$) are the inputs for the inhibitory dendrite FF of basic ENU's within ENU_{1elas} group.

ENU_{1syn} group outputs ($\vec{Z}_{1syn}$) in turn are the inputs for the excitatory dendrite FF of basic ENU's within ENU_{1elas} group. The ENU_{1elas} outputs ($\vec{Z}_{1elas}$) are then inputs for the FF of inhibitory dendrite of ENU_{1syn} (i.e., lateral inhibition).

Finally, inputs for Eck3 and Eck4 are from ENU_{1syn} ($\vec{Z}_{1syn}$) of Eck1 and ENU_{2syn} ($\vec{Z}_{2syn}$) of Eck2 respectively.

		E-DN Node									
		1 or 2						3 or 4		5 or 6	
		ENU Group									
ENU Part		ENU_1 or ENU_2	ENU_{1modu} or ENU_{2modu}		ENU_{1syn} or ENU_{2syn}		ENU_{1elas} or ENU_{2elas}		ENU_3 or ENU_4		ENU_5 or ENU_6
		Basic ENU									
Dend.		$ENU_{1a(b,\ldots,l)}$ or $ENU_{2a(b,\ldots,l)}$	$ENU_{1modu\text{-}a(b,\ldots,l)}$ or $ENU_{2modu\text{-}a(b,\ldots,l)}$		$ENU_{1syn\text{-}a(b,\ldots,f)}$ or $ENU_{2syn\text{-}a(b,\ldots,f)}$		$ENU_{1elas\text{-}a(b,\ldots,l)}$ or $ENU_{2elas\text{-}a(b,\ldots,l)}$		$ENU_{3a(b,\ldots,l)}$ or $ENU_{4a(b,\ldots,l)}$		$ENU_{5a(b,\ldots,l)}$ or $ENU_{6a(b,\ldots,l)}$	
LF	w_{lf}	0.5	-		0.5		5		0.5		0.5	
	τ_{lf}	1	-		1		1		1		1	
FF	w_{ff}	0.5	0.25		$1^{(+)}$	$125^{(-)}$	$1^{(+)}$	$0.5^{(-)}$	1		$0.5^{(+)}$	$2^{(-)}$
	τ_{ff}	10	20		$10^{(+)}$	$30^{(-)}$	$10^{(+)}$	$30^{(-)}$	10		$10^{(+)}$	$40^{(-)}$

Table 3.6. Parameters used for the simulation (Fig. 3.26) of E-DN architecture shown in Figure 3.24. Note the lack of linking field in ENU's within ENU_{1modu} & ENU_{2modu} groups. The parameters for soma/neuromime remain the same as in table 3.1.

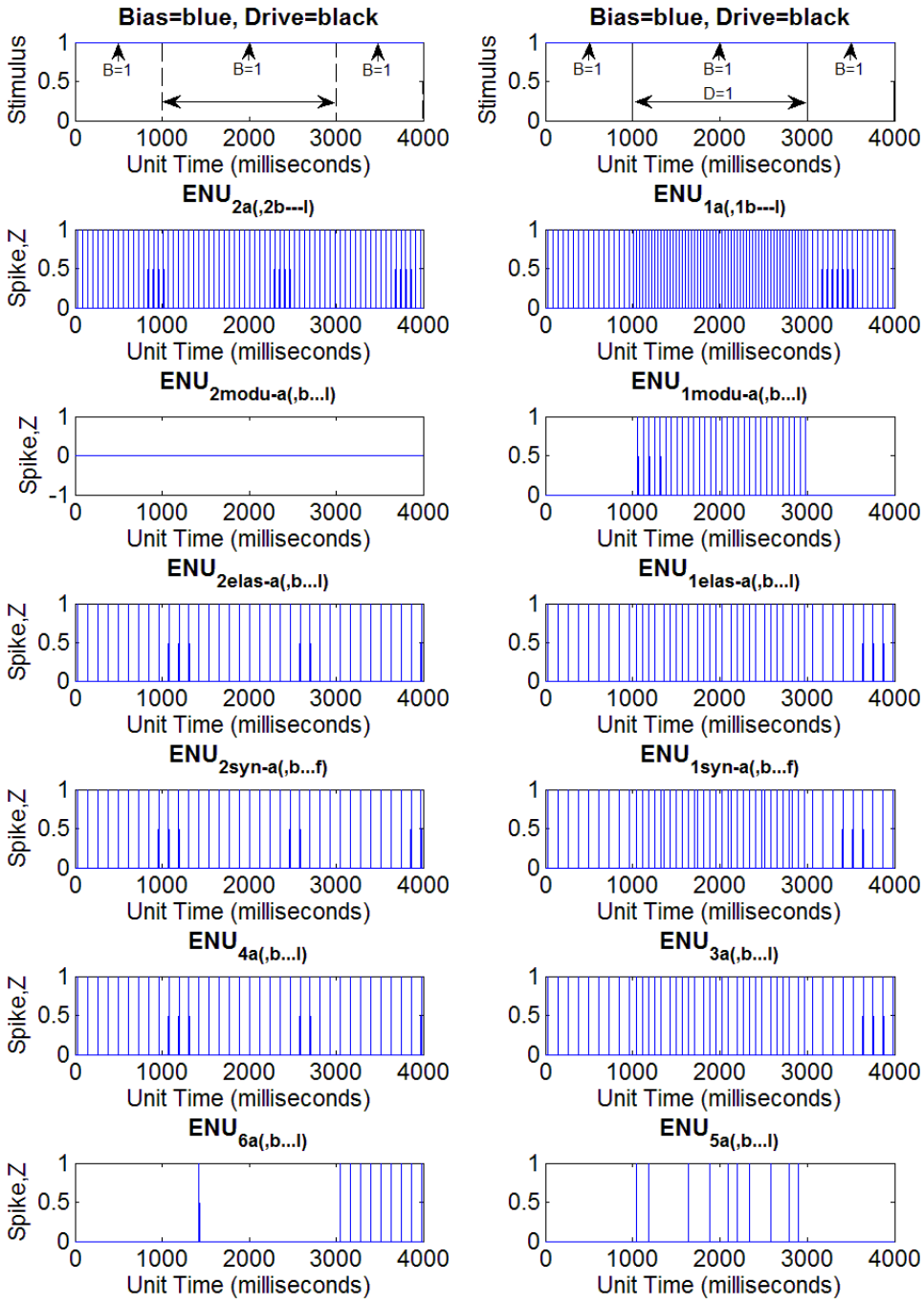

Figure 3.26. Output traces of one basic ENU (ENU_{xa}) implemented (out of 12 each in ENU_1 & ENU_2, 12 each in ENU_{1modu} & ENU_{2modu}, 6 each in ENU_{1syn} & ENU_{2syn}, 12 each in ENU_{1elas} & ENU_{2elas}, 12 each in ENU_3 & ENU_4 and 12 each in ENU_5 & ENU_6 group) in E-DN architecture of Figure 3.24 receiving both B and D-stimulus using parameters (table 3.6).

Output (Fig. 3.26) from Eck5 and Eck6 shows that addition of ENU group (ENU_{1mod} & ENU_{2mod}) responding only during dual-stimuli has altered the spikes. During dual-stimuli and B-stimulus preceding it, Eck5 and Eck6 response is similar to the previous E-DN (Fig. 3.23). However, after removal of D-stimulus spikes occur in Eck6. But this is not the elastic property since it continuously spikes, never getting inhibited from the equally strong pulsed inputs of Eck3.

Five ENU groups within initial nodes (node-1 or Eck1 & node-2 or Eck2)

An alternate connection to the present E-DN (Fig. 3.24 & 3.26) is for ENU_{1elas} and ENU_{2elas} groups to receive excitatory inputs in place of inhibition from ENU_{1mod} and ENU_{2mod} respectively. This would result in ENU_{1syn} group receiving increased inhibition during dual-stimuli. But inhibition by ENU_{1mod} group during dual-stimuli successfully altered the spiking from succeeding nodes (Fig. 3.26). This can be done by decreasing/ weakening the inhibition of ENU_{1syn} and ENU_{2syn} (from respective ENU_{1elas} and ENU_{2elas}) during just B-stimulus to counterbalance the increased inhibition during dual-stimuli.

To achieve the above described network another ENU group is added to the first two nodes (Eck1 & Eck2). The reason is that excitation of ENU_{1elas} group only during dual-stimuli will be from ENU_{1mod}, which is responsive only during this condition while all other ENU groups within Eck1 and Eck2 spike irrespective of this. Thus for weakening the inhibition of ENU_{1syn} and ENU_{2syn}, i.e., inhibiting ENU_{1elas} and ENU_{2elas} (during B stimulus) another ENU group is added in Eck1 ($ENU_{1m\text{-}elas}$) and Eck2 ($ENU_{2m\text{-}elas}$). Thus $ENU_{1m\text{-}elas}$ and $ENU_{2m\text{-}elas}$ outputs occur only during B-stimulus. The new E-DN is shown

in Figures 3.27 and 3.28. Simulation of this network (Fig. 3.29) was done with the parameters given in table 3.7.

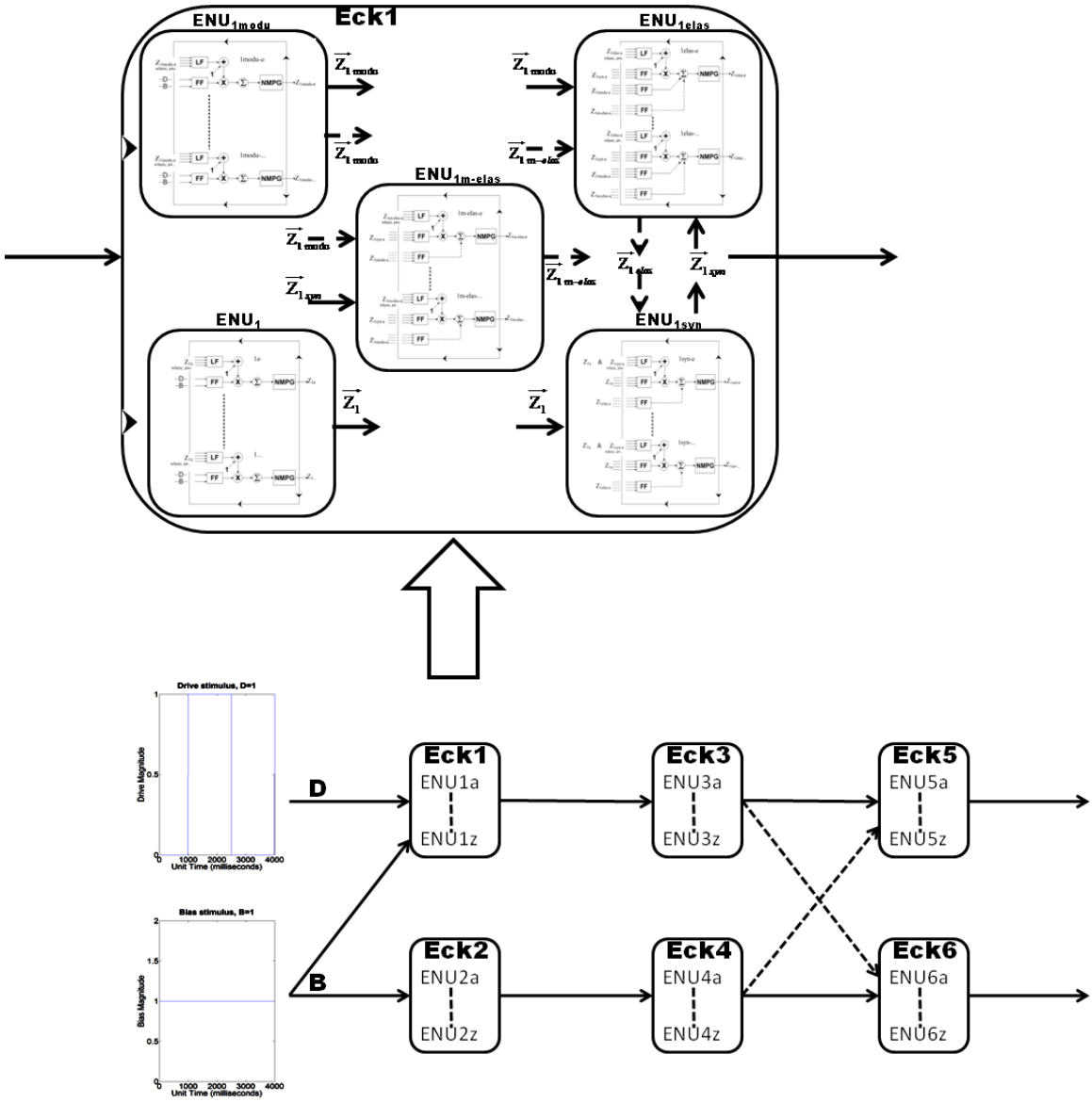

Figure 3.27. E-DN with five ENU groups (ENU_1, ENU_{1syn}, ENU_{1elas}, ENU_{1modu} & $ENU_{1m\text{-}elas}$) in Eck1 (and Eck2) such that ENU_{1elas} receives excitatory pulsed inputs from ENU_{1modu} & ENU_{1syn} but receives inhibitory inputs from $ENU_{1m\text{-}elas}$. The $ENU_{1m\text{-}elas}$ receives excitatory inputs from ENU_{1syn} but inhibitory from ENU_{1modu}.Number of basic ENU's per ENU groups: 12 each in ENU_1 & ENU_2, 6 each in ENU_{1syn} & ENU_{2syn}, 12 each in ENU_{1modu} & ENU_{2modu}, 12 each in ENU_{1elas} & ENU_{2elas}, 12 each in $ENU_{1m\text{-}elas}$ & $ENU_{2m\text{-}elas}$, 12 each in ENU_3 & ENU_4 and 12 each in ENU_5 & ENU_6.

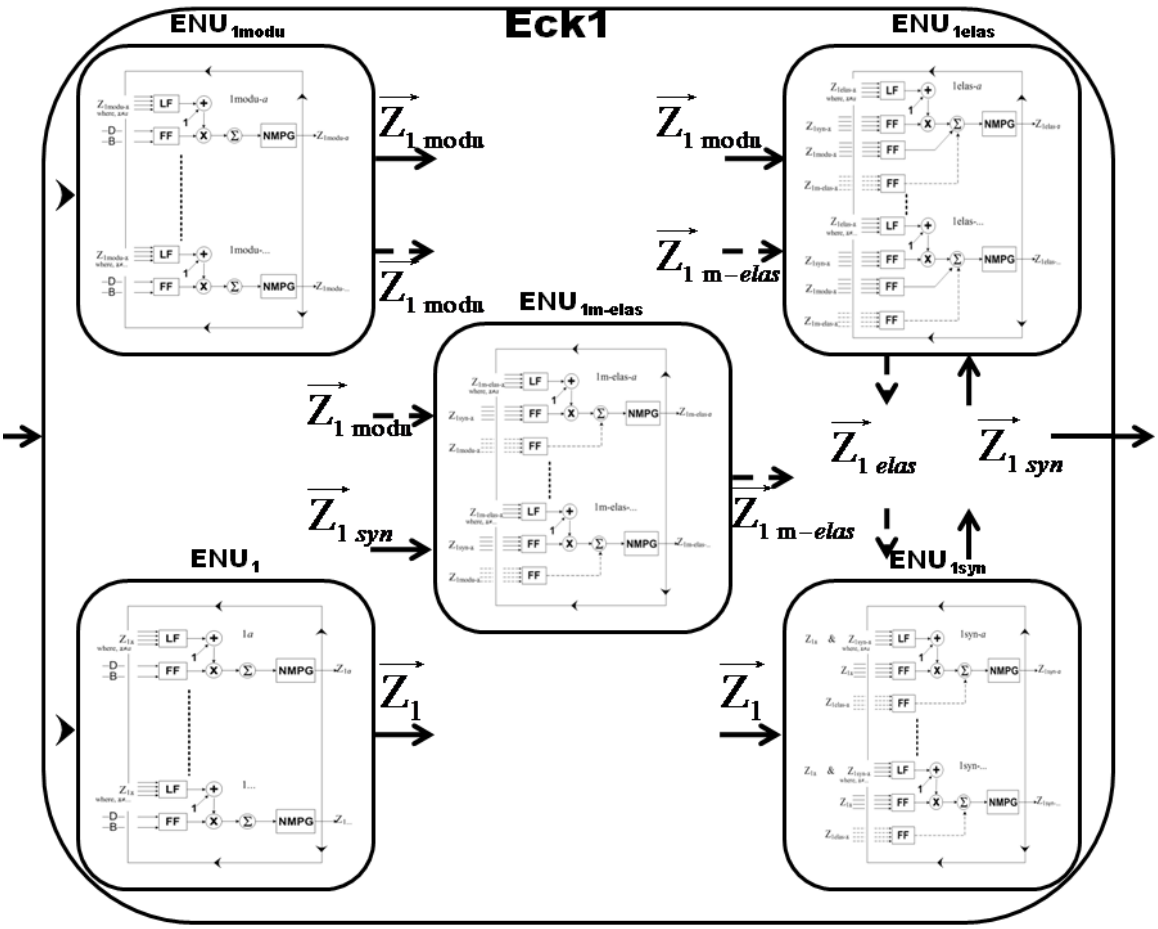

Figure 3.28. Enlarged view of the inset seen in Figure 3.27 showing the configuration of n basic ENU's amongst the five ENU groups (ENU_1, ENU_{1syn}, ENU_{1elas}, ENU_{1modu} & $ENU_{1m\text{-}elas}$) within Eck1.

Feeding field (FF) for all basic ENU's within ENU_1 and ENU_{1modu} group receives input stimulus, which in the case of Eck1 is the drive (D) and bias (B) stimulus as DC. Outputs of ENU_1 group ($\vec{Z}_1$) are the inputs for the excitatory dendrite FF of basic ENU's within ENU_{1syn} group. However, outputs of ENU_{1modu} group ($\vec{Z}_{1modu}$) are the inputs for the excitatory dendrite FF of basic ENU's within ENU_{1elas} group but inputs for inhibitory dendrite FF of basic ENU's within $ENU_{1m\text{-}elas}$ group.

ENU_{1syn} group outputs ($\vec{Z}_{1syn}$) in turn are the inputs for another excitatory dendrite FF of basic ENU's within ENU_{1elas} group and also inputs for excitatory dendrite FF of basic ENU's within $ENU_{1m\text{-}elas}$ group. The $ENU_{1m\text{-}elas}$ outputs ($\vec{Z}_{1m-elas}$) are then inputs for the FF of inhibitory dendrite of ENU_{1elas}.

Finally, ENU_{1elas} outputs ($\vec{Z}_{1elas}$) are the inputs for the FF of inhibitory dendrite of ENU_{1syn} (i.e., lateral inhibition). And inputs for Eck3 and Eck4 are from ENU_{1syn} ($\vec{Z}_{1syn}$) of Eck1 and ENU_{2syn} ($\vec{Z}_{2syn}$) of Eck2 respectively.

		E-DN Node											
		1 or 2								3 or 4		5 or 6	
		ENU Group											
ENU Part		ENU_1 or ENU_2	ENU_{1modu} or ENU_{2modu}	ENU_{1syn} or ENU_{2syn}		ENU_{1elas} or ENU_{2elas}		$ENU_{1m\text{-}elas}$ or $ENU_{2m\text{-}elas}$		ENU_3 or ENU_4		ENU_5 or ENU_6	
		Basic ENU											
Dend.		$ENU_{1a(b,\ldots,l)}$ or $ENU_{2a(b,\ldots,l)}$	$ENU_{1modu\text{-}a(b,\ldots,l)}$ or $ENU_{2modu\text{-}a(b,\ldots,l)}$	$ENU_{1syn\text{-}a(b,\ldots,l)}$ or $ENU_{2syn\text{-}a(b,\ldots,l)}$		$ENU_{1elas\text{-}a(b,\ldots,l)}$ or $ENU_{2elas\text{-}a(b,\ldots,l)}$		$ENU_{1m\text{-}elas\text{-}a(b,\ldots,l)}$ or $ENU_{2m\text{-}elas\text{-}a(b,\ldots,l)}$		$ENU_{3a(b,\ldots,l)}$ or $ENU_{4a(b,\ldots,l)}$		$ENU_{5a(b,\ldots,l)}$ or $ENU_{6a(b,\ldots,l)}$	
LF	w_{lf}	0.5	0.25	0.5		5		0.5		0.5		0.5	
	τ_{lf}	1	1	1		1		1		1		1	
FF	w_{ff}	5	0.25	$1^{(+)}$	$125^{(-)}$	$1^{(+)}$ $0.35^{(+)}$	$1^{(-)}$	$1^{(+)}$	$5^{(-)}$	1		$0.5^{(+)}$	$2^{(-)}$
	τ_{ff}	10	15	$10^{(+)}$	$30^{(-)}$	$10^{(+)}$	$30^{(-)}$	$10^{(+)}$	$40^{(-)}$	10		$10^{(+)}$	$40^{(-)}$

Table 3.7. Parameters used for simulation (Fig. 3.29) of E-DN architecture shown in Figure 3.27. Note: (+) input w_{ff} for ENU_{1elaas} & ENU_{2elas} are different; w_{ff}=1 from ENU_{1syn} & w_{ff}=0.35 from ENU_{1modu}. The parameters for soma/neuromime remain same as in table 3.1.

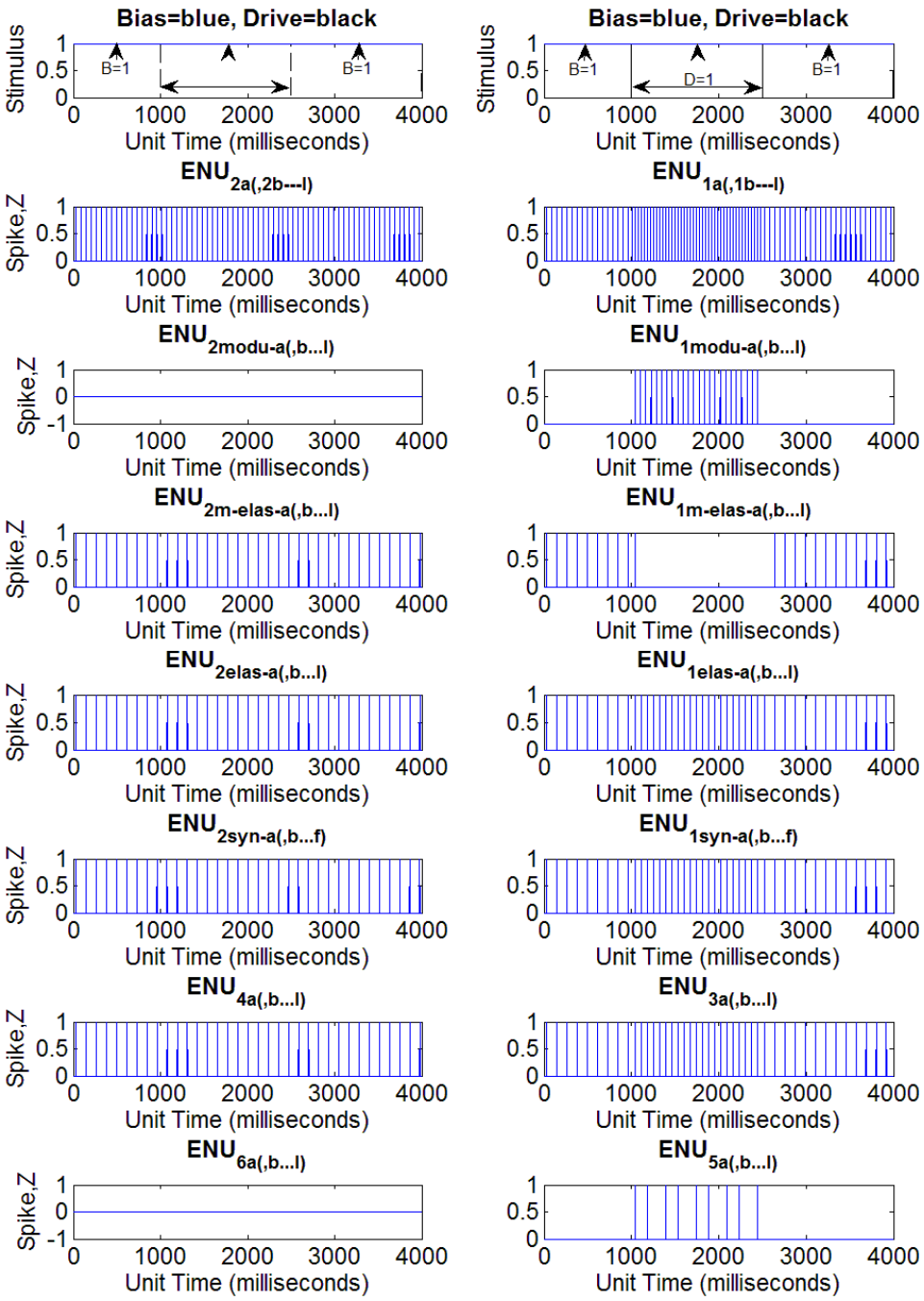

Figure 3.29. Output traces of one basic ENU (ENU_{xa}) implemented (out of 12 each in ENU_1 & ENU_2, 12 each in ENU_{1modu} & ENU_{2modu}, 6 each in ENU_{1syn} & ENU_{2syn}, 12 each in ENU_{1elas} & ENU_{2elas}, 12 each in $ENU_{1m\text{-}elas}$ & $ENU_{2m\text{-}elas}$, 12 each in ENU_3 & ENU_4 and 12 each in ENU_5 & ENU_6 group) in E-DN architecture of Figure 3.27 receiving both B and D-stimulus using parameters in table 3.7.

Outcome of the simulation (Fig. 3.29) resembles the outputs seen earlier (Fig. 3.23) for the E-DN shown in Figure 3.21. This output traces implies increased inhibition of ENU_{1syn} during dual-stimuli. But during B-stimulus the inhibition of ENU_{1elas} and ENU_{2elas} may be insufficient, causing these ENU groups to continue inhibiting ENU_{1syn} and ENU_{2syn} respectively. This is most probably linked with the excessively strong inhibitory feeding field weight ($w_{ff} = 125^{(-)}$) for ENU_{1syn} and ENU_{2syn} (table 3.7). The strong inhibitory feeding field weight parameter has been used since the introduction of ENU_{1elas} and ENU_{2elas} group (Fig. 3.21) with the intent to set a plausible value after achieving the desired network during the build-up process.

Since the introduction of ENU_{1syn} and ENU_{2syn} groups in Eck1 and Eck2 respectively (Fig. 3.17), all pulsed inputs for Eck3 and Eck4 have been from respective ENU_{1syn} and ENU_{2syn} groups. This was also the case in the current E-DN (Fig. 3.27). A different alternative for outputs from first two nodes (Eck1 & Eck2) may be attempted due to failures with networks yet designed.

Inputs for node-3 (Eck3) and node-4 (Eck4) from different ENU groups within the first two nodes (Eck1 & Eck2)

Eck3 and Eck4 inputs from outputs of ENU_1 and ENU_{1syn} (also ENU_2 & ENU_{2syn}) groups within Eck1 might not be the best choice since the main purpose of adding ENU_{1syn} (and ENU_{2syn}) was to achieve synchronization. The output traces (Fig. 3.29) of ENU_{1elas} (and ENU_{2elas}) appear to be similar to ENU_{1syn} (and ENU_{2syn}) and hence will likely produce a similar outcome as Figure 3.29 if outputs from ENU_{1elas} (and ENU_{2elas}) are chosen as inputs for Eck3 (and Eck4). Thus suitable ENU groups can be narrowed

down to a combination of ENU_{1mod} and $ENU_{1m\text{-}elas}$ (also ENU_{2mod} & $ENU_{2m\text{-}elas}$) since during just B-stimulus, outputs from first two nodes (Eck1 & Eck2) would be same due to $ENU_{1m\text{-}elas}$ (and $ENU_{2m\text{-}elas}$) but during dual-stimuli ENU_{1mod} receiving the additional D-stimulus, would be capable of causing spiking in Eck5.

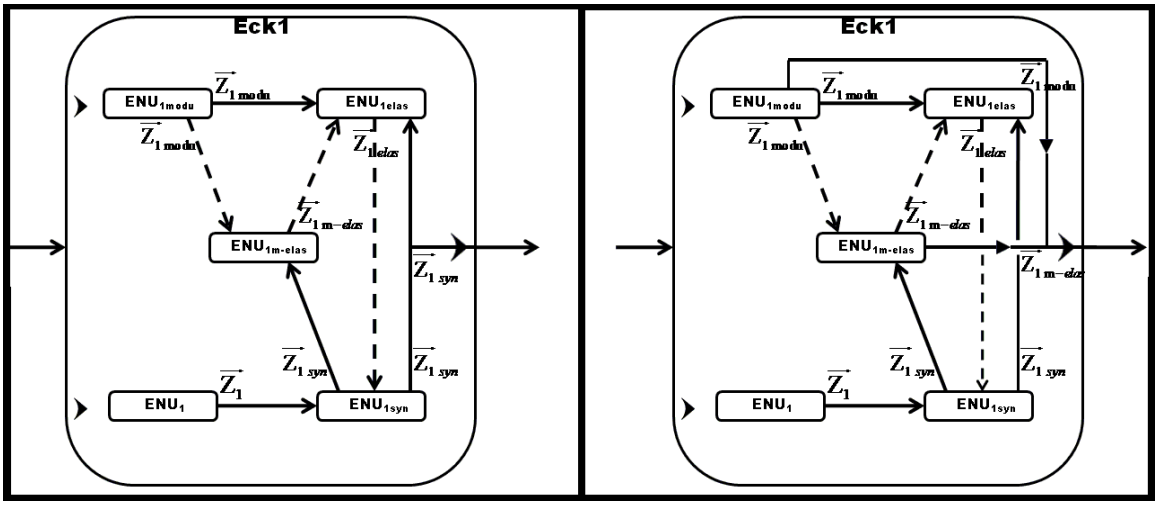

Figure 3.30. Two output configuration for Eck1 (similarly for Eck2, not shown).

Left shows the configuration used for simulating the output traces of figure 3.29 where ENU_{1syn} is the source of pulsed outputs from Eck1 (and similarly ENU_{2syn} for Eck2).

Right shows the new configuration such that both ENU_{1modu} and $ENU_{1m\text{-}elas}$ are the source of output. Both outputs are excitatory (solid line).

Though the figure (right) shows two lines joining to give a single arrow out of Eck1, outputs from the two ENU groups do not summate. However the input vector for Eck3 feeding field has elements of the two ENU group outputs ($\vec{Z}_{1\mathrm{mod}u}$ & $\vec{Z}_{1m-elas}$).

With the new output configuration shown in Figure 3.30 (right) implemented for first two nodes (Eck1 & Eck2) and everything else remaining the same (Fig. 3.27), the new E-DN is derived. The new E-DN was then simulated (Fig. 3.31) with the same parameters (table 3.7) used for previous network.

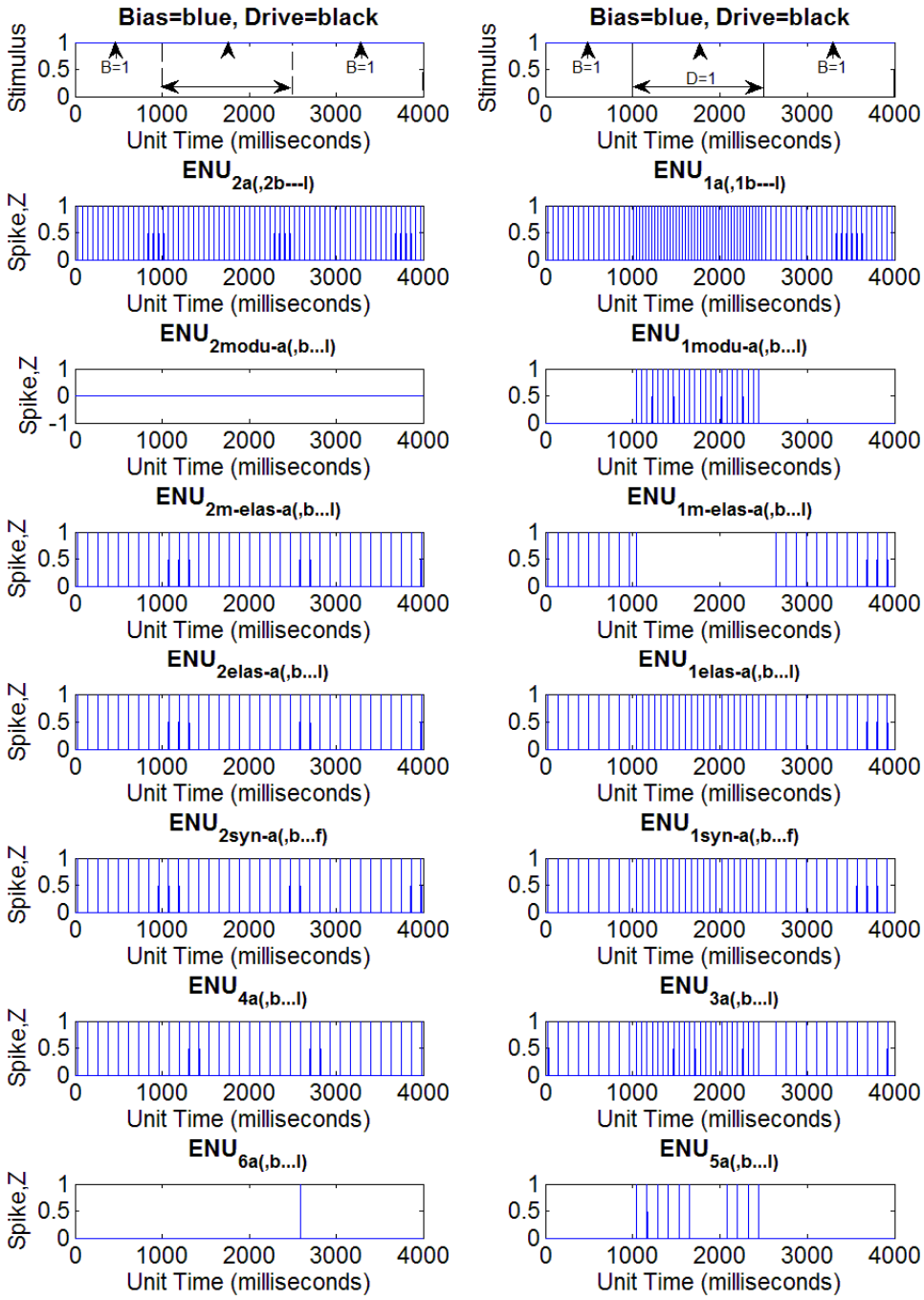

Figure 3.31. Output traces of one basic ENU (ENU_{xa}) implemented (out of 12 each in ENU_1 & ENU_2, 12 each in ENU_{1modu} & ENU_{2modu}, 6 each in ENU_{1syn} & ENU_{2syn}, 12 each in ENU_{1elas} & ENU_{2elas}, 12 each in $ENU_{1m\text{-}elas}$ & $ENU_{2m\text{-}elas}$, 12 each in ENU_3 & ENU_4 and 12 each in ENU_5 & ENU_6 group) in E-DN architecture similar to Figure 3.27 but with output configuration of first two node given by Figure 3.30 (right) receiving both B and D-stimulus using parameters in table 3.7.

The simulation result (Fig. 3.31) shows output in Eck6 soon after the removal of D-stimulus before the equally strong excitatory and inhibitory inputs prevent further outputs from Eck5 and Eck6. This shows that the network, in addition to replicating the property of G-DN encountered in Figure 3.23, also has the potential for replicating the elastic property. The observed results however cannot be considered elastic property since to correspond to the activity seen in G-DN (Fig. 3.7), even though the G-DN activity is very small, Eck6 output should be more than one spike to maintain consistency in activity equivalence mapping between G-DN and E-DN (transformed spikes, Chapter-2, p36-37).

At this stage of network design, with certain amount of success achieved, it was appropriate to refine the E-DN. It should also be mentioned here that the current E-DN has two major problems; some parameter values and the number of basic ENU's implemented. Amongst the parameter values used, the inhibitory feeding field weight ($w_{ff} = 125^{(-)}$) for ENU_{1syn} and ENU_{2syn} is very large (table 3.7). This excessively large w_{ff} for ENU_{1syn} and ENU_{2syn} implies strong inhibition from ENU_{1elas} and ENU_{2elas} respectively. This could be interpreted as, E-DN having many more basic ENU's within ENU_{1elas} and ENU_{2elas} groups (more than 20 each). Hence the two issues are interlinked.

Removal of redundant ENU's and ENU groups

The number of usages of basic ENU's is important not only in terms of computability or computing time but also for making any plausible physical or biological meaning. Basic ENU's are not models at the neuronal level but, due to the absence of reset function, they are abstract model at population level [Wells 2010, Ch.8]. The number of basic ENU's in just the first node (Eck1) of current E-DN is 54 with a total of 166 in all

the six nodes. Considering basic ENU's as population of neurons, usage of such an amount of neuronal resource seems not only unlikely but disadvantageous in the physical world because dipole networks perform a small function in the grand scheme of nervous system.

Refining the current network would therefore mean pruning or removing any redundant ENU groups or basic ENU's within ENU groups. In the current network (Fig. 3.27 but with Eck1 & Eck2 output as shown in Fig. 3.30 right) the purpose of the ENU_{1syn} and ENU_{1elas} groups is eventually to stimulate $ENU_{1m\text{-}elas}$ (similarly for Eck2). Thus only three ENU groups could be implements in the Eck1; ENU_1, ENU_{1modu} and $ENU_{1m\text{-}elas}$ (and similarly for Eck2). This also means that the issue of excessively strong inhibitory feeding field weight ($w_{ff} = 125^{(-)}$) will not exist since ENU_{1syn} (and ENU_{2syn}) is no longer a component of Eck1 (and Eck2). The transformation from 5 ENU groups each per Eck1 and Eck2 to 3 ENU groups is shown in Figures 3.32 through 3.34.

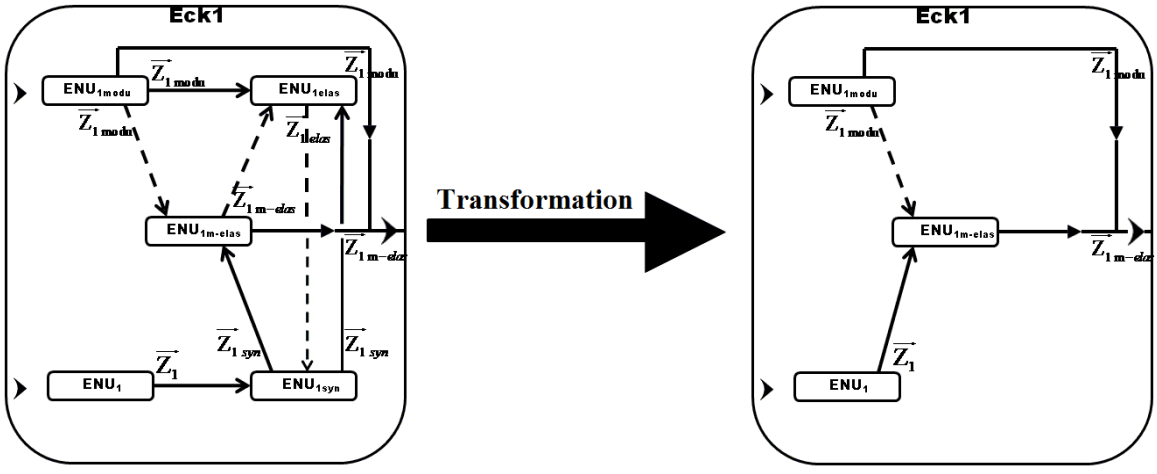

Figure 3.32. Transformation of the components within Eck1 of E-DN following removal of redundant ENU groups (ENU_{1syn} & ENU_{1elas}). Note that though the two ENU groups have been pruned, considering them as redundant, $ENU_{1m\text{-}elas}$ still needs to receive stimulus for it to respond correspondingly to the input (B & D). This is done by receiving excitatory pulsed inputs from ENU_1.

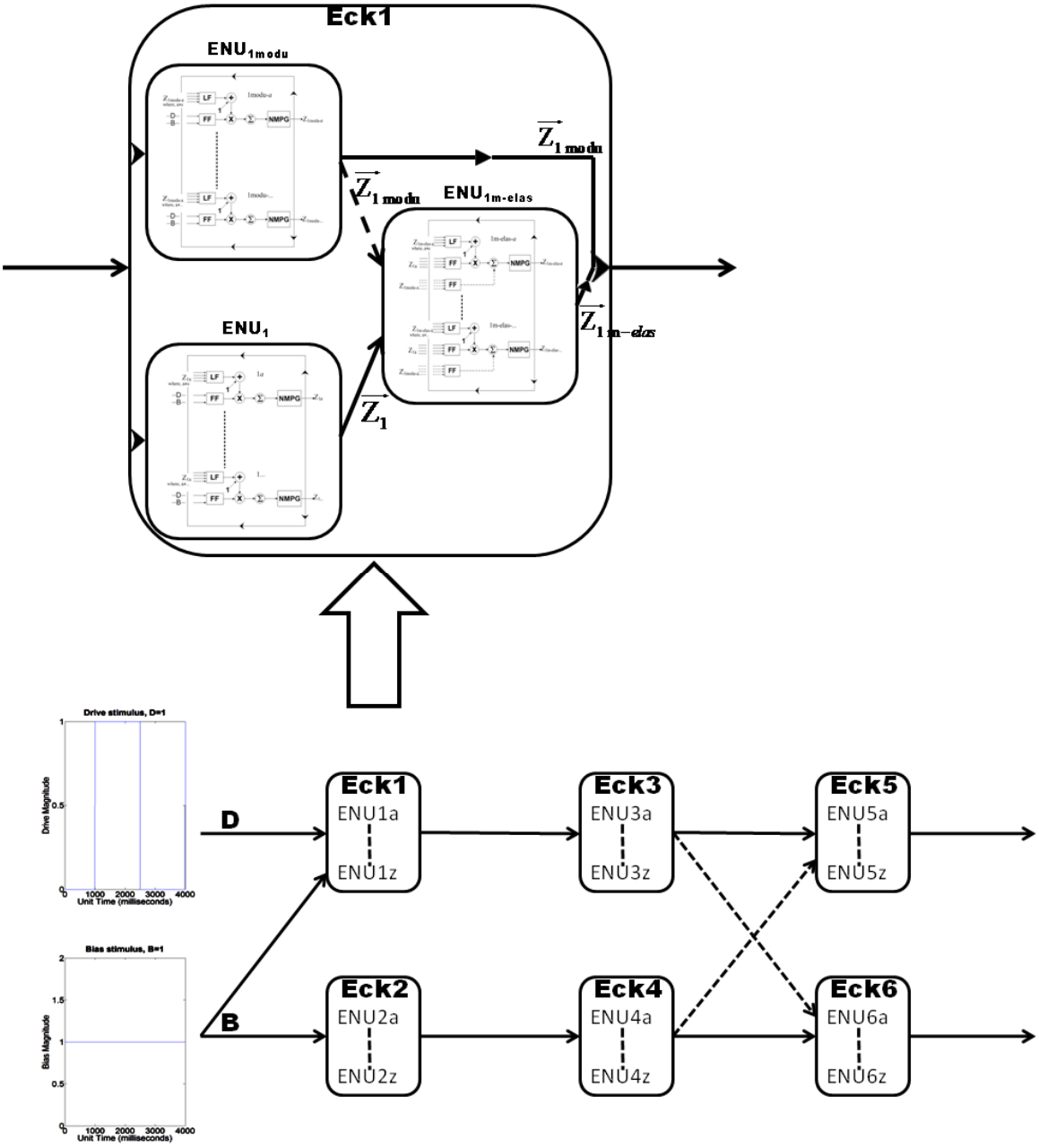

Figure 3.33. E-DN with three ENU groups (ENU_1, ENU_{1modu} & $ENU_{1m\text{-}elas}$) in Eck1 (and Eck2) such that $ENU_{1m\text{-}elas}$ receives excitatory pulsed inputs from ENU_1 but receives inhibitory inputs from ENU_{1modu}. Then both $ENU_{1m\text{-}elas}$ & ENU_{1modu} send outputs for Eck1. Number of basic ENU's per ENU groups: 5 each in ENU_1 & ENU_2, 5 each in ENU_{1modu} & ENU_{2modu}, 5 each in $ENU_{1m\text{-}elas}$ & $ENU_{2m\text{-}elas}$, 2 each in ENU_3 & ENU_4 and 2 each in ENU_5 & ENU_6.

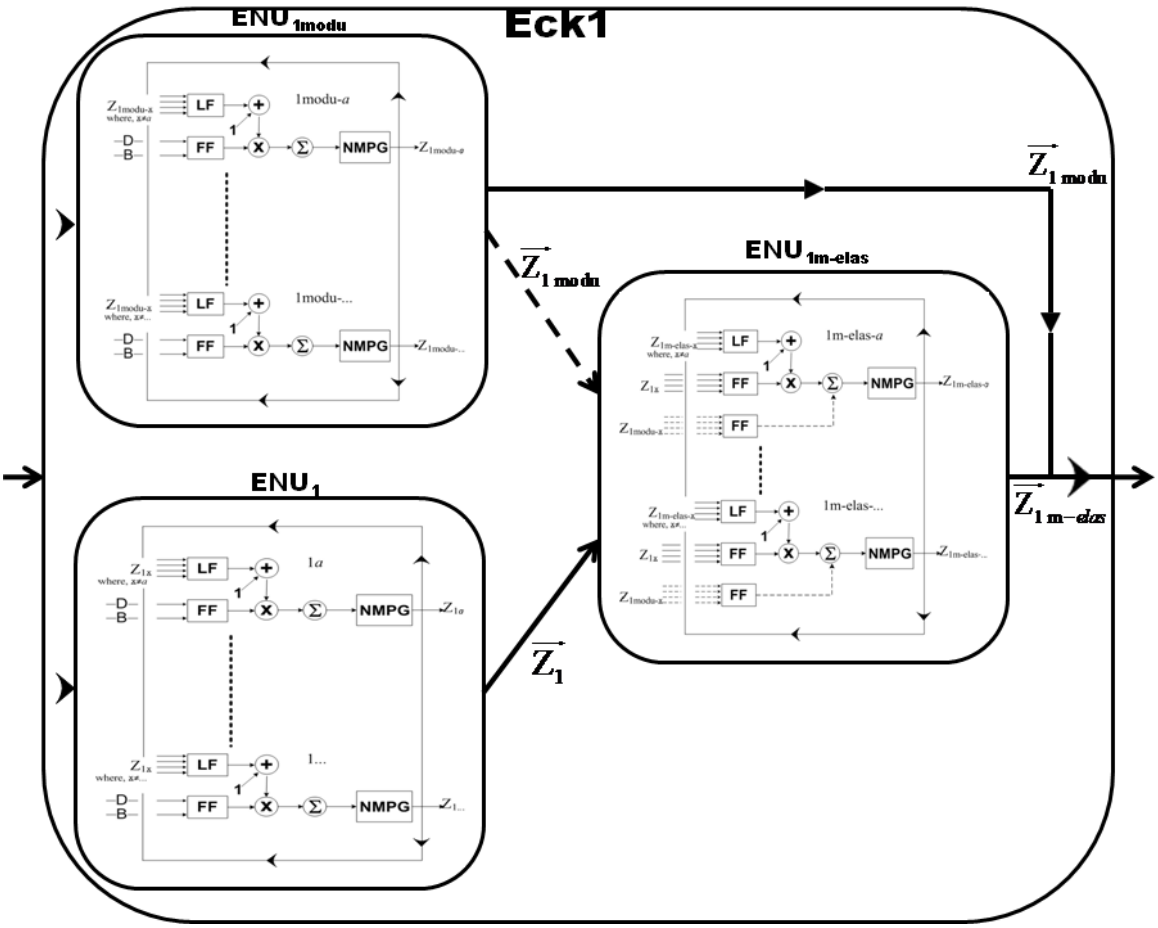

Figure 3.34. Enlarged view of the inset seen in Figure 3.33 showing the configuration of n basic ENU's amongst the three ENU groups (ENU_1, ENU_{1modu} & $ENU_{1m\text{-}elas}$) within Eck1.

Feeding field (FF) for all basic ENU's within ENU_1 and ENU_{1modu} group receives input stimulus which in the case of Eck1 is the drive (D) and bias (B) stimulus as DC. Outputs of ENU_1 group ($\vec{Z}_1$) are the inputs for the excitatory dendrite FF of basic ENU's within $ENU_{1m\text{-}elas}$ group. However, outputs of ENU_{1modu} group ($\vec{Z}_{1modu}$) are the inputs for the inhibitory dendrite FF of basic ENU's within $ENU_{1m\text{-}elas}$ group.

Finally, inputs for Eck3 and Eck4 are from ENU_{1modu} ($\vec{Z}_{1modu}$) and $ENU_{1m\text{-}elas}$ ($\vec{Z}_{1m-elas}$) of Eck1 and from ENU_{2modu} ($\vec{Z}_{2modu}$) and $ENU_{2m\text{-}elas}$ ($\vec{Z}_{2m-elas}$) of Eck2 respectively.

Further pruning of the network can be done by decreasing the number of basic ENU's in other nodes apart from the first two nodes (Eck1 & Eck2) as shown in Figure 3.34 and 3.35. It should be noted that the new E-DN has 15 basic ENU's in Eck1 and a total of 38,

which is considerably less than 54 and 166 total for the previous network. New parameter values (table 3.8) were then used for simulation of the new E-DN. The result is shown in Figure 3.36.

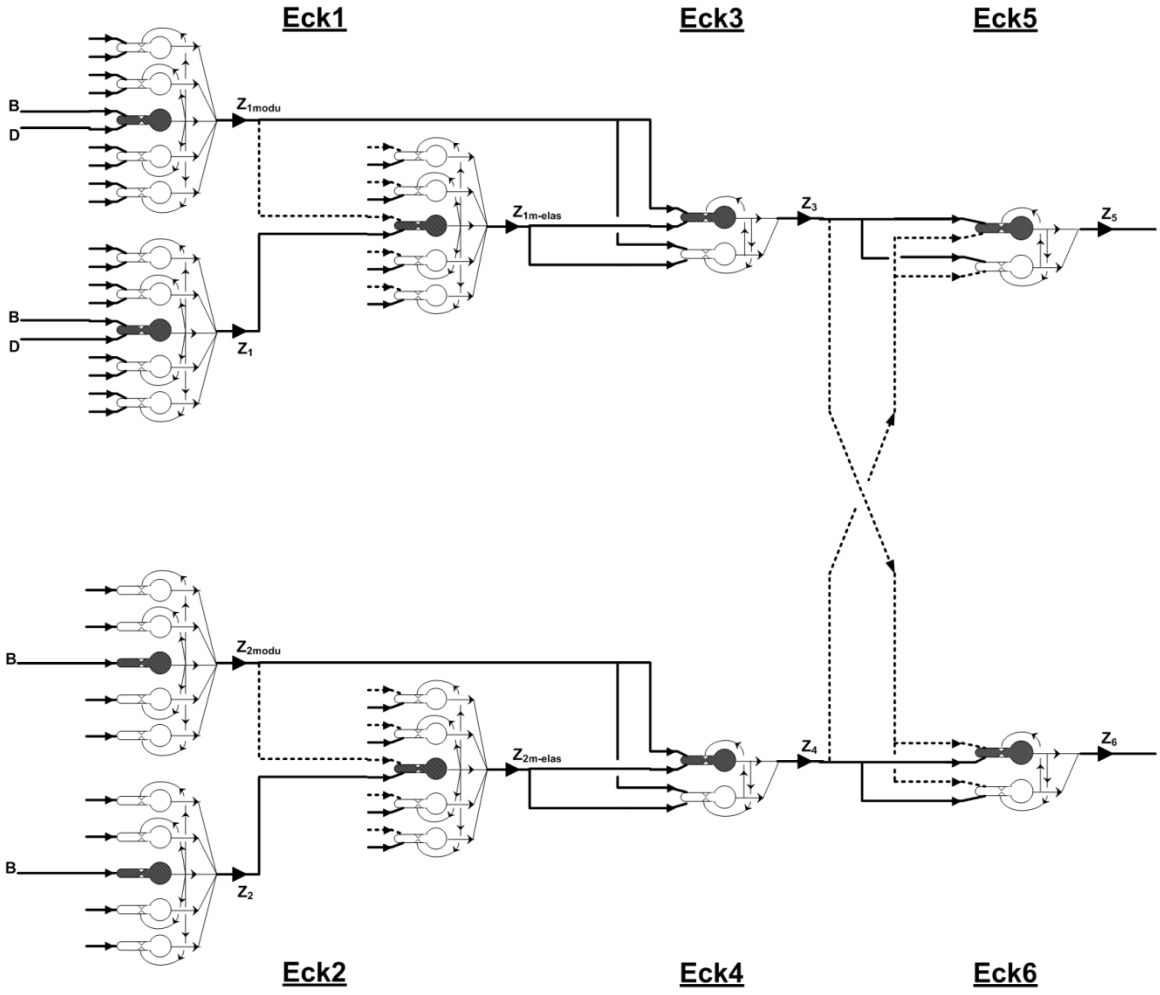

Figure 3.35. Dipole Network using basic ENU as seen in Figure 2.5. Connections of one basic ENU per ENU group in the nodes (shaded basic ENU's) is shown for clarity. Notation for the lines representing connection are same as before (solid for excitatory and dashed for inhibitory).

ENU Part Dend.		E-DN Node						
		1 or 2				3 or 4	5 or 6	
		ENU Group						
		ENU_1 or ENU_2	ENU_{1modu} or ENU_{2modu}	$ENU_{1m\text{-}elas}$ or $ENU_{2m\text{-}elas}$		ENU_3 or ENU_4	ENU_5 or ENU_6	
		Basic ENU						
		$ENU_{1a(b,\ldots,e)}$ or $ENU_{2a(b,\ldots,e)}$	$ENU_{1modu\text{-}a(b,\ldots,e)}$ or $ENU_{2modu\text{-}a(b,\ldots,e)}$	$ENU_{1m\text{-}elas\text{-}a(b,\ldots,e)}$ or $ENU_{2m\text{-}elas\text{-}a(b,\ldots,e)}$		$ENU_{3a(3b)}$ or $ENU_{4a(4b)}$	$ENU_{5a(5b)}$ or $ENU_{6a(5b)}$	
LF	w_{lf}	0.5	0.5	0.5		0.5	0.5	
	τ_{lf}	1	1	1		1	1	
FF	w_{ff}	0.5	0.25	$1^{(+)}$	$12^{(-)}$	$1.2^{(+)}$	$3^{(+)}$	$12^{(-)}$
	τ_{ff}	10	15	$10^{(+)}$	$40^{(-)}$	$10^{(+)}$	$10^{(+)}$	$40^{(-)}$

Table 3.8. Parameters used for simulation (Fig. 3.36) of E-DN shown in Figure 3.33. The parameters for soma remain same as in table 3.1.

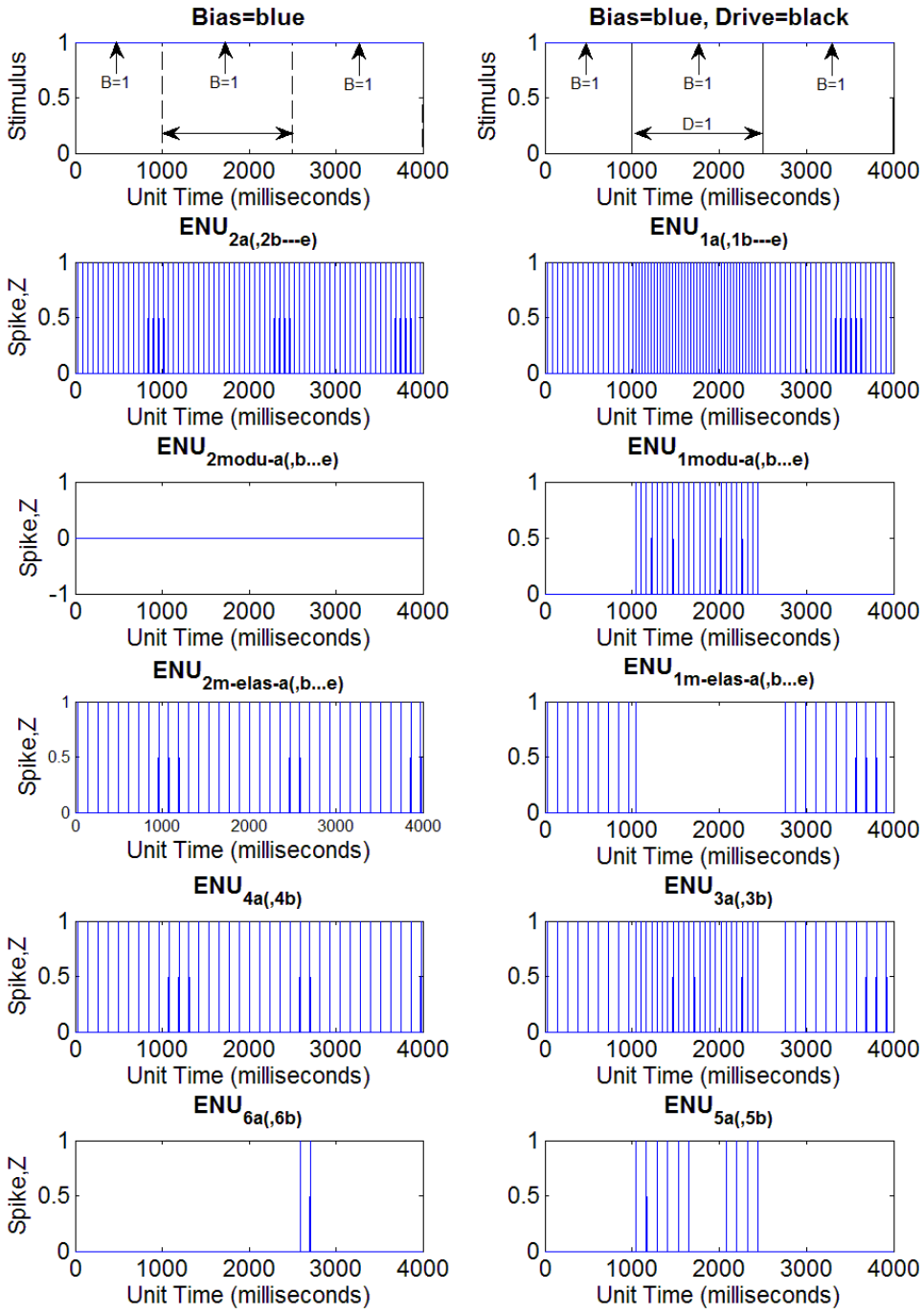

Figure 3.36. Output traces of one basic ENU (ENU_{xa}) implemented (out of 5 each in ENU_1 & ENU_2, 5 each in ENU_{1modu} & ENU_{2modu}, 5 each in $ENU_{1m\text{-}elas}$ & $ENU_{2m\text{-}elas}$, 2 each in ENU_3 & ENU_4 and 2 each in ENU_5 & ENU_6 group) in E-DN architecture of Figure 3.34 & 3.35 receiving both B and D-stimulus using parameters (table 3.8).

Simulation result (Fig. 3.36) for the E-DN (Fig. 3.34 & 3.35) shows that the network has the properties that replicate G-DN seen earlier (Fig. 3.1 & 3.2) and also the elastic property (Fig. 3.6 & 3.7). It should be noted that unlike the earlier output trace (Figure 3.31) the spiking from sixth node after dual-stimuli, though just two spikes, can be considered as an elastic property. This is because the approach that would be implemented for transforming outputs from E-DN to compare the performance of G-DN is based on moving point average.

Pulsed inputs and addition of M-node for the final design (E-N)

As mentioned earlier it should be pointed out that all the designed E-DN's receive DC (constant) input stimulus. Hence for E-DN to be considered a proper PCNN (pulse-coded neural network), the E-DN should be receiving pulsed inputs. That is, basic ENU's of ENU_1 (& ENU_2) and ENU_{1mod} (& ENU_{2mod}) groups within the first two nodes (Eck1 & Eck2) of the E-DN (Fig. 3.35 & 3.36) should receive pulsed inputs corresponding to the DC stimuli. And similarly sensory pulses for the E-N.

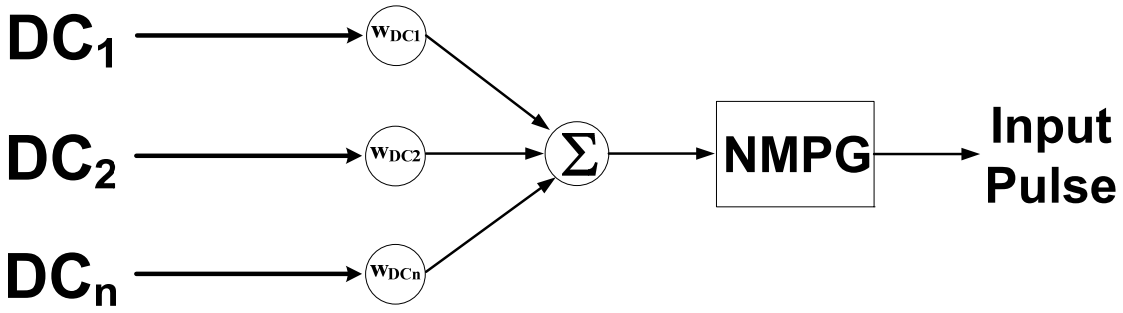

Figure 3.37. General scheme for generating pulsed inputs for E-N architecture shown in Figure 3.38. DC_n is the DC (constant) input for the n^{th} stimulus and w_{DCn} is the weight parameter for respect DC input. Input for the pulse generator (NMPG, neuromime) is therefore $\sum_{\forall n} DC_n \bullet w_{DC_n}$.

Generation of pulsed inputs can be achieved by considering just the neuromime (NMPG) or soma component of the basic ENU such that it receives inputs as the sum of products of DC inputs with respective parameter values (weights), as shown in Figure 3.37. Parameter values of input pulse generators for ENU groups within Eck1 and Eck2, i.e., for ENU_1 (& ENU_2) and ENU_{1mod} (& ENU_{2mod}), and also for the sensory pulses, are shown in table 3.9.

Pulsed Inputs for:	**weights**	**NMPG**		
		V_{pg}	θ_o	τ_{pg}
ENU_1 or ENU_2	$w_B = 0.5$ $w_D = 5 \bullet 10^{-3}$	5	0.5	5
ENU_{1mod} or ENU_{2mod}	$w_B = 5 \bullet 10^{-3}$ $w_D = 0.5$	5	0.5	15
Sensory Pulse	$w_S = 5$	50	0.5	15

Table 3.9. Parameters for pulse generator scheme (Fig. 3.37) for generating input pulses (Fig. 3.38 & 3.39) of E-N architecture shown in Figure 3.39.

Using pulsed inputs in the working architecture of E-DN, the final step is to build the E-N system, i.e., the Eckhorn network (E-N) analogue of Grossberg's network (G-N), which is a dipole network that receives the additional sensory stimulus and whose outputs are sent to a motor node (M-node). Figure 3.38 shows the simulation results (with parameters in table 3.10) during pre-learning stage of the E-N which functionally corresponds to G-N (Fig. 2.7). E-N shown in Figure 3.39 will therefore be the network for comparing the performance with those of G-N to achieve the goal of adaptive PCNN.

ENU Part		**E-DN Node**							**M-Node**	
		1 or 2				3 or 4	5 or 6		M	
		ENU Group								
		ENU_1 or ENU_2	ENU_{1modu} or ENU_{2modu}	$ENU_{1m\text{-}elas}$ or $ENU_{2m\text{-}elas}$		ENU_3 or ENU_4	ENU_5 or ENU_6		ENU_M	
		Basic ENU								
		$ENU_{1a(b,\ldots,e)}$ or $ENU_{2a(b,\ldots,e)}$	$ENU_{1modu\text{-}a(b,\ldots,e)}$ or $ENU_{2modu\text{-}a(b,\ldots,e)}$	$ENU_{1m\text{-}elas\text{-}a(b,\ldots,e)}$ or $ENU_{2m\text{-}elas\text{-}a(b,\ldots,e)}$		$ENU_{3a(3b)}$ or $ENU_{4a(4b)}$	$ENU_{5a(5b)}$ or $ENU_{6a(5b)}$		ENU_{Ma}	
LF	w_{lf}	0.5	0.5	0.5		0.5	0.5		0.5	
	τ_{lf}	1	1	1		1	1		1	
FF	w_{ff}	5	5	$1^{(+)}$	$0.5^{(-)}$	$1.2^{(+)}$	$2.5^{(+)}$	$5\bullet10^{-6(-)}$	$2.5^{(+)}$ $5\bullet10^{-6\,(+)}$	$2.5^{(-)}$
	τ_{ff}	10	10	$10^{(+)}$	$30^{(-)}$	$10^{(+)}$	$10^{(+)}$	$30^{(-)}$	$10^{(+)}$	$30^{(-)}$
SOMA	V_{pg}	50	50	50		50	50		50	
	θ_o	0.5	0.5	0.5		0.5	0.5		0.5	
	τ_{pg}	5	5	7.5		7.5	7.5		7.5	

Table 3.10. Parameters for simulation of E-N (Figs. 3.38 & 3.39). ENU_{Ma} FF weights (w_{ff}) = $2.5^{(+)}$ & $2.5^{(-)}$ with E-DN outputs.

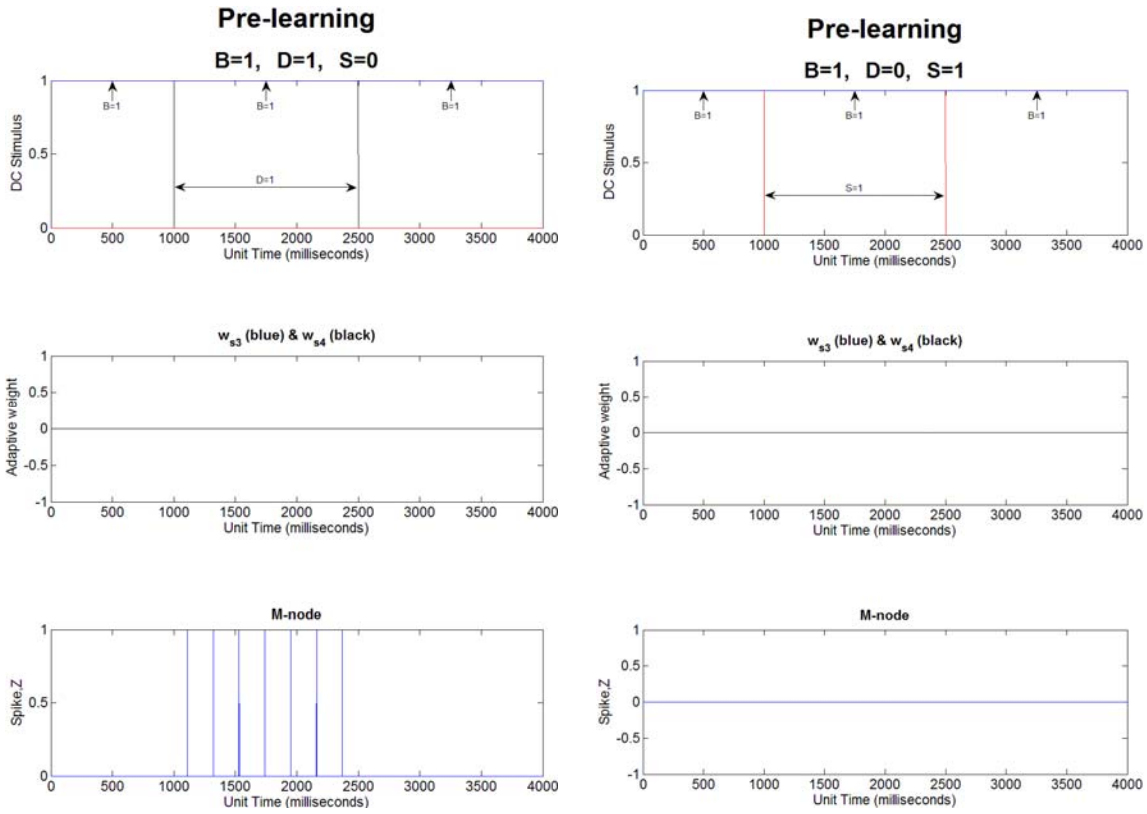

Figure 3.38. Simulation (time-step, $\Delta t=1$) of E-N shows network behavior prior to learning/conditioning which corresponds to simulation for G-N seen in Figure 2.7. [plots for pulsed inputs are not shown in this view]

Left: M-node activity (bottom) during B & D stimulus (top) representing unconditioned response to D-stimulus. No learning takes place (middle).

Right: prior to conditioning and hence before association process between conditioning (S) stimulus and unconditioned (D) stimulus, there is no M-node activity (bottom) with S-stimulus.

In both cases w_{s3} and w_{s4} remains zero, i.e., no learning takes place and hence blue (w_{s3}) and black (w_{s4}) values are overlapping.

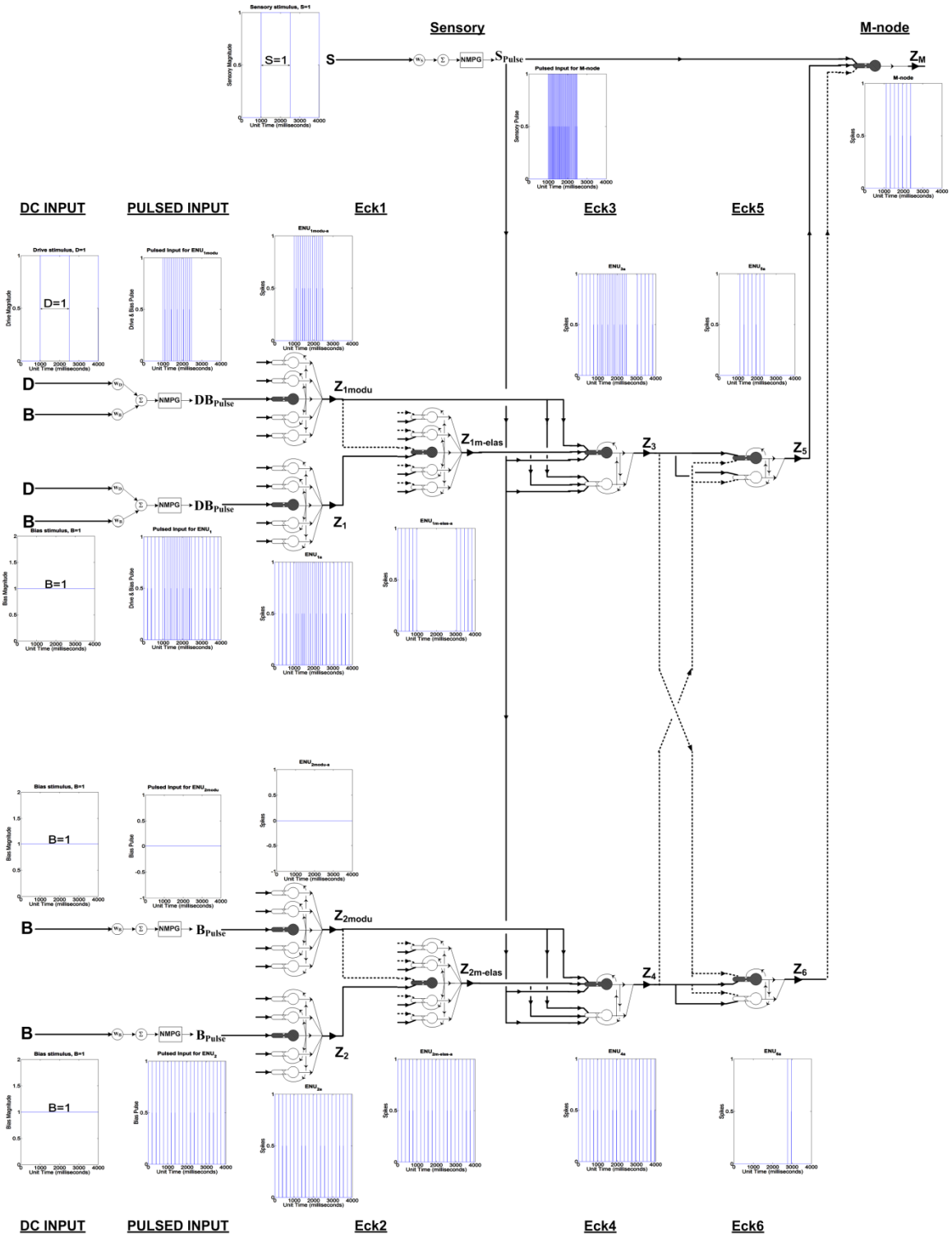

Figure 3.39. E-N for deriving the adaptive PCNN. This E-N is the E-DN (Fig. 3.34 & 3.35) but with input pulses of B, D and also S (sensory) stimulus (Fig. 3.37). The outputs of E-DN, in addition to Sensory pulse (S_{pulse}), are the ENU inputs in M-node (motor node). Notation for the lines representing connection are same as before (solid for excitatory and dashed for inhibitory). The parameters are given in table 3.10.

CHAPTER 4

Understanding the behaviors of E-DN

The reticular formation/system is responsible for 'alert' or 'wakeful' component of consciousness (medical definition). Within the dipole network (DN), tonic arousal is represented by B-stimulus (bias). This means that in a realistic scenario the DN does not receive continuous tonic arousal (B-stimulus) either due to inhibitions preventing arousal or due to exhaustion of neurotransmitters (metabotropic) responsible for arousal (Fig. 4.1).

This chapter deals with the hypothetical case of a single DN receiving continuous tonic arousal (B-stimulus). This is simulated with continuous run of B – D&B – B stimulus trial for number of times. The test run is done in various ways. For instance, duration of the dual-stimuli (D&B) packets is lengthened (from 1.5 to 2 seconds) for the simulation run shown in Figure 4.2.

At least two significantly different DN behaviors (with respect to Eck5 & Eck6 outputs) are observed. From the end of DN channel (Eck6) receiving just B-stimulus, one behavior is the rebound property during B-stimulus following dual-stimuli. Another is continuous spiking from Eck6 in contrast to the short spiking interval for rebound property. This later behavior is a departure from DN behavior (rebound) described in earlier chapter. It should be mentioned here that this is not the case for G-DN, whose behavior remains unchanged. The next step is therefore, investigation for the causes of such behaviors in the E-DN (and also the E-N) to help us better understand the network.

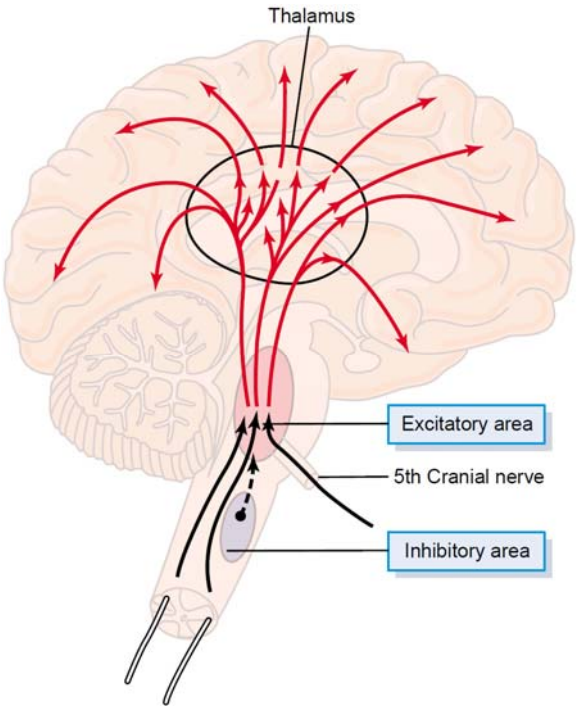

Figure 4.1. Reticular system of the human brain (adapted from [Guyton & Hall 2006]).

Reticular Excitatory area:

Location- This central driving component of reticular system is located in the reticular substance of pons and mesencephalon. This area is also called bulboreticular facilitory area.

Function (Peripheral)- Transmits facilitory signals down the spinal cord to maintain tone in antigravity muscles and control levels of reflex activities.

Function (Central)- Upward signals passing through thalamus can functionally be divided as: 1) fast action-potentials exciting cerebrum for few milliseconds (acetylcholine is the common neurotransmitter), and

2) slow signals (via small slow conducting fibers mainly in intralaminal & reticular nuclei of thalamus) build up progressively for seconds to a minute or more to control long-term background excitability level of the brain.

Reticular Inhibitory area:

Location- medial and ventral regions in medulla.

Function- Inhibit or depress the excitatory (or activation) system. One mechanism on how it does this is by exciting serotonergic neurons secreting inhibitory neurohormone serotonin at specific brain sites. For instance, serotonin released in diencephalons and cerebrum plays an essential inhibitory role to cause sleep.

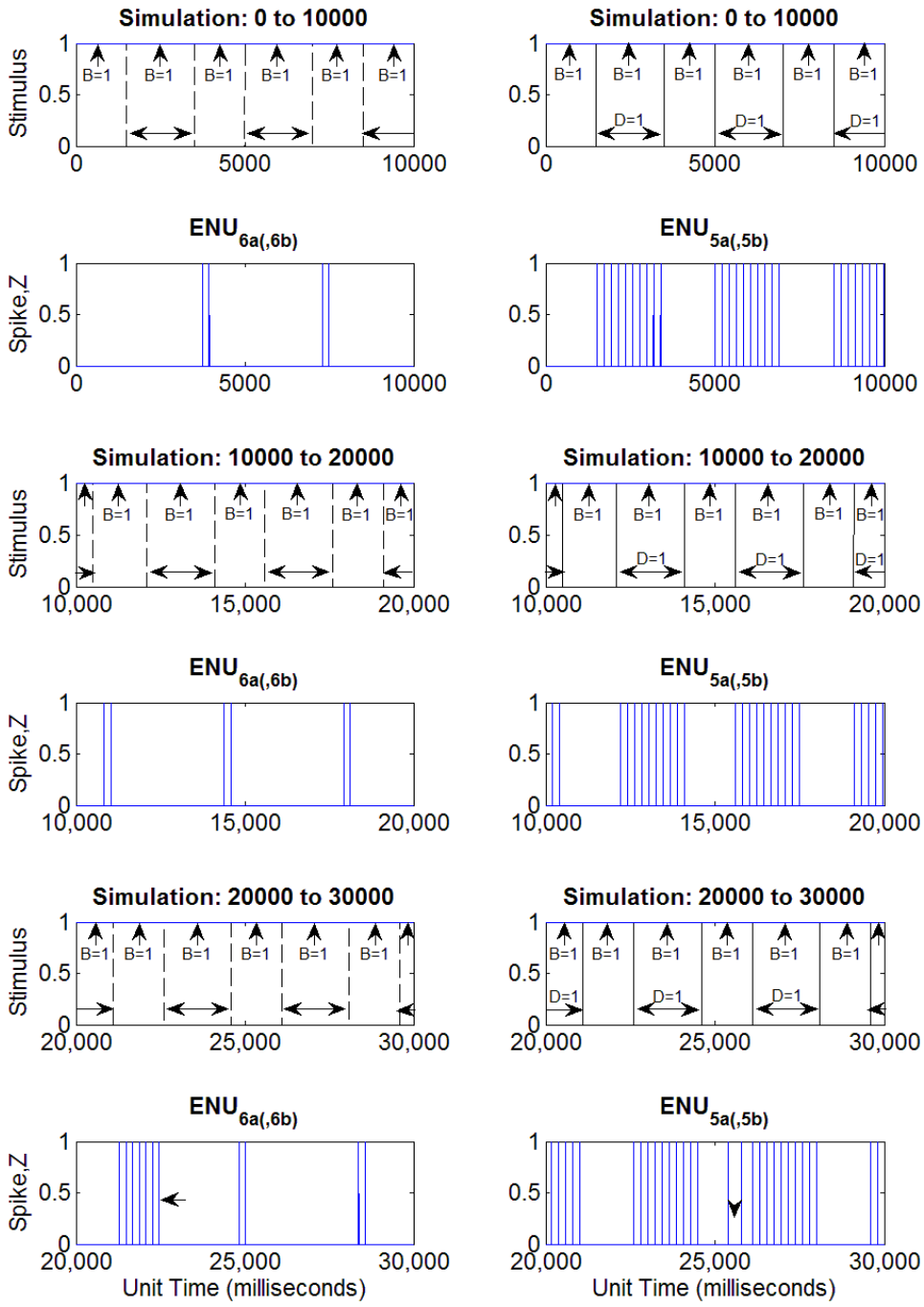

Figure 4.2. Simulation of E-DN part of E-N (Fig. 3.39) with recurring trial of B – D&B – B stimulus, such that duration of B-stimulus is 1500 ms and duration of dual-stimuli packets is 2000 ms. Above shows the simulation for 30 seconds. Arrow (bottom left corner) indicate node-6 (Eck6) spiking continuously during B-stimulus following dual-stimuli. Arrow-head (bottom right) indicate Eck5 spiking prior to dual-stimuli.

Basic ENU's within $ENU_{1m\text{-}elas}$ group at high-pass mode spiking relative to those in $ENU_{2m\text{-}elas}$ (all-pass mode) determines rebound property.

As mentioned earlier $ENU_{1m\text{-}elas}$ group is at the initial node (Eck1) getting inhibition from ENU_{1modu} triggered by dual-stimuli (extinguishing any activity from $ENU_{1m\text{-}elas}$ group). This inhibition forces $ENU_{1m\text{-}elas}$ to fire in high-pass mode while $ENU_{2m\text{-}elas}$ remains in all-pass mode. Thus, during B-stimulus following dual-stimuli $ENU_{1m\text{-}elas}$, now in high-pass mode, fires with a delay. During this delay $ENU_{2m\text{-}elas}$ activated ENU_4 sneaks some excitatory spikes into ENU_6 (but no inhibitory spikes from ENU_5). This triggers spiking from ENU_6. However, whether this ENU_6 spiking demonstrates rebound property depends on the relative spike occurrences between $ENU_{1m\text{-}elas}$ and $ENU_{2m\text{-}elas}$, post dual-stimuli. Note that spiking from either $ENU_{1m\text{-}elas}$ or $ENU_{2m\text{-}elas}$ has the same inter-spike intervals and the resulting spikes from ENU_3 and ENU_4 (both in all-pass mode) respectively are the reflections of their sources.

Figures 4.3 and 4.4 shows that if two ENU_3 spikes (double arrow, Fig. 4.4) activated by $ENU_{1m\text{-}elas}$ (in high-pass mode) after the delay occurs such that ENU_4 spikes (single arrow, Fig. 4.4) within a certain interval between the two ENU_3 spikes, then the ENU_4 spike is unsuccessful in exciting ENU_6 (in Eck6). This is also the case for all succeeding ENU_4 spikes. Thus, ENU_6 spikes during the delay demonstrate rebound property of the network. However, if ENU_4 spiking (single arrow, Fig. 4.6) occurs outside this interval Eck6 spiking ensues. That is, spiking from Eck6 occurs during the whole duration of B-stimulus following dual-stimuli (Fig. 4.5). This does not represent rebound property. We shall call this persistent-Eck6 spiking. Following these observations, next step would be the determination of interval during which ENU6 (within Eck6) spiking occurs.

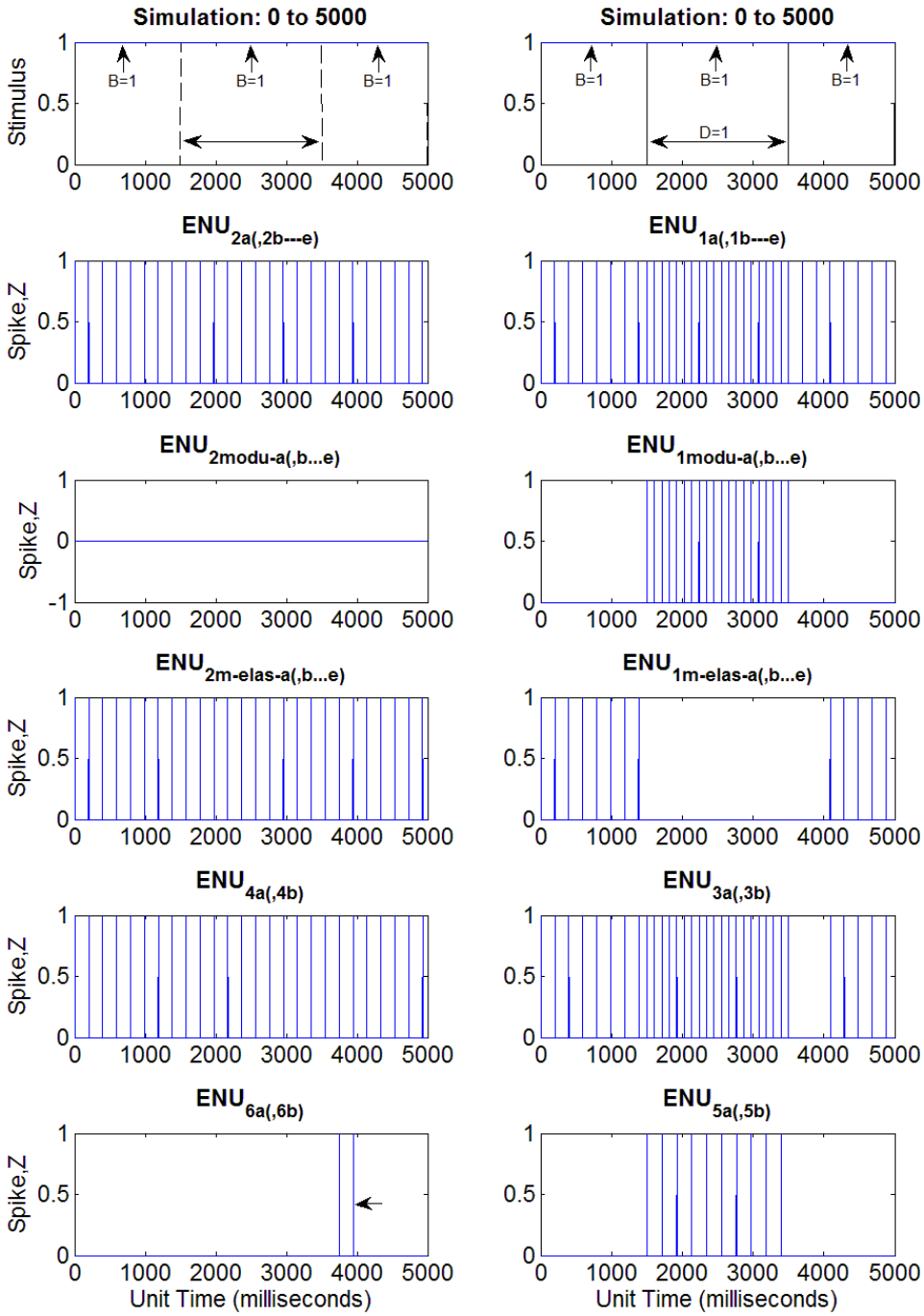

Figure 4.3. First 5 seconds of the simulation shown in Figure 4.2. This shows spiking within each node of E-DN (pulsed-inputs are not shown). During this B – D&B – B trial, the network exhibits rebound property (arrow, bottom left).

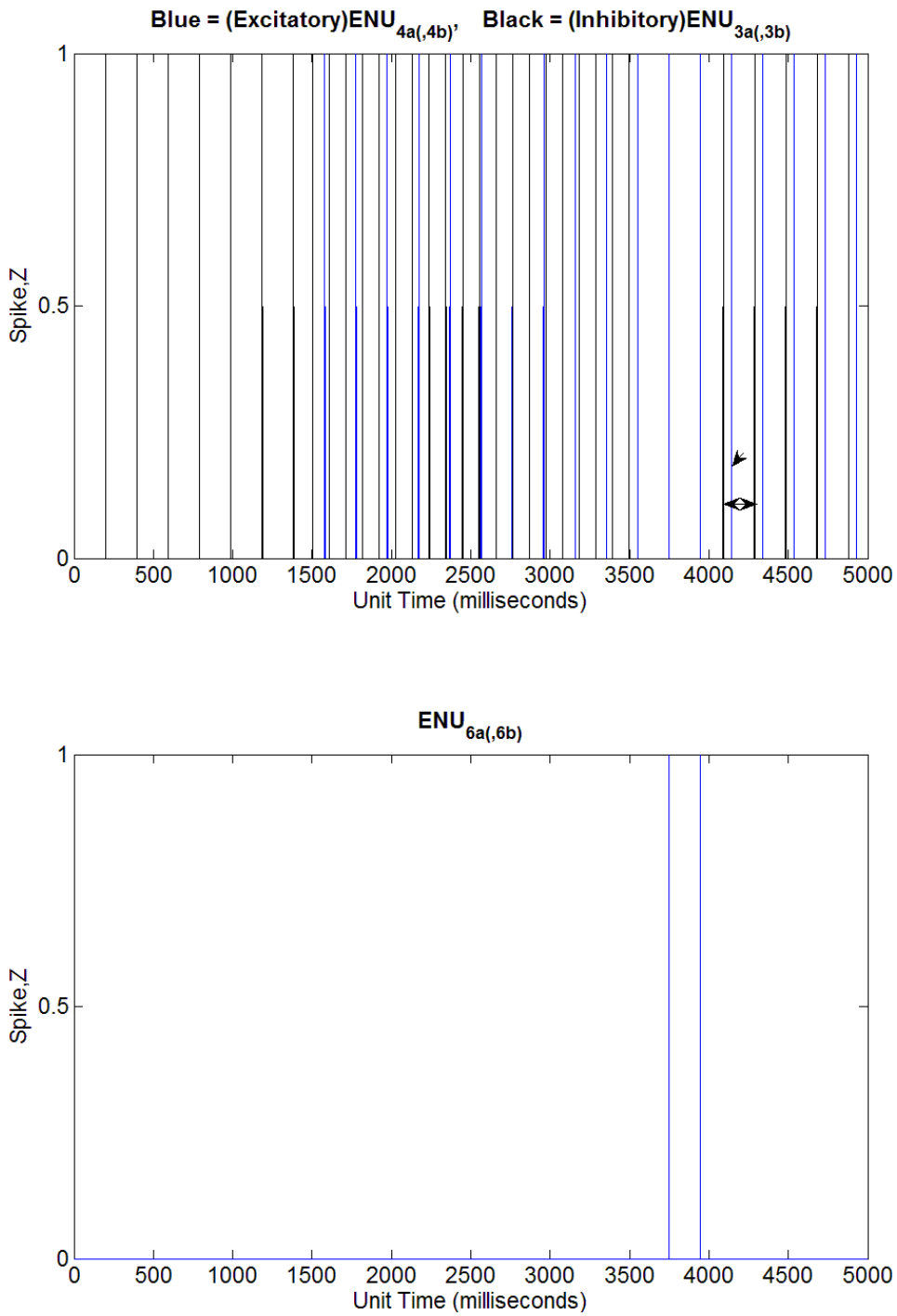

Figure 4.4. (Top) Inputs (spikes) for excitatory (blue) and inhibitory (black) dendrites of ENU_6 (basic ENU in Eck6) as seen in Figure 4.3. When excitatory input (arrow) occur outside a certain region between two inhibitory inputs (double-arrow), Eck6 spiking is not induced (bottom). Note that prior to 1500 ms both inputs (excitatory & inhibitory) occur at same instant.

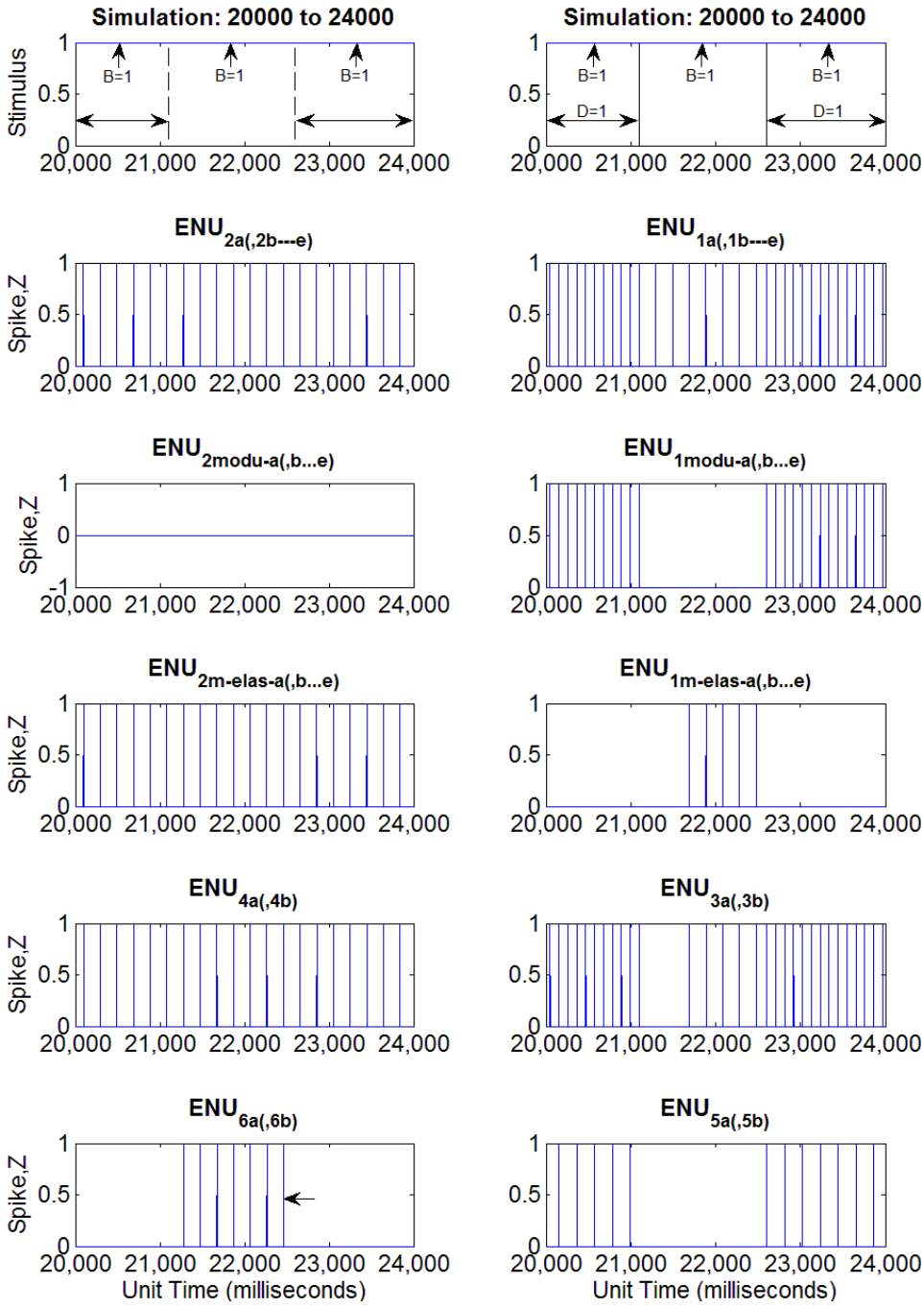

Figure 4.5. Spiking within each node of E-DN during simulation shown in Figure 4.2 (bottom). During this B – D&B – B trial (first B not shown), continuous spiking (arrow, bottom left) from ENU_6 (basic ENU in Eck6) occurs during the whole duration of B-stimulus following dual-stimuli.

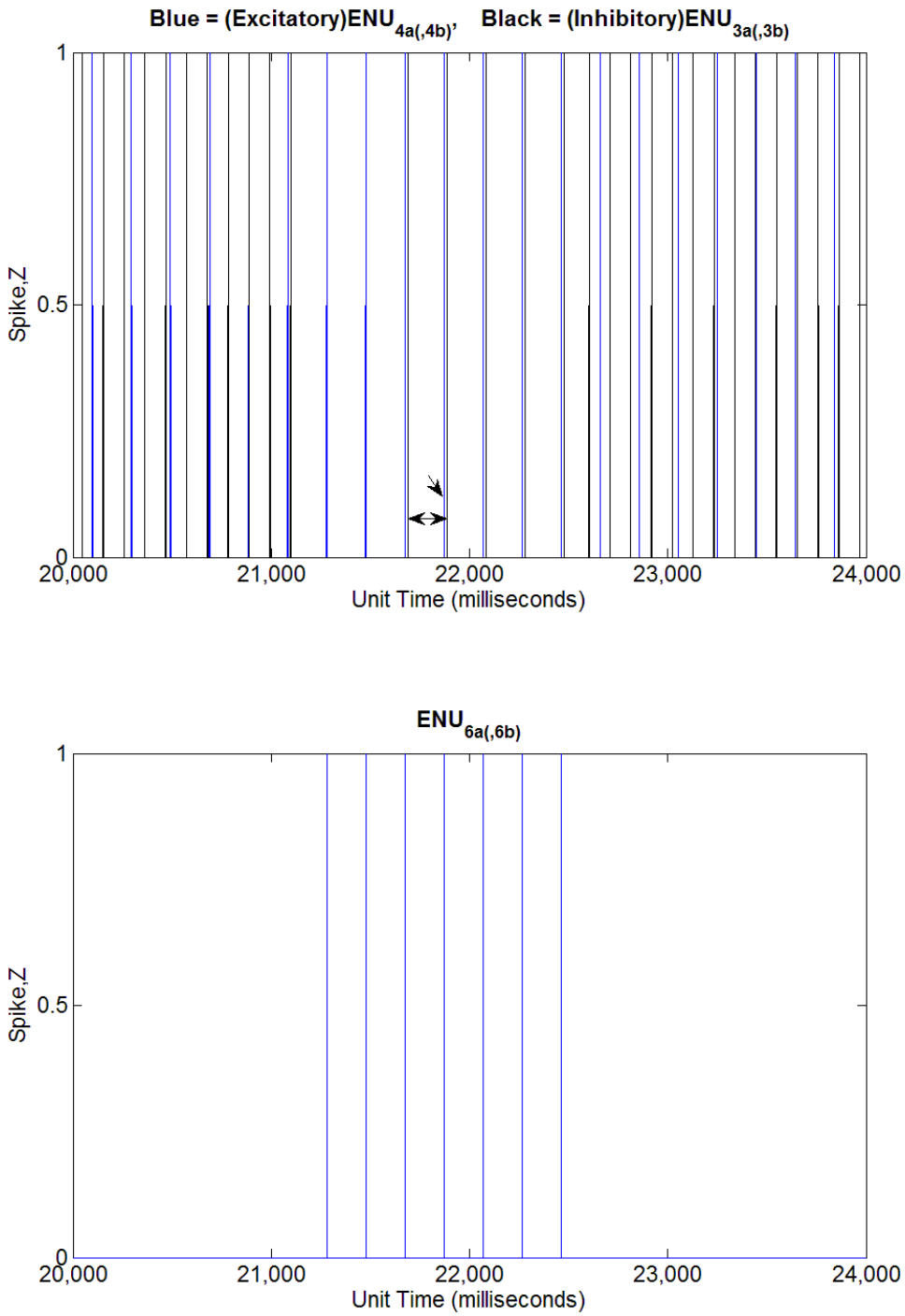

Figure 4.6. (Top) Inputs (spikes) for excitatory (blue) and inhibitory (black) dendrites of ENU_6 (basic ENU in Eck6) as seen in Figure 4.5. When excitatory input (arrow) occur within a certain region between two inhibitory inputs (double-arrow), Eck6 spiking is induced (bottom).

Instant of excitatory dendrite (feeding field) output and inhibitory dendrite output is crucial to soma output

The activated ENU_3 and ENU_4 spikes occurring at same instant of respective $ENU_{1m\text{-}elas}$ and $ENU_{2m\text{-}elas}$ spikes (Fig. 4.3 & 4.5) are the inputs for inhibitory and excitatory ENU_6 dendrites, respectively, and for excitatory and inhibitory ENU_5 dendrites, respectively. Therefore, the interval within which ENU_4 spikes can cause ENU_6 spiking is the interval during which excitatory dendrite output (from an ENU_4 spike) can successfully induce ENU_6 spiking (similarly for ENU_5 spikes but with different/reversed dendrite inputs). The analysis is done by considering ENU_6 (in Eck6) spikes.

For the dendrite components of basic ENU's within Eck6 we can calculate the maximum possible excitatory dendrite output (E_{ff}^{Max}) given by,

$$E_{ff}^{Max} = (1/\tau_{ff}^{E}) \cdot \sum_{i=1}^{n} w_{ff_i}^{E} \cdot (1 + (1/\tau_{lf}^{E}) \cdot \sum_{j=1}^{m} w_{lf_j}^{E}) \qquad (1)$$

where n = number of basic ENU's in either Eck3 or Eck4 and m = l - 1, l = number of basic ENU's in either Eck5 or Eck6. Note that the first component of the equation is of the form $\sum_{i=1}^{n} w_{ff_i}^{E} \cdot Z_i^{E}$. But for E_{ff}^{Max}, $Z_i^{E} = 1$ for all basic ENU's (i.e., for all i's). Thus,

$$\sum_{i=1}^{n} w_{ff_i}^{E} \cdot Z_i^{E} = \sum_{i=1}^{n} w_{ff_i}^{E} .$$

However, the linking field (LF) configuration implemented in E-DN and E-N (Fig. 3.34, 3.35 & 3.39) is such that the LF-component receives inputs from outputs (Z's) of basic ENU's other than itself within its respective ENU group. Thus, if an E_{ff} value is successful in causing a spike, a second peak in E_{ff} occurs (given by Eqn.1) as shown in

Figure 4.7.

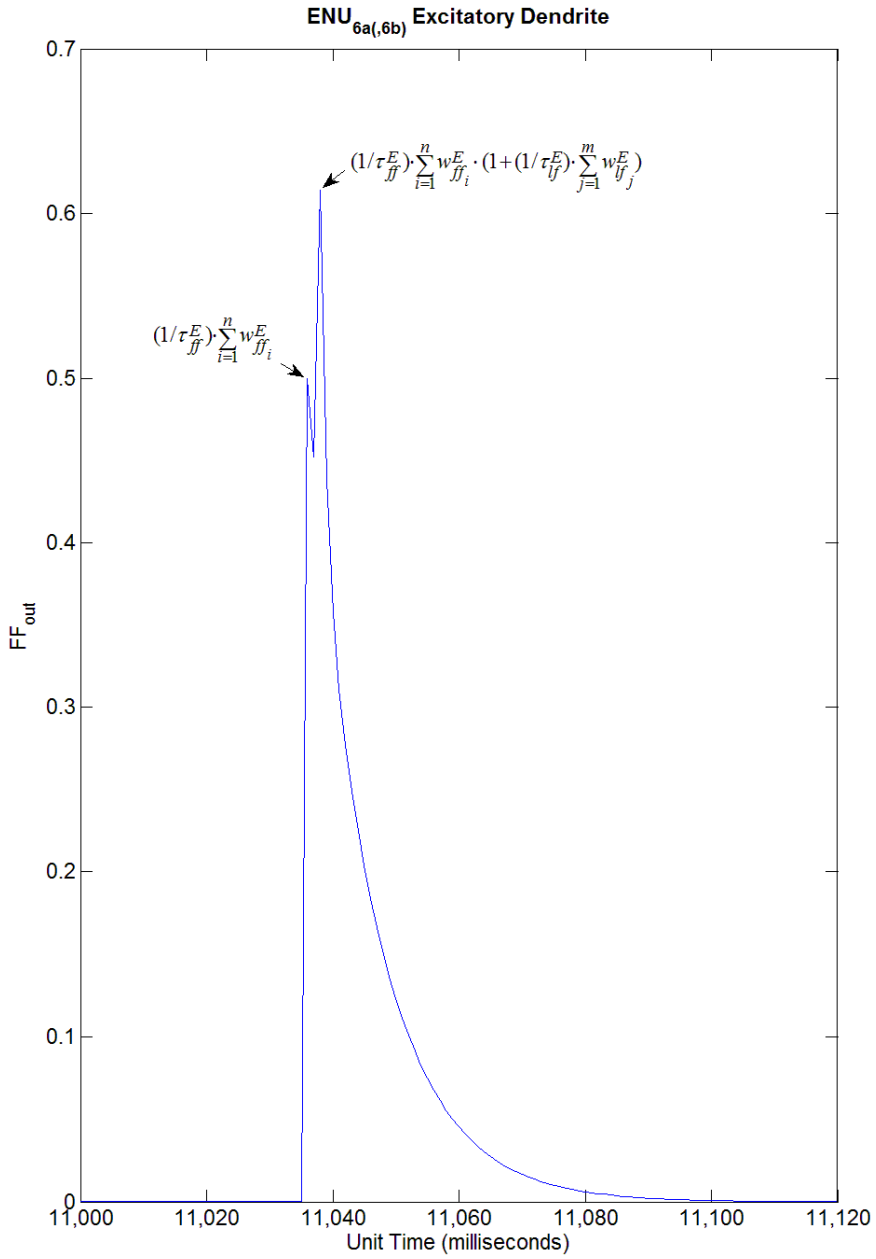

Figure 4.7. Excitatory dendrite output with two peaks. The first peak, if successful in inducing a spike from the soma, results in activating the linking field component of the excitatory dendrite. This is due to the network connection implemented in the network (Fig. 3.34, 3.35 & 3.39). Thus, second peak does not occur if the first does not succeed in causing spike from soma. The causes for the peaks are given by their respective equations. Note that inhibitory dendrites do not have any linking field connection and hence inhibitory dendrite outputs do not exhibit two peaks.

Because of the above reasons and since our interest lies in the first E_{ff} peak that determines spiking, we shall call this E_{ff}, the E_{ff}^{Max} given by

$$E_{ff}^{Max} = (1/\tau_{ff}^{E}) \cdot \sum_{i=1}^{n} w_{ff_i}^{E} \ . \tag{2}$$

Similarly, the maximum possible inhibitory dendrite output (I_{ff}^{Max}) is given by

$$I_{ff}^{Max} = (1/\tau_{ff}^{I}) \sum_{i=1}^{n} w_{ff_i}^{I} \ . \tag{3}$$

In addition to E_{ff}^{Max} and I_{ff}^{Max}, since value of the offset threshold parameter is also known (θ_o from table 3.10), the crucial instant (t_k) is when the inhibitory dendrite output is $I_{ff} = E_{ff}^{Max} - \theta_o$. Thus, if t = 0 and $\Delta t = t_k$, the difference equation for inhibitory dendrite output

$$FF^{I}(t) \ = \ FF^{I}(t-\Delta t) \cdot \exp(-\Delta t / \tau_{ff}^{I}) + (1/\tau_{ff}^{I}) \cdot w_{ff}^{I} \cdot \sum_{\forall j} F_j^{Inhibitory\ inputs} \tag{4}$$

can be re-written as,

$$I_{ff} \ = \ I_{ff}^{Max} \cdot \exp(-t_k / \tau_{ff}^{I}) \tag{5}$$

since, $FF_i(t_k) = I_{ff}$, $FF_i(0) = I_{ff}^{Max}$ and the dendrite does not receive any inputs. Therefore, taking the time when I_{ff}^{Max} precedes E_{ff}^{Max} as the reference (origin, t_o), if t_{spike} is the time from t_o when E_{ff}^{Max} (following I_{ff}^{Max}) occurs, t_k is the crucial time from t_o, and $t_{inter\text{-}inhibitory}$ is the time from t_o to the instant of next I_{ff}^{Max}, then for spiking to occur E_{ff}^{Max} should occur within the interval, $t_k \le t_{spike} < t_{inter\text{-}inhibitory}$. Hence, E_{ff}^{Max} must occur outside this interval for rebound (Fig. 4.8), i.e., no Eck6 spikes after the initial few spikes. On the other hand, E_{ff}^{Max} satisfies the condition (inside the interval) for persistent-Eck6 spiking (Fig. 4.9).

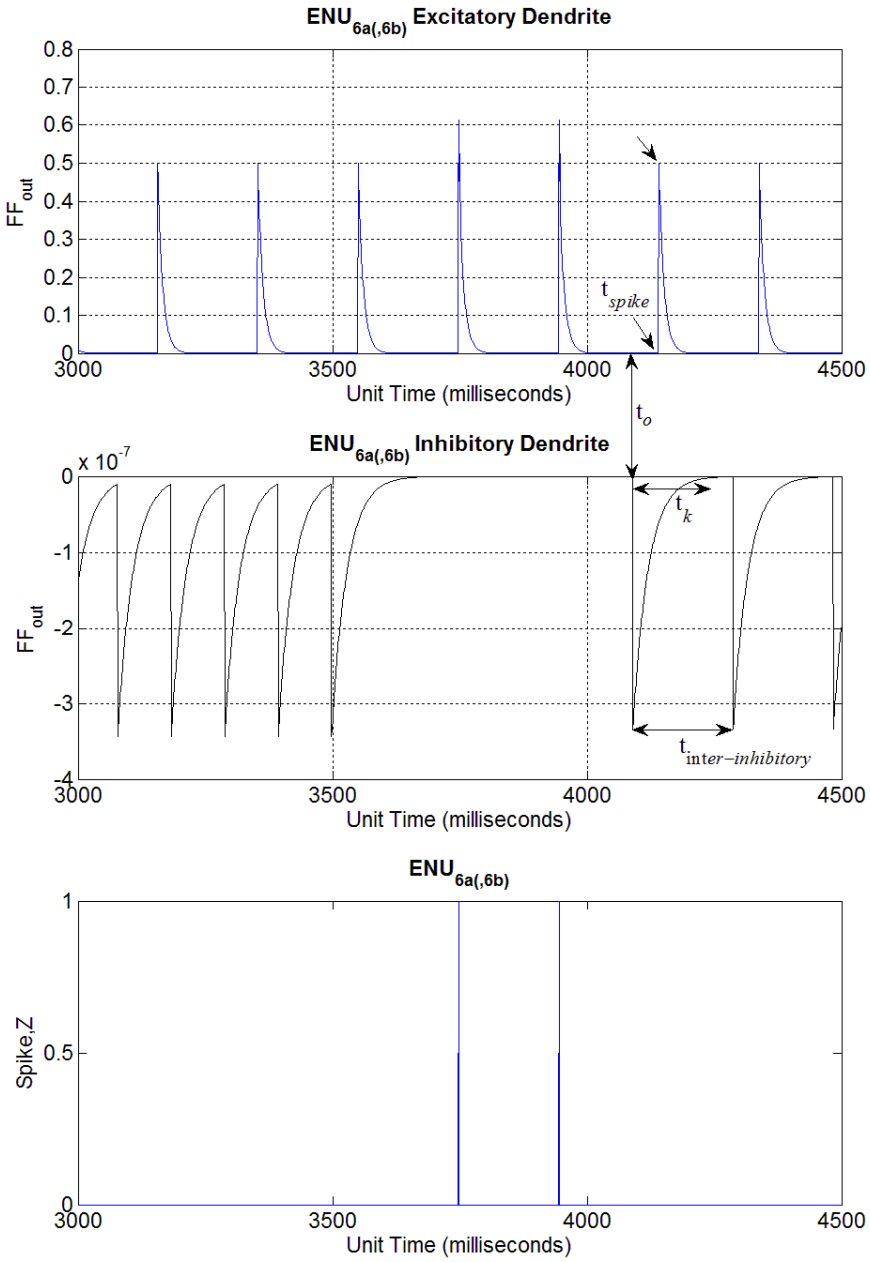

Figure 4.8. Eck6 spiking (rebound) seen in Figures 4.3 (bottom left) and 4.4 is because excitatory dendrite outputs (top, arrow) of ENU_6 during B-stimulus following dual-stimuli does not satisfy the condition, $t_k \leq t_{spike} < t_{inter\text{-}inhibitory}$ after the initial few spikes (which satisfied the condition).

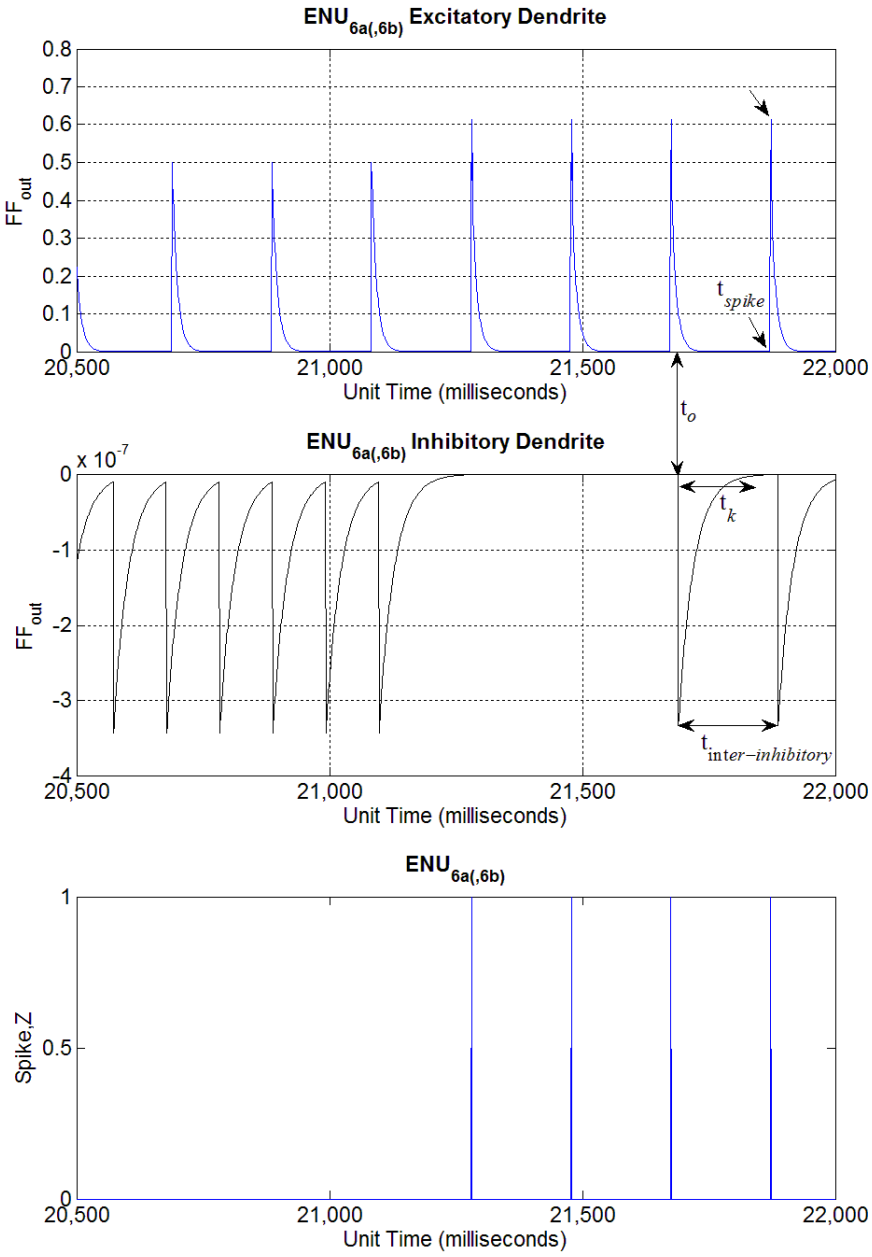

Figure 4.9. Eck6 spiking (persistent-Eck6 spiking) seen in Figures 4.5 (bottom left) and 4.6 is because excitatory dendrite outputs (top, arrow) of ENU_6 during B-stimulus following dual-stimuli satisfies the condition, $t_k \leq t_{spike} < t_{inter\text{-}inhibitory}$.

Instant of stimulus (switching 'on' or 'off') influences network behavior (Eck5 & Eck6 spiking)

Apart from the rebound property and persistent-Eck6 spiking, other network behaviors are also found. Occasionally, spiking from Eck5 occurs during B-stimulus following dual-stimulus (Fig. 4.2 bottom right). The mechanism for Eck5 spiking is the same as for Eck6 spiking described above. That is, E_{ff}^{Max} of ENU_5 must occur within the interval $t_k \leq t_{spike} < t_{inter\text{-}inhibitory}$ for Eck5 spiking.

Similar to persistent-Eck6 spiking (Fig. 4.5, bottom left), the Eck5 spiking during B-stimulus (post dual-stimuli) is also continuous (Fig. 4.10b). However, neither Eck5 spiking nor persistent-Eck6 spiking occur in the next trial of B – D&B – B. Figure 4.10c and 4.10d shows that if the duration of dual-stimulus is changed, spiking from Eck5 no longer occurs. Therefore, persistent-Eck6 and Eck5 spiking during B-stimulus following dual-stimuli do not occur frequently as their occurrence is dependent on stimulus instant.

In conclusion, occurrences of persistent-Eck6 and/or Eck5 spiking during B-stimulus following dual-stimuli will not take place if the network does not receive continuous tonic arousal (B-stimulus). Since tonic arousal for either G-N or E-N represents 'alertness' or attention-drive, the likelihood of continuous B-stimulus as a feasible scenario biologically and psychologically requires future investigation. This study establishes that timing and duration of B-stimulus input in this spiking–mode neural network produces emergent network properties that are not captured by the Grossberg-level models. The origin and characterization of the source of B and D inputs is beyond the scope of this thesis.

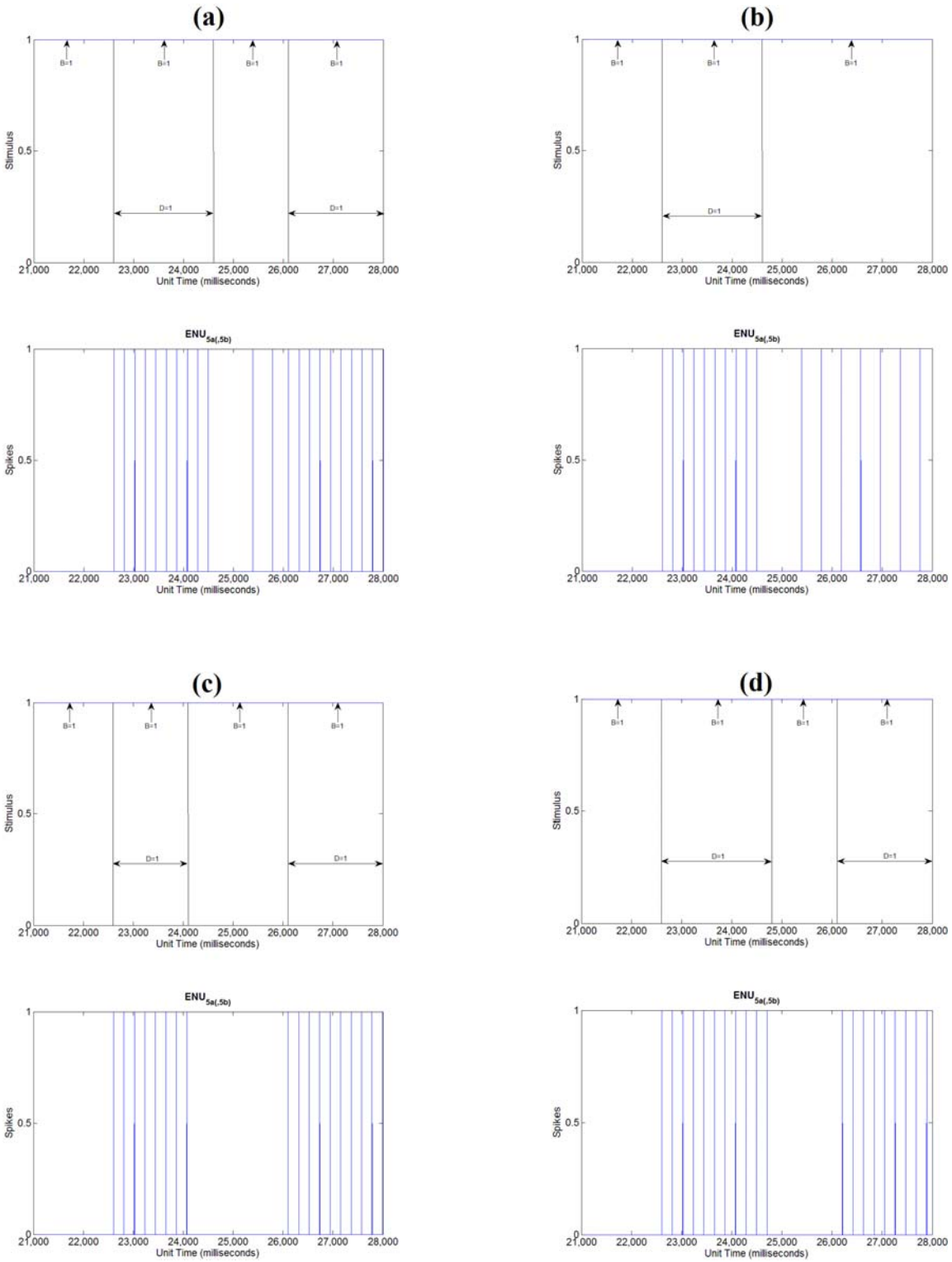

Figure 4.10. a) Simulation seen in Figure 4.2 (bottom right). b) Simulation as in a) but with extended B-stimulus (2nd B of B – D&B – B trial). Notice that Eck5 spiking occurs during B-stimulus following dual-stimuli. c) and d) Simulation with shorter (c) or longer (d) duration of dual-stimuli leads to no Eck5 spiking seen in a) and b).

CHAPTER 5

Results

Performance Surface

Following the scheme shown in second chapter (Fig 2.12 & 2.13), the performance surface of the derived network (Fig. 3.39) is first empirically obtained for individual adaptive weight pairs (w_{O3} & w_{O4} with weight step, $\Delta w = 0.1$ between 4.5 to 6.5 and $\Delta w = 0.25$ else) as shown in Figures 5.1, 5.2 and 5.3. The performance surface is obtained with the E-N receiving B and S-stimulus but no D-stimulus. Thus, also called conditioned performance surface. Note that w_{O3} is the feeding field weight for ENU's in Eck3 (network end with additional drive stimulus) at the receiving end of sensory stimulus while w_{O4} is the adaptive weight for Eck4 ENU's (network end with just bias stimulus). The performance index is defined by

$$P = \left(\text{Desired}_{GN} - \text{Transformed}_{EN}\right)^2 \qquad (1).$$

Starting from initial weights, $w_{O3} = 0$ and $w_{O4} = 0$, the surface remains flat at maximum P but with increasing weight values the surface has regions of local minima (arrow head, Fig. 5.1) and a global minima (arrow, Fig. 5.1). With further increase in weight values the surface climbs, eventually reaching maximum P when adaptive weight for the dipole channel with inhibitory connection to the M-node increases beyond a certain value ($w_{O4} \geq 4.9$). It should be noted that beyond a certain value of adaptive weights (either w_{O3} or $w_{O4} > 8.4$) ENU's in Eck3 or Eck4 gets into saturated (unwanted) firing mode thus, causing loss of functional performance.

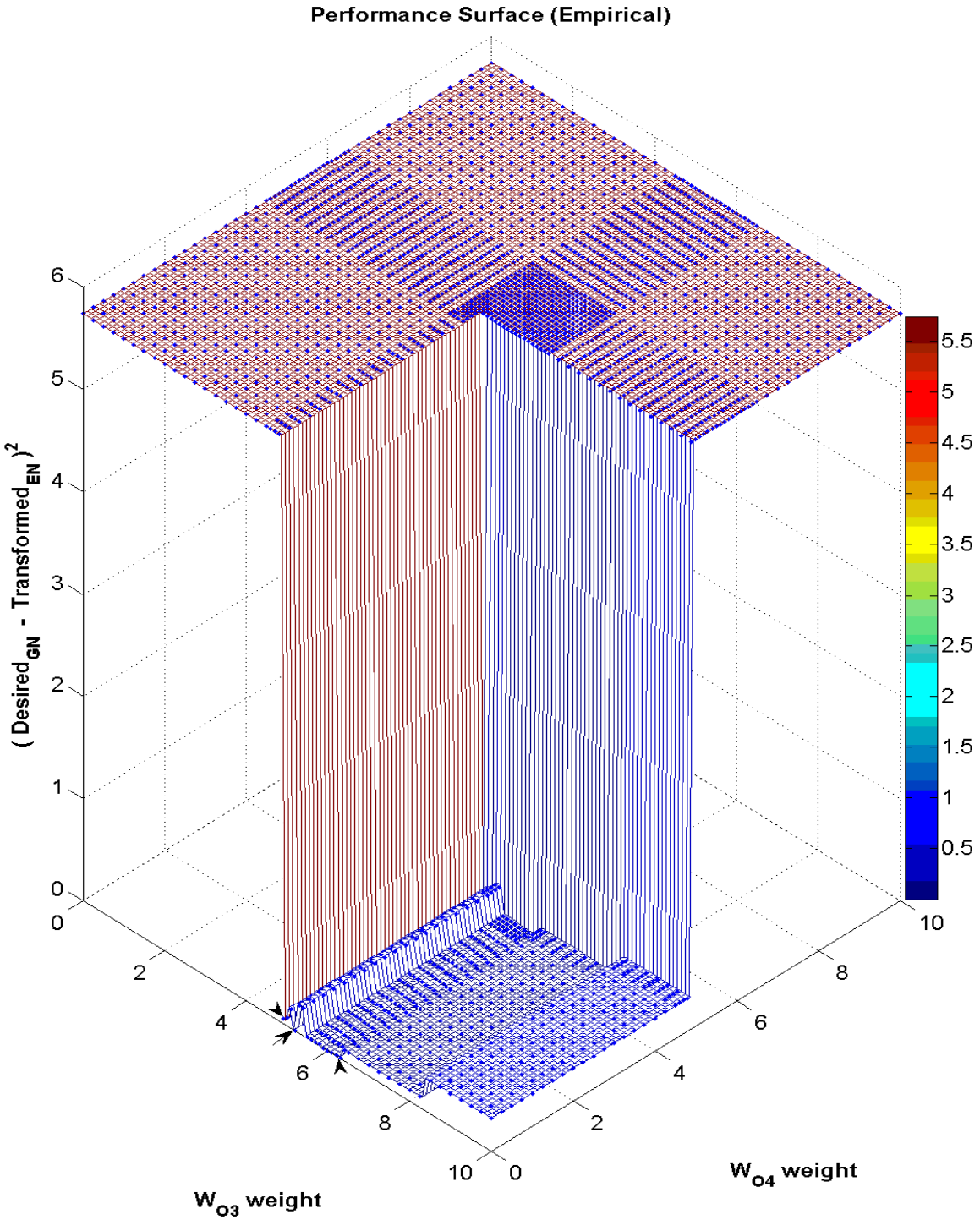

Figure 5.1. Performance surface (conditioned) of Eckhorn network obtained empirically by manually (weight step, $\Delta w = 0.1$ between 4.5 to 6.5 and $\Delta w = 0.25$ else) adjusting the adaptive weight pairs (w_{O3} & w_{O4}). Blue dots on the performance represent data points. Weight w_{O3} is the adaptive weight in ENU's of Eck3 while weight w_{O4} is for ENU's of Eck4. A global minimum (arrow) is situated between the two local minima (arrowheads). Note that for the E-DN in this particular E-N, Eck3 is on the channel with excitatory connection to M-node while Eck4 is on the channel with inhibitory connection.

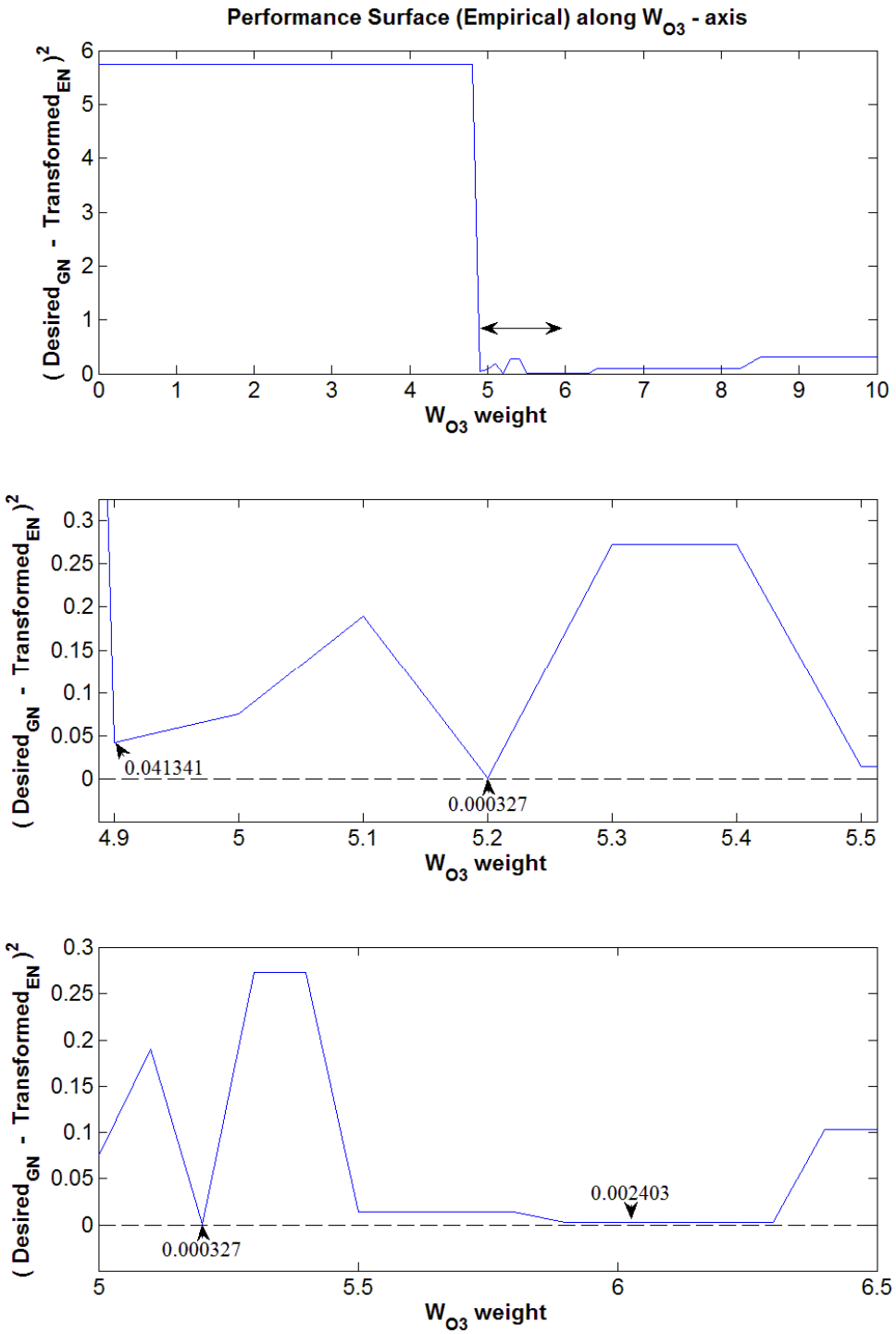

Figure 5.2. Side views along w_{O3} weight axes of the 3D-performance surface (Fig.5.1). Top: Performance index (P) decreases to local minima, global minima, local minima and then climbs such that beyond a certain w_{O3} value (>8.4) the surface becomes non P-selective. The regions of minima (double arrow) are enlarged in bottom two sub-figures. Middle: Shows the first local minima and the global minima with their respective P values. Bottom: Shows the global minima and second local minima with respective P values. The dashed horizontal line in lower two figures indicates P = 0 (for reference).

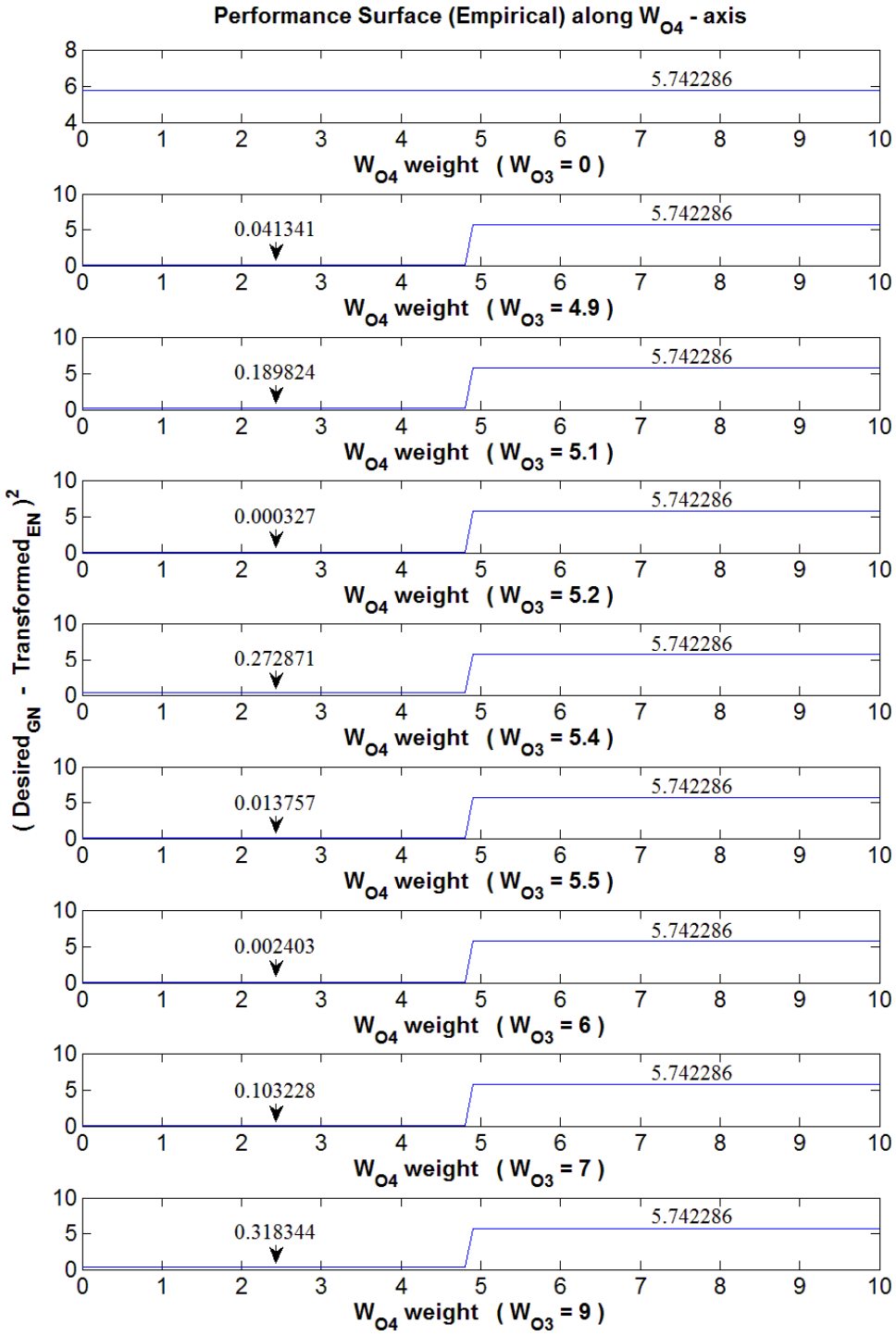

Figure 5.3. Side views along w_{O4} weight axes at various slices (different fixed w_{O3} values) of the 3D-performance surface (Fig.5.1). The numbered arrows give respective P values. The 2nd row figure (w_{O3} = 4.9) is the slicing at the region of first local minima (first arrow head, Fig. 5.1) within a certain range of w_{O4} beyond which P increases to its maximum value (P = 5.742286). Similarly, the 4th row figure (w_{O3} = 5.2) is the slicing at global minima (arrow, Fig. 5.1) and 7th row figure (w_{O3} = 6) the slicing at second local minima (second arrow head, Fig. 5.1).

Adaptation Algorithm

Though the global minimum is located between local minima, the minima values are very close to each other. For instance, difference between the global minimum and the larger local minima is of the order 10^{-2}. Thus adaptive weight values within the region of minima do not cause any practical difference whether it is local minima or global minimum. Under the set membership paradigm for adaptive systems, these miniscule differences place the minimum points within the same solution set [Zadeh 1963, Combettes 1993]. Thus steepest descent method can be implemented around the region of minima. However a gradient method cannot be used in regions with constant gradient and also between regions with different constant (gradient) regions due to sudden (steep) changes between them. Therefore, the principle of gain scheduling is implemented for performance outside the region of the minima. The performance surface is therefore divided into two regions:

- Region 1 (R1) when $|\text{Gradient}| \leq G_{\text{Minimum}}$, region of flat spot,
- Region 2 (R2) when $|\text{Gradient}| > G_{\text{Minimum}}$.

This checking for region of flat spot is given by the scalar,

$$\text{Gradient} = \frac{P(w_{O3}+\delta,\ w_{O4}+\delta) - P(w_{O3}-\delta,\ w_{O4}-\delta)}{2 \bullet \delta \bullet \sqrt{2}} \qquad (2)$$

where, performance index (P) is measured for both weight perturbation ($\delta = 5/10^3$).

The adaptation for the network is such that the adaptive procedure in R1 pushes the weights (w_{O3} & w_{O4}) a constant amount. The purpose of this adaptive procedure is to push the adaptive weights until performance gets to R2, where steepest decent method can be used.

The push-weight procedure is given by

$$W_{k+1} = W_k + Push_{Uniform} + Push_{Extra} \quad (3)$$

where, $W = \begin{bmatrix} w_{O3} \\ w_{O4} \end{bmatrix}$,

$Push_{Uniform} = \begin{bmatrix} c \\ c \end{bmatrix}$ and

$$Push_{Extra} = \begin{bmatrix} b \bullet (Conn_{5,M} - Conn_{4,M})_0^1 \\ b \bullet (Conn_{4,M} - Conn_{5,M})_0^1 \end{bmatrix}$$

such that the extra push parameter, b is determined by the connection function,

$$Conn_{i,M} = \begin{cases} +1, \textit{if} \text{ excitatory} \\ -1, \textit{if} \text{ inhibitory} \end{cases}$$

where *i* is the node end (Eck*i*) of the E-DN channel connected to M-node. For the reception of b by the adaptive weight in question, connection function of the opposing channel is subtracted from the function of channel carrying the adaptive weight whose outcome is given by the Heaviside step function,

$$(S)_0^1 = \begin{cases} 1, \textit{if } S > 0 \\ 0, \textit{if } S \le 0 \end{cases}.$$

Therefore the adaptive weight of the channel with excitatory connection receives b and hence $Push_{Extra}$. The need for $Push_{Extra}$ in the push-weight procedure arises because with just $Push_{Uniform}$, the increasing adaptive weight (wo3 & wo4) due to the push could pass diagonally across the performance surface (Fig. 5.1) missing the region of minima.

This problem of determining b and of invoking $Push_{Extra}$ is closely related to the "context-dependent choice" problem [Grossberg 1978]. That is, the same sensory cue can result in different responses depending upon the context. Here, the word context is used

to mean events or processes (physical & mental) characteristic of a particular situation which has a behavioral impact [Reber 2001]. Grossberg articulated some possible approached to context-dependant choice. Figure 5.4 illustrates one of these [Wells 2011b].

The E-DN shown in this thesis is just part of a map or network system. Thus the connection types (excitatory and inhibitory) from E-DN to M-node occur in complementary pairs [James 1980, Plutchik 1980]. In other words, if for a particular context, the connection of E-DN channel with M-node is excitatory than in another context the connection for the same channel may be inhibitory (Fig. 5.4).

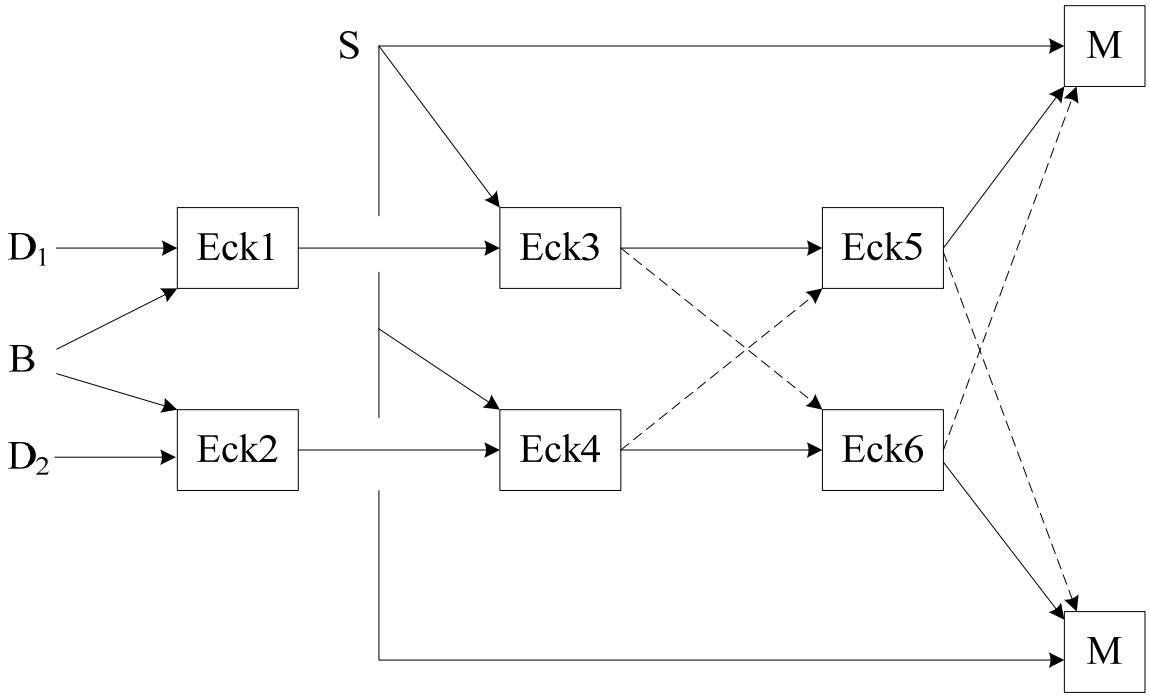

Figure 5.4. An architectonic solution to the "context-dependant choice". The figure shows contradictory unconditioned stimulus (D_1 & D_2) resulting in respective responses (M-node output). Thus adaptation of the network is dependent on which of the two dipole channels receive unconditioned stimulus. Solid lines represent excitatory connection while dashed lines represent inhibition.

During the learning stage, E0N receives a bias, drive and sensory stimulus. Thus Eck5 and Eck6 spiking will differ during dual-stimuli. An alternative $Push_{Extra}$ equation is

$$Push_{Extra} = \begin{bmatrix} b \bullet (Spikes_{ENU3} - Spikes_{ENU4})_0^1 \\ b \bullet (Spikes_{ENU4} - Spikes_{ENU3})_0^1 \end{bmatrix}$$

where, $Spikes_{ENUx}$ is the total spike output from the respective ENU node (EckX) during adaptation conditions (that is, when the E-N receives a bias, drive and sensory stimulus). Thus the $Push_{Extra}$ parameter follows a Hebbian rule. Either of the above $Push_{Extra}$ equations can be used in the push-weight procedure.

Finally, if the performance is located in region R2 on the performance surface, adaptation procedure switches over to steepest descent method which is given by

$$W_{k+1} = W_k + r \bullet \hat{\nabla} \qquad (4)$$

such that rate $r = 5/10^6$ and the gradient estimate is

$$\hat{\nabla} = \begin{bmatrix} \dfrac{P(w_{O3} + \delta) - P(w_{O3} - \delta)}{2 \bullet \delta} \\ \dfrac{P(w_{O4} + \delta) - P(w_{O4} - \delta)}{2 \bullet \delta} \end{bmatrix}$$

where performance index (P) is measured for individual weight perturbations ($\delta = 5/10^3$). Since flat region R1 can also occur in region of minima triggering the push-weight procedure, an increase for P following the procedure is checked. Therefore, no P increase means it is not in region of minima. However, for P in region of minima, adaptive weights are set to the values responsible for P minima. That is, set to the weights prior to P increase. Figure 5.5 shows the flowchart implementing the adaptive procedure, i.e., adaptation algorithm for the Eckhorn network.

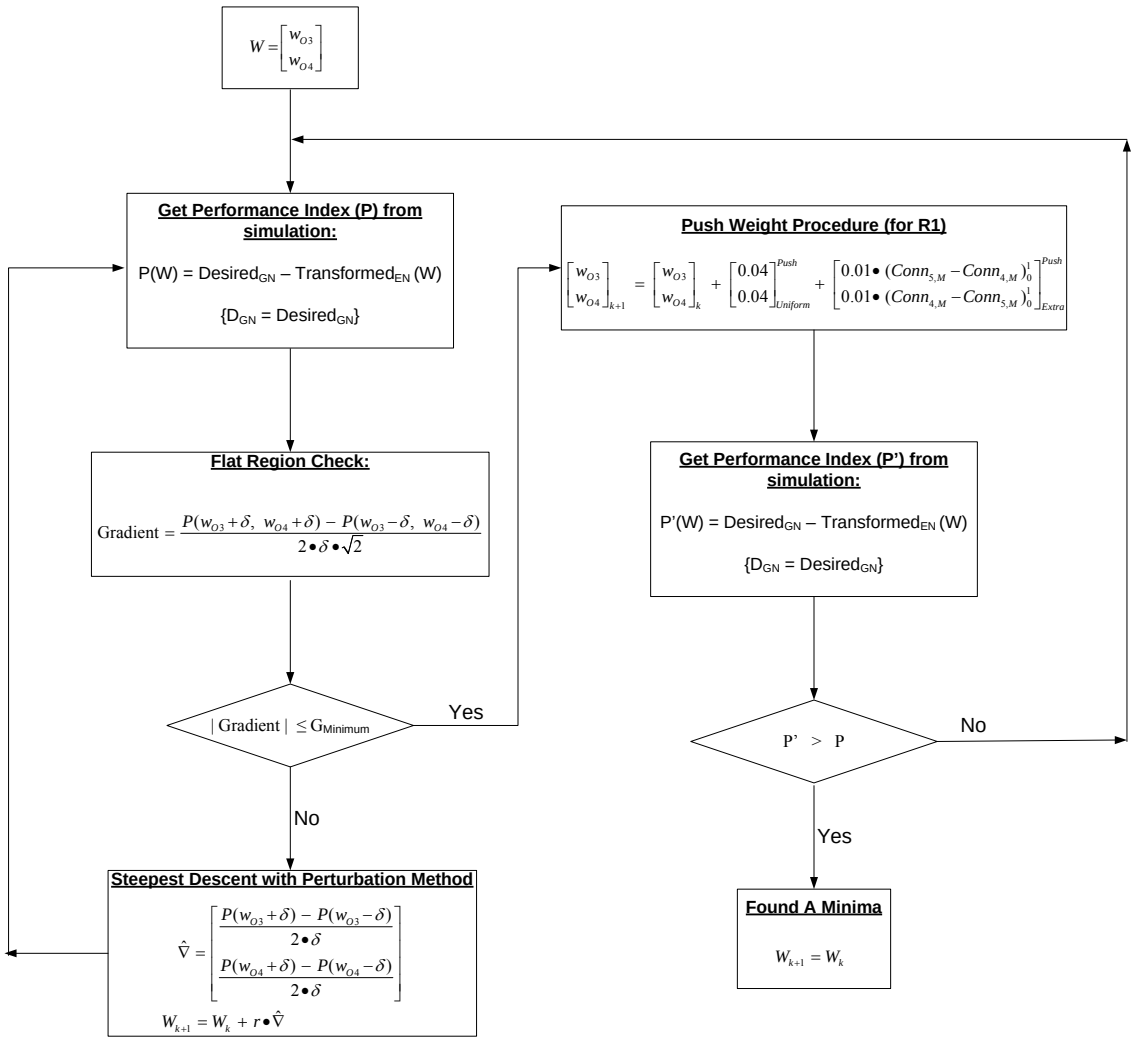

Figure 5.5. Flowchart showing the adaptive algorithm for the Eckhorn network. First, P is obtained from the initial weight inputs (W) which is then used for calculating the gradient for flat region check by simultaneously perturbing both the adaptive weights. Depending upon where P is located on the performance surface, flat region or not, either the Push-Weight procedure or the steepest descent method is chosen to update W (W_{k+1}) for the next weight input. In region of minima the P' caused by the push-weight is compared with P. Thus in minima, P' > P and algorithm is stopped with adaptive weights, $W_{k+1} = W_k$. Note that the parameters for Push-Weight procedures $Push_{Uniform}$ & $Push_{Extra}$ are different.

Learning Curve and Weight Curves

The performance surface of E-N during conditioning (i.e., with B, D and S-stimulus) is different from conditioned performance surface (Fig. 5.6). Though the later performance surface (Fig. 5.6a) is what matters for the adapted weights, the dynamics of the adapting weights depends on the former performance surface (Fig. 5.6b). That is, during adaptation and hence during conditioning the P used for estimating the gradient for flat region check and $\hat{\nabla}$ for the steepest-descent method (Fig. 5.5) is based on the conditioning performance surface (Fig. 5.6b). However, the P of the E-N with the adapted weight is evaluated against the conditioned performance surface (Fig. 5.6a).

Implementing the algorithm (Fig. 5.5) with initial weights $w_{O3} = 0$ and $w_{O4} = 0$ of E-N (Fig. 3.39) during conditioning, the learning curve was obtained (Fig. 5.8a). Figures 5.7 and 5.8 shows P in the learning curve settles at weight values which correspond to a solution set performance region (arrows, Fig. 5.7 & 5.8b) in both performance surfaces. Superimposing $P_{Conditioned}$ (Fig. 5.7b) and $P_{Conditioning}$ (Fig. 5.7d), one notices that regardless of the initial dip amount, the instant of the dip for both $P_{Conditioned}$ and $P_{Conditioning}$ coincides with the same weight values (arrow, Fig. 5.8b). As mentioned earlier, the weight values within the region of minima do not cause any practical difference whether it is local minima or global minimum of the conditioned performance surface. Similarly, though P in the learning curve dips and then rise to a plateau (arrow, Fig. 5.8a) the difference between the least P and P value at plateau is of the order 10^{-2}. The apparent rise of P from the minimum P in the learning curve to its plateau, especially when considered with respect to the conditioned performance surface, becomes less significant. Thus the minimum and plateau P values are within the solution set as per set membership.

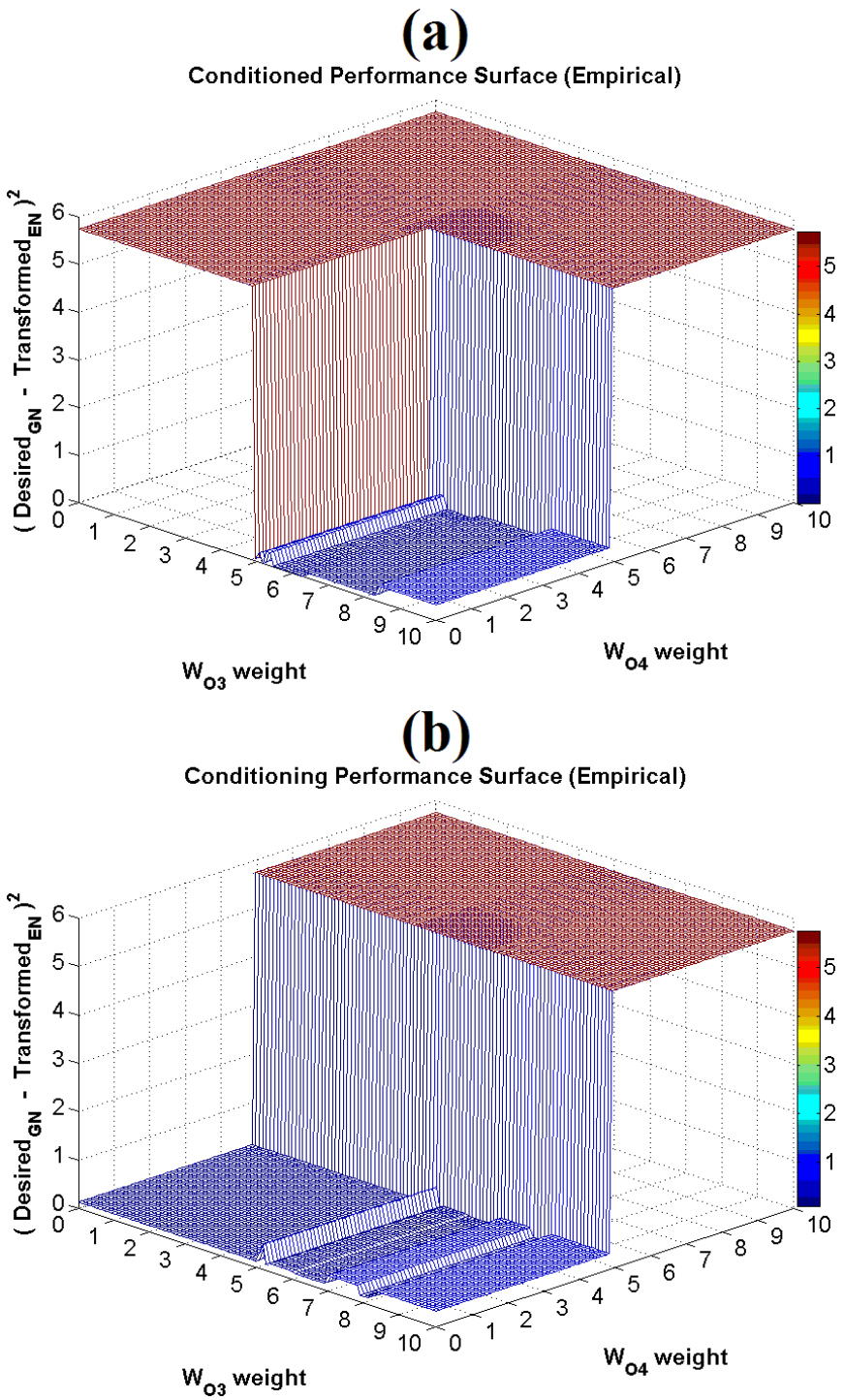

Figure 5.6. Conditioned (a) and Conditioning (b) Performance surface of Eckhorn network obtained empirically by manually (weight step, $\Delta w = 0.1$ between 4.5 to 6.5 and $\Delta w = 0.25$ else) adjusting the adaptive weight pairs (w_{O3} & w_{O4}). (a) Same as Figure 5.1 is the surface during E-N receiving B and S-stimuli while for (b) E-N receives all three stimuli, B, S and D. Weights w_{O3} and w_{O4} are adapting in (b) and adapted in (a). Thus, adaptation algorithm follows the conditioning performance surface (b).

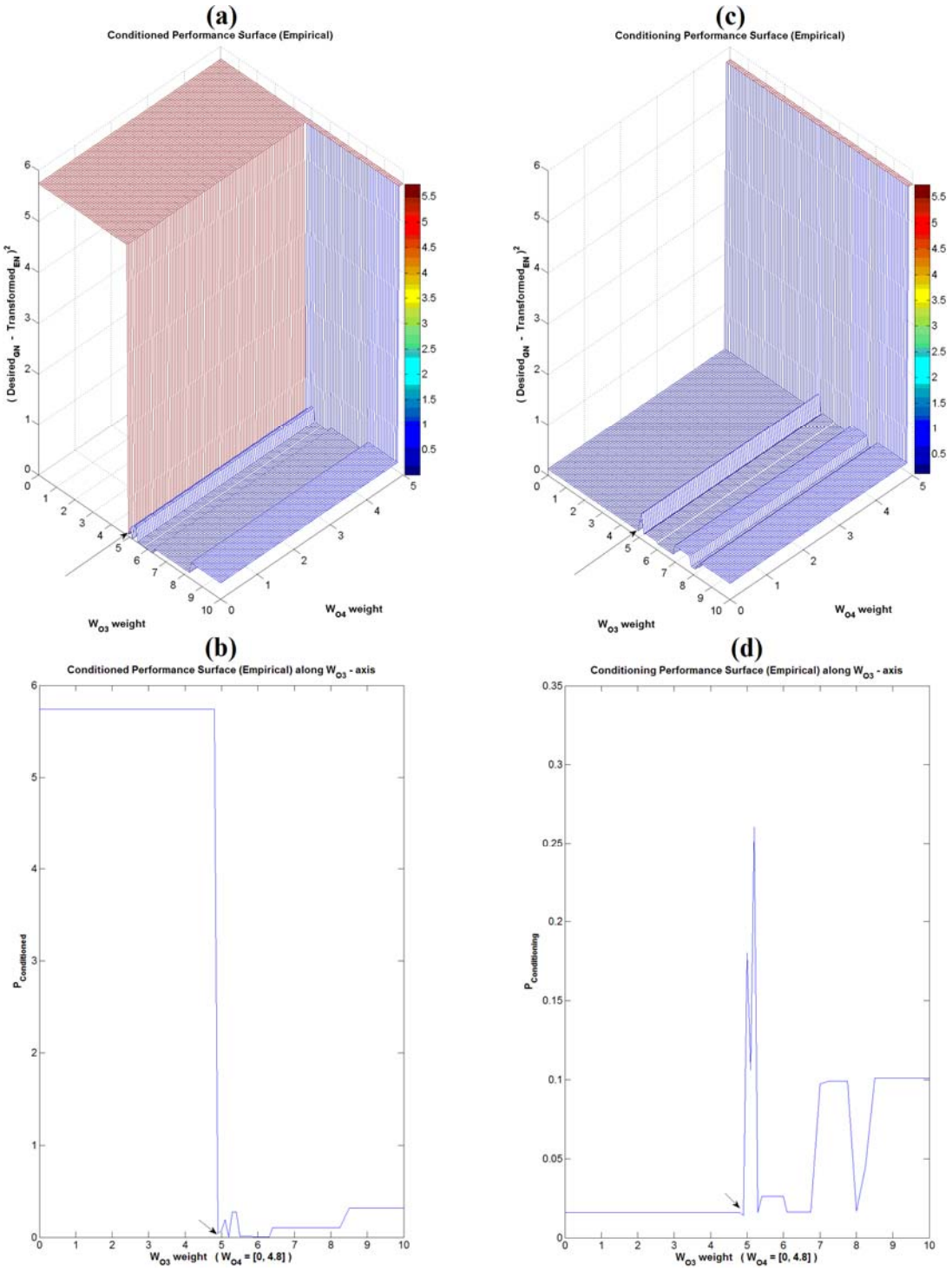

Figure 5.7. Conditioned and Conditioning Performance surface of Eckhorn network. (a) and (c) are conditioned and conditioning surface sections respectively from their whole surface (Fig. 5.6). The sections include weight ranges, $w_{O3} \in [0, 10]$ and $w_{O4} \in [0, 4.8]$. Bottom figures, (b) and (d) are sections of respective figures (a) and (c) taken along w_{O3} weight axes of the above 3D-surfaces. The arrows in all four figures indicate the dip from the initial plateau. The dip (arrow) correspond to when $w_{O3} \approx 4.9056$ and $w_{O4} \in [0, 4.8]$.

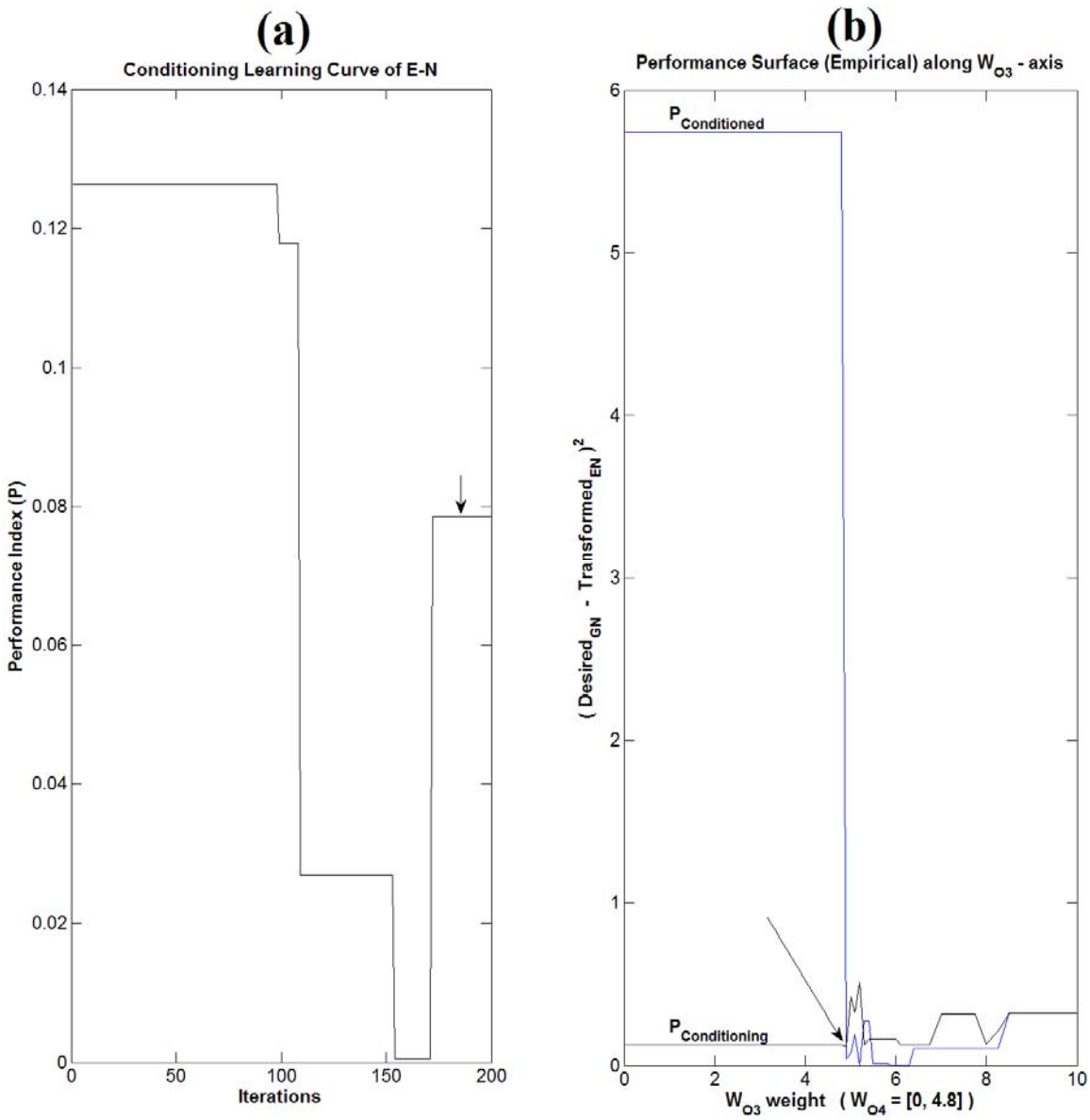

Figure 5.8. Conditioning learning curve (a) of E-N and performance surface (b) along w_{O3} - axis. (b) is obtained by superimposing Figures 5.7b and 5.7d.

(a). P starts out in the region of flat spot (R1) and remains in same R1 with increasing adaptive weights (push-weight procedure) until at 172nd iteration it moves down into new R1 (arrow) at the region of minima where the adaptation stops because beyond this point the performance gets worse (P increases). Note the y-axis scale (P value) in (a).

(b). P for the learning curve (a) follows $P_{Conditioning}$(b) during adaptation. The plateau (arrow (a)) in the learning curve after the fall in P corresponds to adaptive weight values at the dip (arrow (b)) in $P_{Conditioning}$. (b) also shows that the adaptive weights in learning curve plateau (arrow (a)) and hence the adapted weights also correspond to the dip of $P_{Conditioned}$.

The dynamics of the learning curve is shown in Figure 5.9. After the 99th iteration, |Gradient| > $G_{Minimum}$ (middle Fig. 5.9) thus, choosing steepest-descent method in the algorithm (Fig. 5.5). The steepest-descent method causes $\hat{\nabla}_{w_{O3}}$ to change (bottom Fig. 5.9) but $\hat{\nabla}_{w_{O4}}$ remains at zero. However after around 172nd iteration, the gradient estimate for flat region check and $\hat{\nabla}_{w_{O3}}$ fluctuates, though at different magnitudes. Therefore, after 172nd iteration onwards this $\hat{\nabla}_{w_{O3}}$ fluctuation results in an average w_{O3} value. The average w_{O3} (≈ 4.9056) and a non-changing w_{O4} (3.92) values causes the P plateau in the learning curve (double arrow in top Fig. 5.9). In other words, the P plateau in the learning curve (arrow, Fig. 5.10a) is due to the loop operation along the steepest-descent method path of the adaptive algorithm (Fig. 5.10b). This is merely the usual misadjustment property of gradient descent [Widrow & Stearns 1985]. The changes in the adaptive weights (w_{O3} & w_{O4}) responsible for the performance shift in the learning curve are shown in Figure 5.11.

Figures 5.12 and 5.13 shows the weight-learning curves for Grossberg's and Eckhorn's network respectively. The initial values for the adaptive weights are zero in Grossberg's network. The curves are plotted with same time axis (milliseconds) for one-on-one comparison. Due to the outstar-rule implemented in Grossberg's network, the adaptive weight for the node receiving B and no D stimulus ($w_{O4(Grossberg)}$) remains zero while $w_{O3(Grossberg)}$ (node with additional D stimulus) keeps getting bigger until it reaches a steady-state (optimal) value (≈ 0.4972). Adaptive weights in Grossberg's network reaches optimal value at around 110 sec or 1.83 min. However, adaptive weights in Eckhorn's network reaches optimal value at around 258 sec or 4.3min. That is, adaptation for the Eckhorn network is about two and half times slower (2.4 x). Investigation on

optimization techniques for speeding up the adaptation is outside the scope of this thesis.

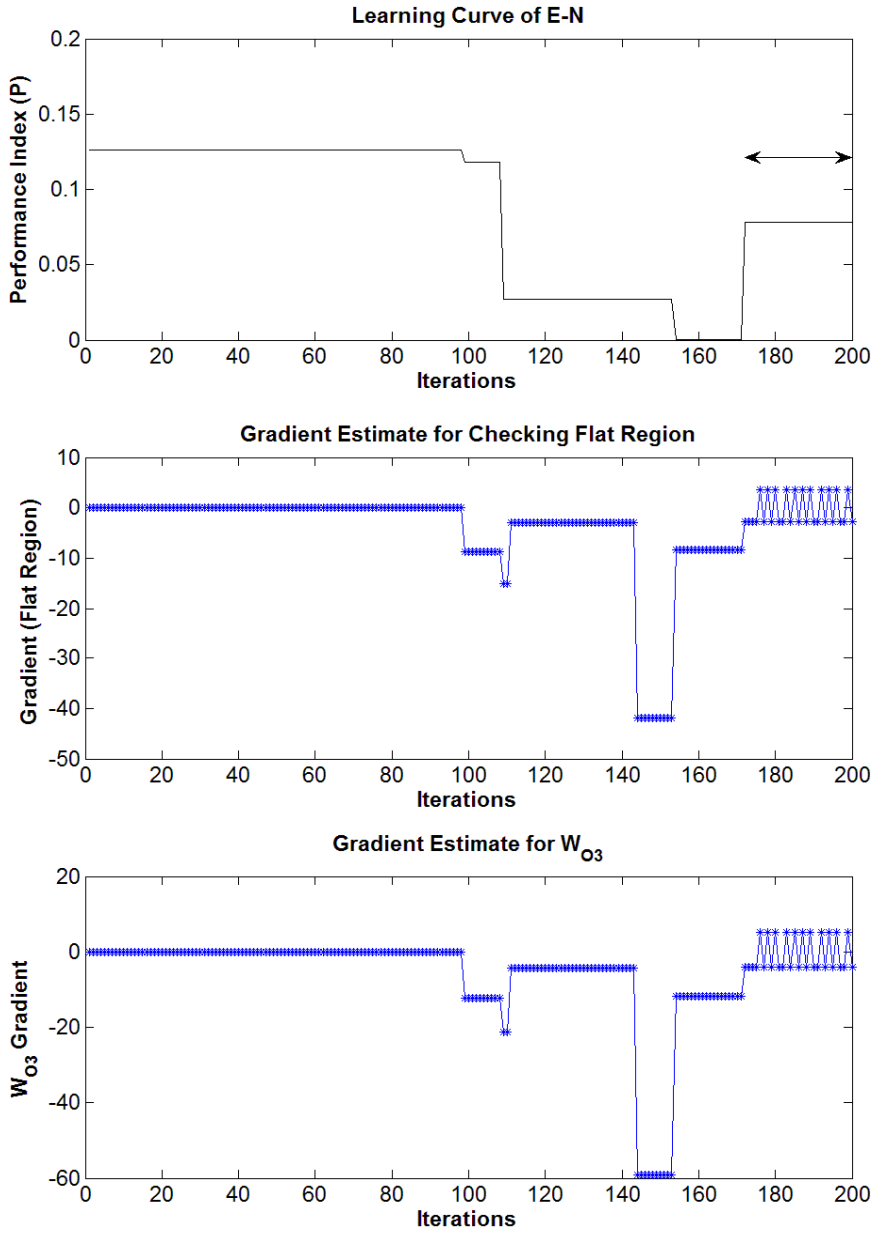

Figure 5.9. Learning curve of E-N with gradient estimates for flat region and w_{O3}. Learning curve or conditioning learning curve (a) is the same curve seen in Figure 5.8a. The double arrow indicates the plateau region (arrow, Fig. 5.8a) which begins at 172nd iteration. During the first 99 iterations the gradient estimate for flat region check (middle figure) is | Gradient | $\leq G_{Minimum}$, thus adaptive weights follow push-weight procedure (Fig. 5.5). However during succeeding iterations | Gradient | > $G_{Minimum}$, thus undergoing steepest descent procedure (Fig. 5.5). In the plateau region (double arrow), the gradient fluctuates by the same quantity. This fluctuation corresponds to those of w_{O3} gradient estimate ($\hat{\nabla}_{w_{O3}}$), bottom figure. $\hat{\nabla}_{w_{O4}} = 0$ (not shown) during the adaptation process.

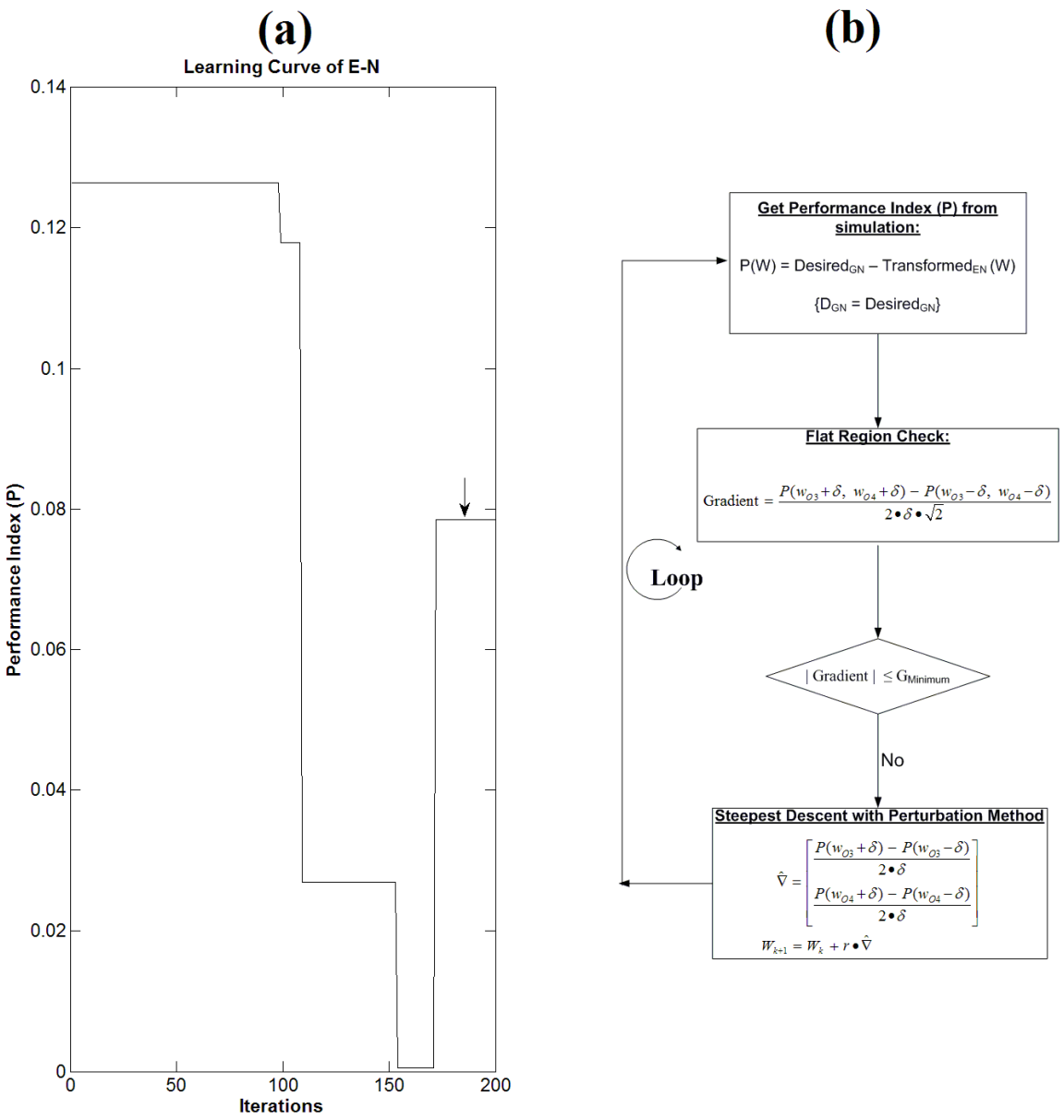

Figure 5.10. Learning curve of E-N. The plateau (arrow) in conditioning learning curve (a) beginning at 172nd iteration corresponds to fluctuation in gradient estimate for flat region check (middle Fig. 5.9), thus following the steepest descent method (b). During this plateau, $\hat{\nabla}_{w_{O3}}$ also fluctuates (bottom Fig. 5.9) resulting in an average w_{O3} value. The fluctuations in flat region gradient estimate and $\hat{\nabla}_{w_{O3}}$ results in repetition (b) along the steepest descent method of the adaptive algorithm.

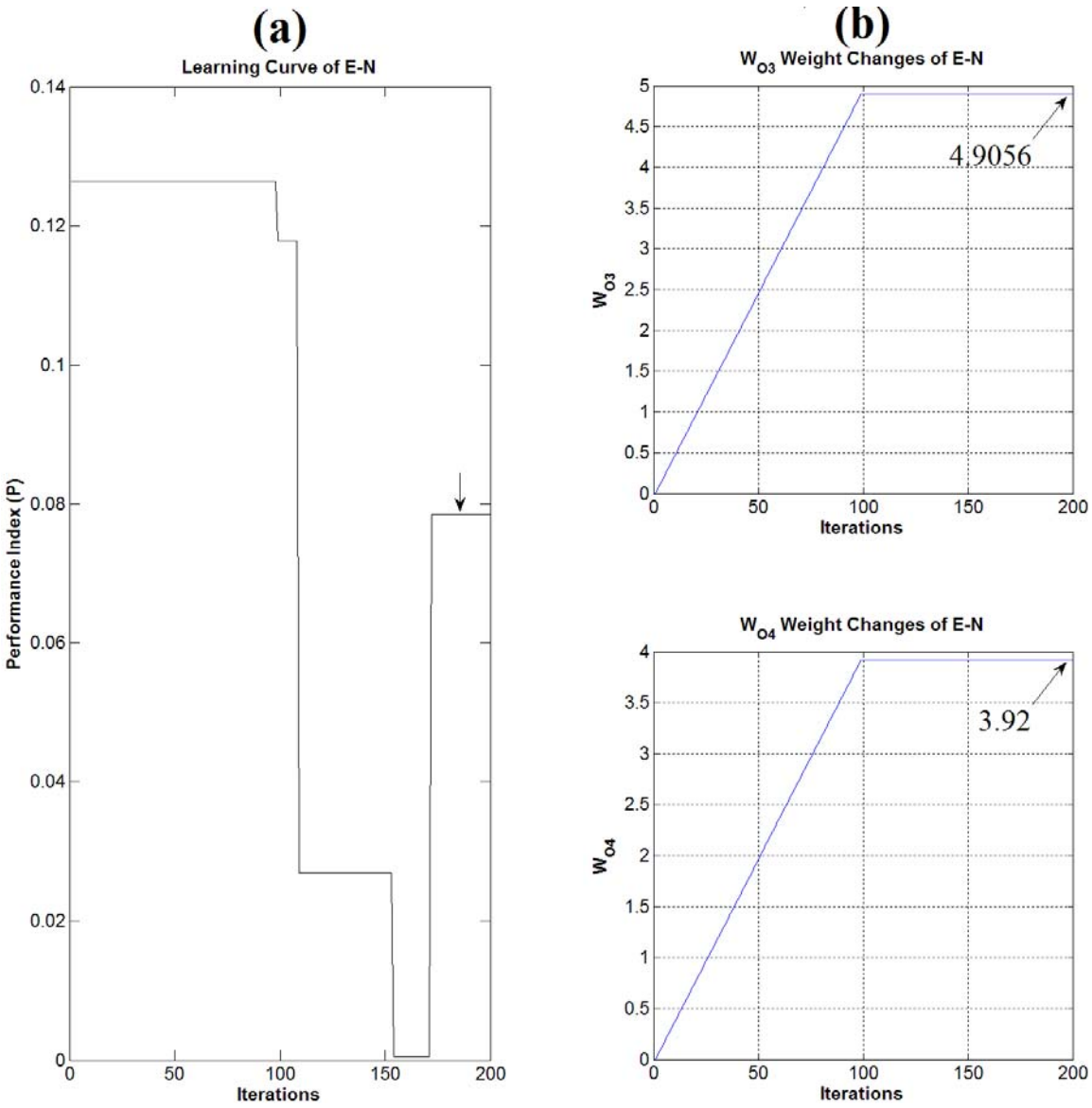

Figure 5.11. Weight changes (b) of Eckhorn network responsible for the learning curve (a). The adaptive weights (w_{O3} & w_{O4}) increases (push-weight procedure) in R1 of the initial plateau (Fig. 5.6) until it settles at the region of minima (arrow, (a)). The weights reach optimal values (arrows) at 172nd iteration. The labeled values ($w_{O3} \approx 4.9056$, $w_{O4} = 3.92$) corresponds to the P plateau seen in the learning curve (Fig. 5.10a). Note that $w_{O3} \approx 4.9056$ is an average value due to the $\hat{\nabla}_{w_{O3}}$ fluctuations (bottom Fig. 5.9).

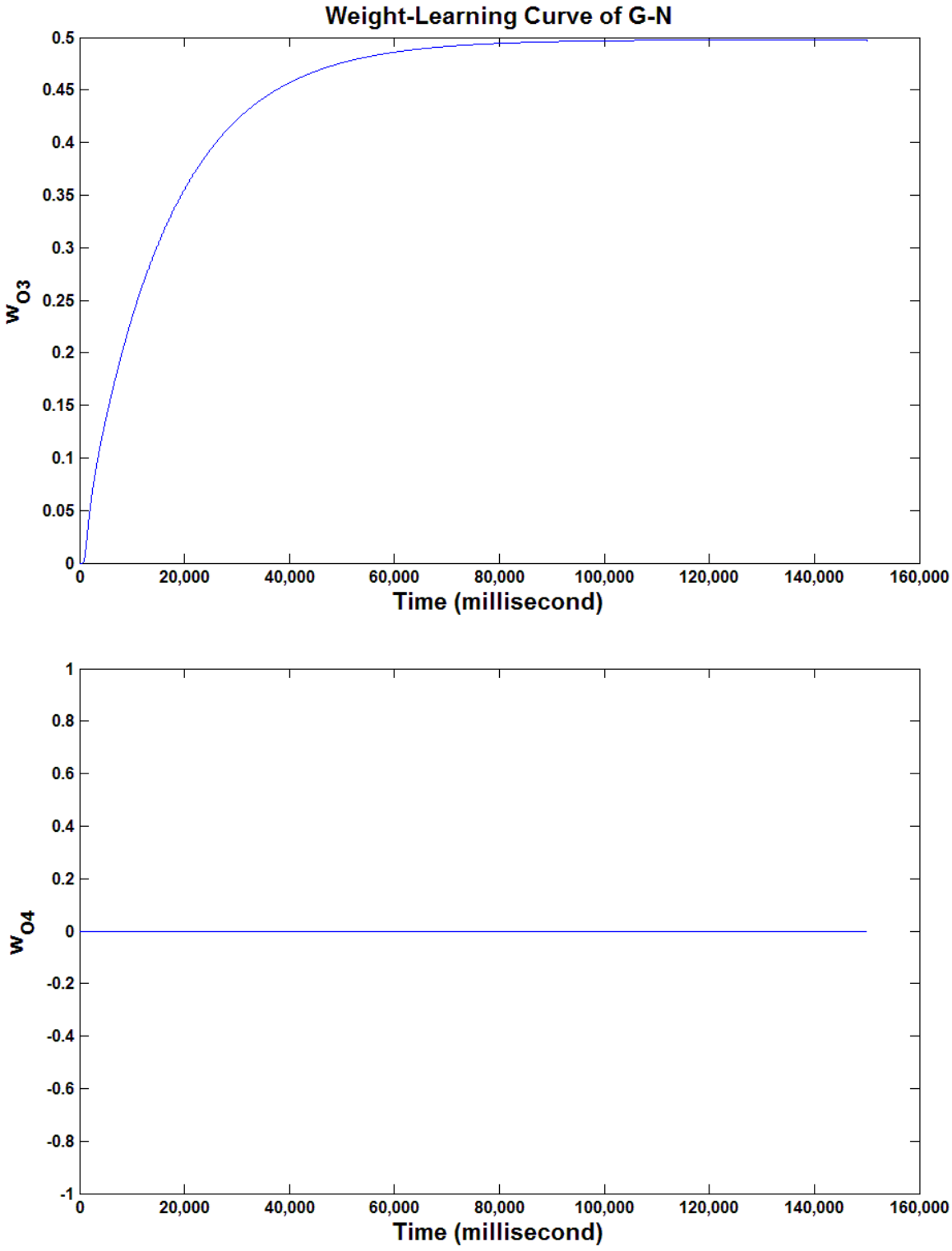

Figure 5.12. Weight-Learning curves of Grossberg's network plotting the adaptive weights ($w_{O3(Grossberg)}$ & $w_{O4(Grossberg)}$) against time in milliseconds. The weights reach optimal values ($w_{O3(Grossberg)} \approx 0.4972$) at 110 sec or 1.83 min.

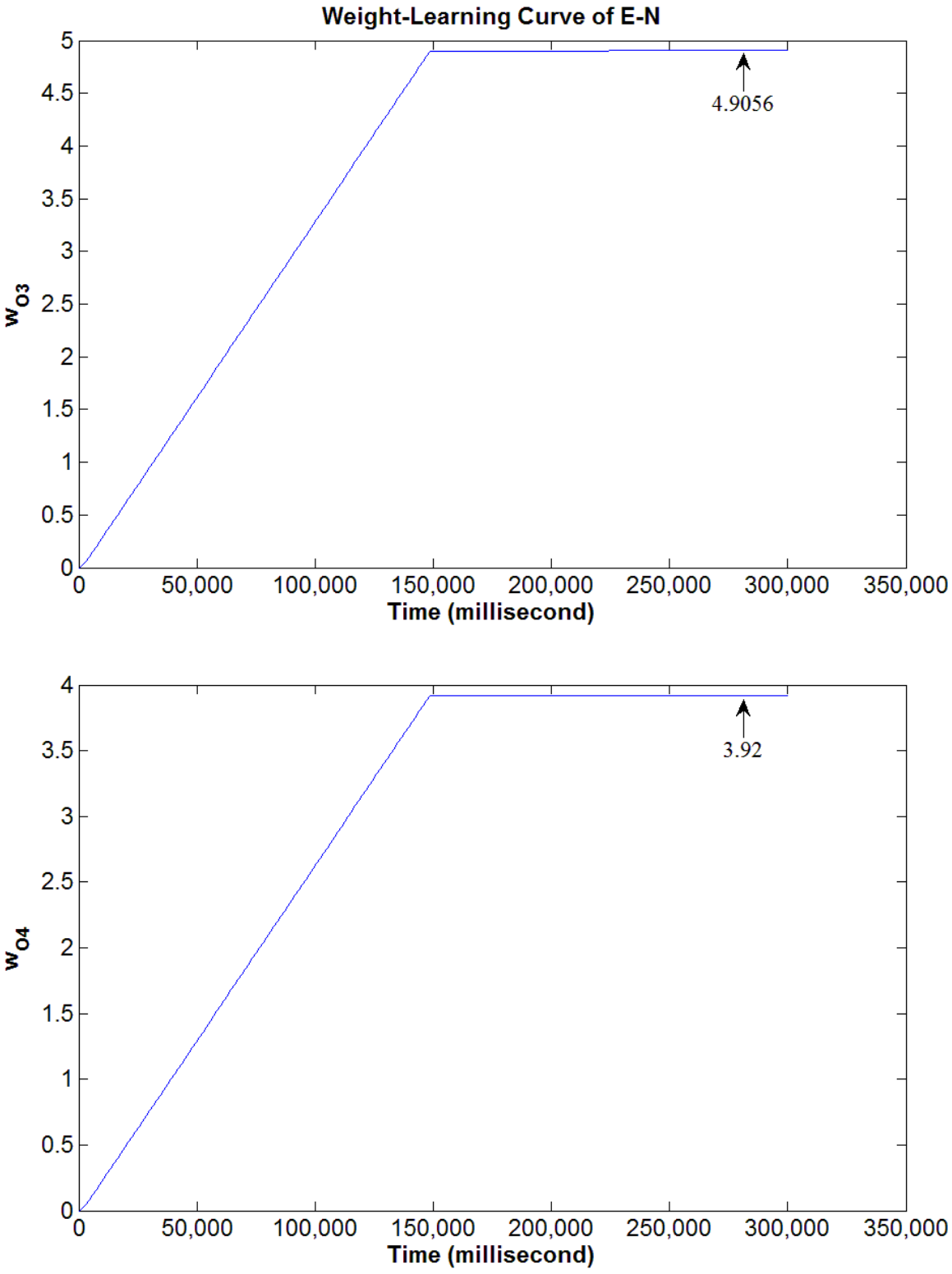

Figure 5.13. Weight-Learning curves of Eckhorn's network plotting the adaptive weights ($w_{O3(Eckhorn)}$ & $w_{O4(Eckhorn)}$) against time in milliseconds. The weights reach optimal values ($w_{O3(Eckhorn)} \approx 4.9056$ and $w_{O4(Eckhorn)} = 3.92$) at around 258 sec or 4.3 min (172nd iteration).

CHAPTER 6

Conclusion

This thesis has successfully incorporated the adaptive property of a phenomenological large scale neural model into a smaller-scale neural network by taking the approach of scientific reduction and using the model reference principle. The original contributions made by this thesis are as follows.

- An Eckhorn dipole network (E-DN) was designed that has the elastic rebound capability of a Grossberg dipole network (G-DN). But unlike G-DN, the rebound is achieved by network design and not as counterpart to Grossberg's elastic weight equations.
- The timing and duration of B-stimulus input in the E-DN produces emergent network properties that are not captured in the G-DN.
- Eckhorn network (E-N) performance evaluation is achieved by comparing the Grossberg network (G-N) output with a transformed E-N output. The transformation is a moving-point average (MPA) as defined in Figure 2.13 of chapter 2.
- The E-N has a performance surface that exhibits steep changes between regions of one performance index to another, indicating the need for using techniques such as gain-scheduling. In other words, during the transitions on the performance surface, use of gradient methods is not effective.
- The issue of "context-dependant choice" seen in level-coded model [Grossberg 1978] is also encountered in the E-N, as seen in the push-weight procedure of the algorithm.

- The conditioning performance surface (on which the adaptation is based on) is different from the conditioned performance surface as shown in Figure 5.6.
- The adaptive algorithm employed was successful in adapting the E-N; the learning rate is about 2.4x slower than that of the reference model, G-N. However, this performance factor can be optimized and the result reported here does not mean E-N adaptation is inherently slower.

The network developed in this work is a new network topology for pulse-coded neural networks. Although its constituent building block is a standard Eckhorn layer of linked Eckhorn neural units (ENU), the novelty in the network topology lies in the manners by which these layers are interconnected with one another. The resulting network is significantly more functionally purposive than the few standard Eckhorn topologies previously reported. The network is also much more biologically plausible than is the PCNN system commonly used in engineering applications [Lindblad & Kinser 2005].

This thesis has demonstrated that the employment of model-reference adaptation (MRA) technique is a powerful design tool for the development of new function-oriented pulse-coded neural networks (PCNNs). Network function is defined at the higher network system level by the G-N. MRA is then used to produce an adaptation performance surface. The performance surface is a key and fundamental tool for future development of entirely PCNN-level adaptation algorithms.

This thesis has also demonstrated that mapping from the G-N level of modeling to the E-N level of modeling is a non-trivial task. E-N level networks are shown to exhibit

emergent properties that are not exhibited at the G-N level. The full implications of this finding are not yet known.

Topics for future research

The unexpected (non-elastic) property of E-DN described in chapter 4 is most likely a consequence of either the way in which elastic modulation is effected in this particular pulsing-mode network or a consequence of elastic modulation of weights as proposed by Grossberg. The presence of the elastic weights mechanism at the Grossberg modeling level cannot help but be reflected at the pulse-modeling level. Changes in the level signals in a Grossberg model must correspond to changes in spiking rate and/or spiking time in a pulse-coded network.

The fact that such changes in the phasing of spike train packets produces emergent properties, as demonstrated in chapter 4, raises the issue of the biological substrate for Grossberg's elastic weights. There is little doubt Grossberg was inspired by short-term synaptic potentiation and depression when he introduced the notion of elastic weights. But at the scale of the Grossberg model, weights are not synapses and so, if the elastic weight hypothesis is correct, the elastic function cannot be immediately due to such low-level synaptic phenomena. The nature of elastic weight modulation due to network-level fatigue effect is not clear. Chapter 4 results raise this as a significant research question.

By raising this question, one also raises the question of what sort of changes in Eckhorn network behaviors would be introduced if elastic weight dynamics were somehow directly introduced into the feeding field weights of the basic Eckhorn dendrite model (of an ENU). Grossberg's differential equation for weight elasticity is not directly

implementable in pulse-mode neural networks. Therefore the question is raised: what is the pulse-mode functional counterpart to Grossberg's differential equation? This, too, is a topic for future research.

For this thesis, the transformation of spiking activities from the Eckhorn network to level-activities is based on MPA. This means that activity is proportional to spiking frequency. For instance, consider two cases with only two spikes. If case-1 has spiking interval T_1 and T_2 for case-2, such that $T_1 < T_2$, then $MPA_1 > MPA_2$. Consider a third case, where three spikes occur with $T_{2a} + T_{2b} = T_2$. Though case-3 has three spikes, $MPA_1 > MPA_3$. Application of this transformation procedure assumes that functional neuroenergetics of the cortex is proportional to the ensemble firing frequency [Smith 2002]. Apart from the work done by Smith et al. in the somatosensory cortex, research on the calibration of fMRI activities with electrical activities in the cortex with respect to various neurotransmitter systems and brain regions is still an open field. Therefore, an accurate transformation process from a spiking-model neural network in the future should have a stronger neurophysiological basis of fMRI.

The performance index (P) for the algorithm is based on the conditioning performance surface of E-N. Performance surface of E-N during conditioning (i.e., with B, D and S-stimulus) is different from conditioned performance surface. This difference in shape of performance surface with and without D-stimulus should have further investigation.

The objective of this thesis was to get a PCNN adaptive based on foundations that are close to psychology and biology. However, we have not yet investigated any optimization

techniques that can speed the adaptation. For future research, optimization techniques such as dynamic programming might be implemented to achieve the optimum parameter values.

Using the model-reference method, this thesis has shown that adaptation of PCNN is possible based on Hebb's laws. Thus, the next step would be to develop new methods by which the Eckhorn network can auto-adapt without the need of Grossberg reference as the "teacher".

Bibliography

Balkenius, C. (1995). “Modelling Learning” in *Natural Intelligence in Artificial Creatures* PhD Thesis. Lund University Cognitive Studies, 37, Sweden: Lund Offset, pp. 127-159, 1995. (http://www.lucs.lu.se/christian.balkenius/PDF/Balkenius.1995.Thesis.pdf).

Broussard, R.P. (1997). “Physiologically-Based Vision Modeling Applications and Gradient Descent-Based Parameter Adaptation of Pulse Coupled Neural Networks” PhD Thesis. Air Force Institute of Technology, Wright-Patterson Air Force Base, OH, USA. (http://handle.dtic.mil/100.2/ADA327028)

Burkitt, A.N. (2006a). “A review of the integrate-and-fire neuron model. I. Homogeneous synaptic input”. *Biol Cybern*. Jul; 95(1):1-19, 2006.

Burkitt, A.N. (2006b). “A review of the integrate-and-fire neuron model. II. Inhomogeneous synaptic input and network properties”. *Biol Cybern*. Aug; 95(2):97-112, 2006.

Combettes, P. (1993), "The foundations of set theoretic estimation," Proceedings of the IEEE, vol. 81, no. 2, pp. 182-208, 1993.

Eckhorn, R., Bauer, R., Brosch, M., Jordan, W., Kruse, W., Munk, M. and Reitboeck, H.J. (1988a). "Are form- and motion-aspects linked in visual cortex by stimulus-evoked resonances? Multiple electrode and cross-correlation analysis in cat visual cortex", *EBBS-Workshop on "Visual Processing of Form and Motion”*, Tubingen, Confer. Abstr., p. 7, 1988.

Eckhorn, R., Bauer, R., Brosch, M., Jordan, W., Kruse, W., Munk, M. and Reitboeck, H.J. (1988b). "Coherent oscillations: A mechanism of feature linking in the visual cortex? Multiple electrode and correlation analysis in the cat", *Biol. Cybern*. vol. 60, pp. 121-130, 1988.

Eckhorn, R., Bauer and Reitboeck, H.J. (1989a). "Discontinuities in visual cortex and possible functional implications: Relating cortical structure and function with multi-electrode/correlation techniques", in *Springer Series in Brain Dynamics*, E. Basar, Ed., Vol. 2, Springer-Verlag. Berlin, Heidelberg, 1989.

Eckhorn, R., Reitboeck, H.J., Arndt, M. and Dicke, P. (1989b). "Feature linking via stimulus-evoked oscillations: experimental results from cat visual cortex and functional implications from a network model". Proceed. Int. Joint Conf. Neural Networks, Washington. *IEEE TAB Neural Network Comm.*, San Diego, I, 723-730, 1989.

Eckhorn, R., Reitboeck, H.J., Arndt, M. and Dicke, P. (1990). "Feature linking via synchronization among distributed assemblies: Simulations of results from cat visual cortex". *Neural Computat.*, 2: 293-307, 1990.

Freeman, W.F. (1972). “Waves, pulses, and the theory of neural masses”. *Progress in Theoretical Biology*. Vol.1., John Wiley and sons, New York, pp. 1-34, 1972.

Gazzaniga, M.S., Senior, C. and Russell, T. (2006). “Functional Magnetic Resonance Imaging”, pp. 193-235 and “Electroencephalography” pp. 237-262 in *Methods in Mind (Cognitive Neuroscience)*. Cambridge, MA: MIT Press. 2006.

Grossberg, S. (1969a). “Embedding fields: A theory of learning with physiological

implications". *J. Math. Psycho*. 6, 209-239, 1969.

Grossberg, S. (1969b). "On the production and release of chemical transmitters and related topics in cellular control". *J. Theoret. Bio*. 22, 325-364, 1969.

Grossberg, S. (1971). "Embedding Fields: Underlying philosophy, mathematics, and applications to psychology, physiology, and anatomy". *J. Cybernet*. 1, 28-50, 1971.

Grossberg, S. (1972a). "A neural theory of punishment and avoidance, I: Qualitative theory". *Mathematical Biosciences*, 15, 39-67, 1972.

Grossberg, S. (1972b). "A neural theory of punishment and avoidance, II: Quantitative theory". *Mathematical Biosciences*, 15, 253-285, 1972.

Grossberg, S. (1972c). "Pattern learning by functional-differential neural networks with arbitrary path weights". In K. Schmitt (Ed.), *Delay and functional-differential equations and their applications*. New York: Academic Press, pp.121-160, 1972.

Grossberg, S. (1978). "A theory of human memory: Self-organization and performance of sensory-motor codes, maps, and plans". *In Progress in theoretical biology Volume 5*. Edited by: Rosen R, Snell S. New York: Academic Press; pp. 233-374, 1978.

Grossberg, S., Commons, M.L. and Staddon, J.E.R. (1991). "A neural network architecture for Pavlovian conditioning: reinforcement, attention, forgetting, timing". Ch.4 in *Neural Network Models of Conditioning and Action: A volume in the quantitative analyses of behavior series*. New Jersey: Lawrence Erlbaum Assoc., Inc. pp. 69-122, 1991.

Guyton, A.C. and Hall, J.E. (2006). "Behavioral and Motivational Mechanisms of the

Brain – The Limbic System and the Hypothalamus", Ch.58 in Textbook of Medical Physiology (11th ed). Pennsylvania: Elsevier Inc. pp. 728-729, 2006.

Hebb, D.O. (1949). *The organization of behavior*. New York: Wiley & Sons.

Hill, R., MacPherson, Q. and Wells, R.B. (2009). "Affect-driven learning in an avalanche neural network modeling early sensorimotor intelligence". 18th Ann. Computational Neuroscience Meeting (CNS 2009), July 18-23, 2009, Berlin, Germany. Published in *BMC Neuroscience* 2009, 10 (Suppl 1):P143.

Hodgkin, A.L. and Huxley, A.F. (1952). "A quantitative description of membrane current and its application to conduction of excitation in nerve," *J. Physiology*, 117: 500-544, 1952.

James, W. (1980). *The Principles of Psychology* (in two volumes), New York, Dover Publications, 1950.

Johnson, J.L., and Ritter, D. (1993), "Observation of periodic waves in a pulse-coupled neural network," *Optics Letters* 18: 1253-1255.

Johnson, J.L. (1994), "Pulse-coded neural networks: Translation, rotation, scale, distortion, and intensity signal invariance for images," *Applied Optics* 33: 6239-6253.

Lindblad, T. and Kinser, J.M. (2005). *Image Processing Using Pulse-Coupled Neural Networks*, 2nd revised ed., NY: Springer, 2005.

MacGregor, R.J. and Lewis, E.R. (1977). "Neuromimes" in *Neural Modeling*, New York: Plenum Press, pp. 195-223, 1977.

Morrison, F. (2008). “Pertubation Theory – Type II”. Ch.15 in *The Art of Modeling Dynamic Systems: Forecasting for Chaos, Randomness and Determinism*, Dover Ed., New York: Dover Pub., 2008.

Plutchik, R. (1980). *Emotion: A Psychoevolutionary Synthesis*, NY: Harper & Row, 1980.

Reber, A.S. and Reber, E.S. (2001). The Penguin Dictionary of Psychology, 3rd ed., London: Penguin Books, 2001.

Rulkov, N.F. (2002). "Modeling of spiking-bursting neural behavior using two-dimensional map," *Phys. Rev. E*, vol. 65, 041922, pp. 041922-1 to 041922-9, 2002.

Smith, A.J., Blumenfeld, H., Behar, K.L., Rothman, D.L., Shulman, R.G. and Hyder, F. (2002) “Cerebral energetics and spiking frequency: the neurophysiological basis of fMRI”. *Proc. Natl. Acad. Sci. U. S. A.* Aug 6; 99(16):10765-70, 2002.

von der Malsburg, C. (1999). "The what and why of binding: The modeler’s perspective," *Neuron*, 24: 95-104, 1999. (Christoph von der Malsburg)

von Neumann, J. (1958). *The Computer and the Brain*, 2nd Ed., New Haven, CN: Yale Univ. Press.

Wells, R.B., Garrett, N. and Richner, T. (2006). "Investigation of Physiological Mechanism For Linking Field Synapses," MRCI Technical Report, Sept. 20, 2006, Moscow, ID: The MRC Institute, Univ. Idaho. (http:\\www.mrc.uidaho.edu/~rwells/techdocs).

Wells, R.B. (2010). *Introduction to Biological Signal Processing and Computational*

Neuroscience (draft manuscript), Moscow, ID: The MRC Institute, Univ. Idaho., available from the author.

Wells, R.B. (2011a). “On Critical Doctrine of Method in Brain-theory” MRCI Technical Report, March 31, 2011, Moscow, ID: The MRC Institute, Univ. Idaho. (http:\\www.mrc.uidaho.edu/~rwells/techdocs).

Wells, R.B. (2011b). Private conversation with Prof. Richard B. Wells on May 6, 2011, Moscow, ID: The MRC Institute, Univ. Idaho.

Werbos, P. (1992). “Neurocontrol and supervised learning: An overview and evaluation” in *Handbook of Intelligent Control: Neural, Fuzzy and Adaptive Approaches*, D.A White and D.A Sofge (eds), NY: Van Nostrand Reinhold, pp. 65-89, 1992.

Werbos, P. (1998). “Stable Adaptive Control Using New Critic Designs” NSF Sept. 25 1998. Room 675, Arlington, Virginia. (http://arxiv.org/html/adap-org/9810001)

Whittaker, E. T. and Robinson, G. (1967). "Graduation, or the Smoothing of Data." Ch. 11 in *The Calculus of Observations: A Treatise on Numerical Mathematics*, 4th ed. New York: Dover, pp. 285-316, 1967.

Widrow, B. and Stearns, S.D. (1985). *Adaptive Signal Processing*. New Jersey: Prentice-Hall, Inc., 1985.

Zadeh, L.A. (1963). “On the Definition of Adaptivity”. *Proceedings of the IEEE*, March 1963, vol.51, Issue 3, pp.469-470, 1963.